# KINETICS AND MECHANISMS OF ANION ADSORPTION AND DESORPTION AT THE GOETHITE–WATER INTERFACE USING PRESSURE–JUMP RELAXATION

by

Pengchu Zhang

A dissertation submitted to the Faculty of the University of Delaware in partial fulfillment of the requirements for the degree of Doctor of Philosophy

May, 1990

© 1990 Pengchu Zhang
All Rights Reserved

# KINETICS AND MECHANISMS OF ANION ADSORPTION AND DESORPTION AT THE GOETHITE–WATER INTERFACE USING PRESSURE–JUMP RELAXATION

by

Pengchu Zhang

Approved: Donald L. Sparks

Donald L. Sparks, Ph.D.
Chairman of the Department of Plant Science

Approved: Donald F. Crossan

Donald F. Crossan, Ph.D.
Dean of the College of Agricultural Sciences

Approved: Carol E. Hoffecker

Carol E. Hoffecker, Ph.D.
Acting Associate Provost for Graduate Studies

I certify that I have read this dissertation and that in my opinion it meets the academic and professional standard required by the University as a dissertation for the degree of Doctor of Philosophy.

Signed: Donald L. Sparks

Donald. L. Sparks, Ph.D.
Professor in charge of dissertation

I certify that I have read this dissertation and that in my opinion it meets the academic and professional standard required by the University as a dissertation for the degree of Doctor of Philosophy.

Signed: Jeffry J. Fuhrmann

Jeffry J. Fuhrmann, Ph.D.
Member of dissertation committee

I certify that I have read this dissertation and that in my opinion it meets the academic and professional standard required by the University as a dissertation for the degree of Doctor of Philosophy.

Signed: William F. Ritter

William F. Ritter, Ph.D.
Member of dissertation committee

I certify that I have read this dissertation and that in my opinion it meets the academic and professional standard required by the University as a dissertation for the degree of Doctor of Philosophy.

Signed: J. Thomas Sims

J. Thomas Sims, Ph.D.
Member of dissertation committee

## ACKNOWLEDGMENTS

I wish to thank Dr. Donald L. Sparks, my major professor, for his guidance and patience. I am very grateful for the helpful suggestions, the criticism, and the encouragement that he has offered me during the past three years. I also thank Drs. Jeffry J. Fuhrmann, William F. Ritter and J. Thomas Sims for serving on my committee and for offering suggestions on this dissertation. I express my gratitude to Gerald Hendricks for his help in the laboratory. In addition, I thank the graduate students, postdoctoral fellows, and visiting professors in our soil chemistry group who provided advice and suggestions about my research. They also created an environment of intense fascination which made my graduate school life unforgettable.

The author also thanks his father, brother and sisters and their families; without their continuous encouragement, this project would not have been nearly so successful. My wife, Hong, and son, Scott, have provided me their love and confidence which made the completion of the research possible. The author expresses his deepest gratitude to his late Mom, Yuqing; her love and high expectation are always remembered and cheeried.

Finally, I wish to thank the University of Delaware for providing me with a graduate research fellowship to fund this project.

# TABLE OF CONTENTS

CHAPTER

## LIST OF FIGURES

## LIST OF TABLES

## ABSTRACT

The mechanism(s) and *chemical kinetics* of adsorption and desorption of inorganic ions on soils and soil constituents cannot be determined by the traditional kinetic methods such as batch, miscible displacement, and stirred–flow techniques. A pressure–jump (p–jump) relaxation apparatus with conductivity detection was employed to investigate the mechanism(s) and chemical kinetics of $MoO_4$, $SO_4$, $SeO_4$ and $SeO_3$ adsorption/dsorption on goethite in aqueous suspensions. Single relaxations were observed in the $SO_4$–goethite and $SeO_4$–goethite systems. The mechanism for adsorption of $SO_4$ and $SeO_4$ on goethite involved simultaneous protonation of surface functional OH group and adsorption of the anion on this surface. The intrinsic rate constants showed that the adsorption process,($logk^{int}_{ads.SO_4} = 8.3$, $logk^{int}_{ads.SeO_4} = 8.55$), was much faster than the desorption process, ($logk^{int}_{des.SO_4} = -0.84$, $logk^{int}_{des.SeO_4} = 0.52$).

Double relaxations were observed for the $MoO_4$– and $SeO_3$–goethite systems. The overall reaction for both systems consisted of two steps. An outer–sphere surface complex forms during the first step and occurs at the $\beta$ layer, in which the intrinsic forward rate constants, ($logk^{int}_{1,MoO_4} = 3.6$, $logk^{int}_{1,SeO_3} = 10.6$), are much larger than those for the second step ($logk^{int}_{2,MoO_4} = 0.28$, $logk^{int}_{2,SeO_3} = -4.0$). A ligand exchange process occurred in the second step resulting in the formation of inner–sphere surface complexes.

The modified triple layer model was successfully used to describe the adsorption of $MoO_4, SO_4, SeO_4$, and $SeO_3$ on goethite with the assumption that adsorbed ions may be located at either the $\alpha$ or $\beta$ layer. Electrostatic parameters, such as surface potentials computed from the model were employed in the relaxation equations to derive the intrinsic rate constants. Excellent agreement was found between the intrinsic equilibrium constants determined from TLM model calculations ($logK^{int}_{SO_4,model} = 9.6$, $logK^{int}_{SeO_4,model} = 8.64$, $logK^{int}_{MoO_4,model} = -0.47$, $logK^{int}_{SeO_3,model} = 20.42$ for $HSeO_3$ and 15.48 for $SeO_3$)

and between measurements from p-jump ($logK^{int}_{SO_4,kinetic}$ = 9.14, $logK^{int}_{SeO_4,kinetic}$ = 8.02, $logK^{int}_{MoO_4,kinetic}$ = −0.33, $logK^{int}_{SeO_3,kinetic}$ = 19.99 for $HSeO_3$ and 16.24 for $SeO_3$). These results indicate that a combination of equilibrium and kinetic studies can and must be used to ascertain mechanisms for anion adsorption/desorption on soil constituents.

# CHAPTER 1
# INTRODUCTION

Investigations on the kinetics of adsorption/desorption processes result in interesting information being obtained about mechanism(s) of these processes which take place at the solid/solution interface (Sposito, 1985; Sparks, 1989) and about the state of bonding at the adsorbed phase (Wedler, 1976). To properly understand the dynamic interactions between fertilizers, pesticides, herbicides, sludges, and wastes with soils, as well as to predict the mineral equilibria and geochemical behavior of elements in soils, one must have kinetic information. Additionally, to fully model organic and inorganic reactions in soils, a knowledge of their rates and mechanisms is fundamental (Sparks, 1987; Rai and Muraka, 1987). An assessment of the kinetic aspects of an inorganic ion-soil interaction must precede the application of the thermodynamics-based model (Sposito, 1985).

Traditional batch and miscible displacement flow techniques may not be suitable methods for investigating kinetics of adsorption/desorption of ions on soils and soil constituents (Chou and Wollast, 1984; Sparks, 1985; Ogwada and Sparks, 1986; Carski and Sparks, 1985). A newly developed stirred–flow technique has a number of advantages over traditional batch and flow methods including: maintaining constant experimental conditions, obtaining rapid measurements, diminishing transport and mass transfer processes, and removing desorbed ions during the reaction process (Carski and Sparks, 1985). However, the fastest measurement one can make is about 1 min. Many reactions on soil constituents are very rapid with some occurring on millisecond or even microsecor ' time scales. These reactions can not be studied using batch and flow methods (Sparks; 1989).

Numerous equilibrium models have been developed to describe the adsorption of ions at the solid/aqueous interface in terms of surface complexes. These include the constant capacitance (Hohl and Stumm, 1976), triple layer (Davis and Leckie, 1978), and

generalized model or four layer model (Barrow et al., 1980; Bowden et al., 1980; Barrow 1985). However, these models do not reveal information about kinetics and mechanisms of ion adsorption. To obtain this information, a knowledge of kinetics and/or a spectroscopic analysis is necessary.

In this dissertation, a pressure–jump relaxation technique was used to study the kinetics of sulfate, molybdate, selenite and selenate adsorption/desorption on goethite, an important soil constituent, in aqueous solution. For each anion studied, the research consisted of three parts: 1) investigating the rates of adsorption/desorption of at goethite/water interface using pressure–jump relaxation; 2) evaluating mechanisms for adsorption/desorption using thermodynamic and kinetic information; and 3) examining the applicability of surface complexation models for describe anion adsorption/desorption at the goethite/water interface in combination with kinetic data.

# CHAPTER 2
# LITERATURE REVIEW

## 2.1 Introduction

For many years, anion adsorption on oxides and clay minerals has been of interest to soil and environmental scientists and to geochemists concerned with ion retention in soils. Oxides and clay minerals have been employed to remove harmful anions from wastes (Muljade et al., 1966; Yates and Healy, 1973; Anderson et al., 1976; Mikami et al., 1983). In the past few years, many mechanisms, based solely on equilibrium studies, have been proposed to explain anion adsorption phenomena ( Breeuwsma and Lyklema, 1973; Huang, 1975; Anderson and Malotky, 1979; Davis and Leckie, 1980).

Much attention has been given over the last 50 years to equilibrium processes in soil. This information has proved valuable in understanding many aspects of adsorption processes; however, these studies do not assist one in understanding the kinetics of these reactions (Sparks, 1986). In fact, many of the equilibrium studies on anion adsorption/desorption are confusing and often contradictory. Therefore, it is necessary to examine extensively and properly the proposed mechanisms for anion adsorption on soils and soil constituents by studying both thermodynamics and kinetics.

## 2.2 Anion Adsorption and Desorption

### 2.2.1 Static Studies

The adsorption of an anion on a soil surface will be governed by the properties of both the anion and the surface. The anions of interest in soil chemistry are divided into two classes. The first class concludes $Cl^-$, $NO_3^-$, $ClO_4^-$, and probably $Br^-$, which are

referred to as nonspecifically adsorbed anions. All other anions, including organics, fall into a second class known as specifically adsorbed species (Mott, 1981).

The generic term *specific adsorption* is often used to describe the effects of inner-sphere surface complexation with surface functional groups of oxides, clay minerals and organics. The term *nonspecific adsorption* can be applied to outer-sphere surface complexation of ions with the above functional groups (Sposito, 1984).

#### 2.2.1.1 Nonspecific Adsorption

When an anion is nonspecifically adsorbed on soil constituents, it is electrostatically attracted to positive charges on the colloidal surfaces. If $H^-$ is adsorbed on a surface in excess of $OH^-$, the net positive charge will be balanced by adsorption of the spectator (nonspecifically adsorbed) anion from solution. At the pH where equal amounts of $H^-$ and $OH^-$ are adsorbed, the surface has no net charge and there is no spectator anion or cation adsorption (Hingston et al., 1972). This pH value is commonly referred as to the zero point of charge (zpc). On the acid side of the zpc, an increase in ionic strength leads to an increase in the activity product $[(H^+)(\text{anion})]^{\frac{1}{2}}$ (Atkinson et al., 1967) and hence to an increase in $H^+$ adsorption. The anion balancing the positive charge is in either the outer Helmholtz layer, which refers to the *3* layer in the triple model reported by Davis (1981), or the diffuse layer (Parks and deBruyn, 1962; Atkinson et al., 1967). The adsorption of $H^+$ has the same effect on surface charge as the desorption of $OH^-$, the adsorption of $H^+$ appears to be a replacement of a surface $OH^-$ by the nonspecifically adsorbed anion.

#### 2.2.1.2 Specific Adsorption

On the other hand, specifically adsorbed ions form chemical bonds with the surface groups. The free energy for this process is negative and the surface groups are very stable at a given pH (Mott, 1981). Specific adsorption refers to exchange of a ligand for an adsorbed anion and is thus referred to as ligand exchange (Sposito, 1984). Hingston et al. (1972) proposed that ligand exchange occurs when anions having a specific affinity for metal atoms in a hydroxylated mineral enter the coordination layer of the mineral

surface and are adsorbed out of all proportion to their concentration or activity in aqueous solution. Hingston et al. (1972) showed that anions of incompletely dissociated acids, such as phosphate, are adsorbed beyond the neutralization of positive surface sites and even on a surface having a negative charge. Protonated anions can be adsorbed onto a negative charged surface after dissociation of their protons, which then react with surface hydroxyls to form water molecules that in turn can be readily replaced by the anions. The role of the protonated anion in this mechanism as a proton donor has since been disputed (Rajan et al., 1974; Hingston, 1981; White, 1981), because protonation-proton dissociation reactions of the hydroxylated mineral surface alone are adequate to explain the pH dependence of anion adsorption (Stumm et al., 1980).

With ligand exchange, adsorbed anions are not released (desorbed) with the same amount of energy as occurred with adsorption. This may indicate that the reaction is not thermodynamically reversible. Mott (1981) has quantified such observations by introducing the concept of "desorbability" which is the percentage of the actual amount of anion remaining on the solid after two washes to the expected amount of anion remaining on the solid.

Adsorption isotherms have been studied for many anion adsorption reactions on soil constituents. The typical isotherm curve – an adsorption envelope – which is a graph of maximum adsorption versus pH, usually exhibits a broad peak at a pH value near the $pK_a$ for the conjugate Bronsted acid (Hingston et al., 1967; Hingston et al., 1968; Hingston et al., 1972; Sposito, 1983). Anion isotherm curves illustrate the tendency and influence of pH on anion adsorption and desorption on mineral surfaces (Sposito, 1983). However , the adherence of experimental adsorption data to a particular adsorption isotherm provides no evidence as to the actual mechanism of the sorption process. To explain mechanisms, one must employ spectroscopy or kinetics. An example of the latter is illustrated in the work of Alvarez and Sparks (1985) who reported polymerization of silicate anions in solution at low concentrations using laser Raman spectroscopy. These results showed that polymerization occurs at concentrations commonly used by investigators who have concluded that adsorption of silicate ions is occurring. To prevent erroneous conclusions about sorption data, Alvarez and Sparks (1985) pointed out that any mechanisms and

models that are proposed to describe anion sorption on sesquioxides should consider that silicates, and probably other tetrahedral-forming anions, may not be present in solution solely as monomeric ionic species.

With specific adsorption, the pzc usually shifts to more acidic values (Mott, 1980). This shift was observed for phosphate, silicate, selenite, and fluoride (Hingston et al., 1967; 1968; Hingston et al., 1972). Contrastingly, Arnold (1977) reported that for sulfate sorption on a tropical soil, the zpc is not reduced but raised and the same effect was observed by Rajan (1978) for sulfate adsorption.

### 2.2.1.3 Spectroscopic Studies

Direct spectroscopic evidence for ligand exchange on mineral surfaces using infrared spectroscopy was found by Goldberg and Sposito (1985). Russell et al.,(1976) have shown the singly coordinated surface hydroxyls on goethite and the OD signal disappeared after phosphate saturation. Parfitt and Russell (1977), using infrared spectroscopy, reported that $HPO_4^{2-}$, $SO_4^{2-}$ and oxalate are adsorbed by ligand exchange and form binuclear bridging complexes whereby two singly coordinated A-type $OH^-$ groups are replaced by two oxygen atoms of one ligand. Martin and Smart (1987) measured the characteristics of anion adsorption on goethite with X-ray photoelectron spectroscopy (XPS). Their results confirmed the conclusions reached in other studies, namely, that phosphate, selenite and sulfate replaced A-type hydroxyls when they were adsorbed on goethite.

Hayes et al. (1987) used extended X-ray absorption fine structure (EXAFS) to measure the interaction between selenate and selenite and goethite in aqueous suspension. Measurements showed that selenate forms a weakly bonded, outer-sphere surface complex and that selenite forms a strongly bonded, inner-sphere complex. The adsorbed selenite ion was directly bonded to the goethite surface in a bidentate fashion with two Fe atoms 3.38 nm from the selenium atom. Adsorbed selenate has no Fe atom in the second coordination shell of selenium, which indicates retention of its hydration sphere upon sorption (Hayes et al., 1987).

### 2.2.1.4 Effect of Surfaces on Adsorption and Desorption

The effect of mineral surface type on adsorption phenomena has not been studied as extensively as the type of ions. Mineral surfaces are generally not homogeneous. Rather, kinks, steps, edges, dislocations, or point defects may provide reactive zones (Davis and Hayes, 1986) for adsorption/desorption. Microcrystalline preparation of solids, which are frequently used in labrotary sorption experiments, may have several cleavage planes with different site energies. The importance of the high energy sites that result from these imperfections is well recognized particularly for dissolution and crystal growth processes (Dibble and Tiller, 1981). For example, Hingston et al. (1974) have found that goethite provides a stronger ligand bond for most anions than gibbsite, and consequently, desorbability is significantly higher.

Finally, it is necessary to realize that the term adsorption which is used by most researchers refers to loss of solute from an aqueous solution. Sposito (1986) suggested that the general term sorption should be used if the mechanism for the loss is not known since sorption includes three principal processes: adsorption, absorption and surface precipitation. It is increasingly clear, as pointed out by Davis and Hayes (1986), that the macroscopic approaches that have been commonly used to study sorption processes, e.g. adsorption isotherms, solubility calculations, and kinetic methods, cannot unequivocably distinguish between processes such as adsorption and surface precipitation.

### 2.2.2 Anion Adsorption and Desorption: Kinetic Studies

A number of studies have recently appeared in the scientific literature on kinetics of cation adsorption on clays and soils (Sawhney, 1966; Jardine and Sparks, 1984; Sparks et al., 1980; Ogwada and Sparks, 1986a, b). However, few studies have been conducted on the rate of anion adsorption on soil constituents. Limited studies have been conducted on sulfate (Rajan, 1978; Tripathi et al., 1975), borate (Griffin and Buran, 1974; Peryea and Bingham, 1985), and phosphate adsorption (Kuo and Lotse, 1972; Novak and Adriano, 1975; Fiskell et al., 1979; Barrow, 1985).

Mott (1981) states that unlike nonspecifically adsorbed ions, ligand exchanged ions do not have adsorption and desorption isotherms that are identical kinetically. For ligand exchanged ions, desorption at constant pH is a much slower process than adsorption.

One of the biggest problems in studying the rates of anion adsorption on soil constituents is the methodology one employs. Two basic techniques have traditionally been used to study kinetics of ionic reactions on soil constituents: batch and flow (Sparks, 1985, 1986). The traditional batch (tube) technique involves placing an adsorbent and adsorbate in a vessel such as a centrifuge tube which is agitated. Then the suspension is usually centrifuged or filtered to obtain a clear supernatant solution for subsequent analysis. There are a number of disadvantages to this traditional batch technique including: not being able to observe rapid reactions if centrifugation is required: determining proper mixing rates: and, not removing exchanged species remaining in solution which could cause hysteresis and secondary precipitation during dissolution of soil minerals (Chou and Wollast, 1984; Sparks, 1985).

A modified batch technique which lacks many of the disadvantages given above was developed by Zasoski and Burau (1978). It has successfully been used by Harter and Lehmann (1983) to measure metal adsorption reactions on soils. With this technique, one can measure reactions at fairly rapid intervals and can easily maintain constant suspension pH and soil:solution ratios. However, there are problems with not removing desorbed species and difficulty in monitoring desorption kinetics.

Flow or miscible displacement methods have recently been used in several kinetic studies (Sivasubramaniam and Talibudeen, 1972; Sparks et al., 1980; Miller et al., 1986; Chou and Wollast, 1984; Carski and Sparks, 1985). The technique first introduced by Sivasubramaniam and Talibudeen (1972) and later modified by Sparks et al., (1980) enables measurement of reactions at 2 min. intervals, effects constant removal of desorbed species, and maintains a constant soil:solution ratio.

Unfortunately, some problems exist with the original flow method of Sparks et al. (1980). The colloidal sample is not dispersed and significant mass transfer exists (Ogwada and Sparks, 1986b) due to lack of mixing. Moreover, transport and chemical

kinetics phenomena are occurring simultaneously, which makes strict kinetic interpretation difficult. Additionally, dilution errors can exist (Carski and Sparks, 1985).

Most of these problems can be eliminated by use of a stirred–flow method developed by Carski and Sparks (1985). With this technique, the sample is continuously mixed to greatly diminish transport and significantly reduce mass transfer processes. The stirred-flow method has successfully been used to study K reactions on clay minerals and soils (Carski and Sparks, 1986). It also appears from recent studies that diffusion processes are greatly reduced using the stirred-flow technique and that one can calculate thermodynamic parameters from kinetic measurements, *viz.*, $k_a/k_d = K_{eq}$, where $k_a$ is the adsorption rate coefficient and $k_d$ is the desorption rate coefficicent, using this method (Ogwada and Sparks, 1986a: Carski and Sparks, unpublished data). This method seems to have real promise in studying anion adsorption-desorption kinetics on minute or longer time scales.

Ogwada and Sparks (1986b) investigated kinetic methodology effects on $k_a$ values and energies of activation for adsorption ($E_{aa}$) using several techniques. These data clearly show the effect of mixing on equilibration time and degree of diffusion-controlled exchange. Except for a rapid vortex method, significant diffusion existed as evidenced by low $E_{aa}$ values.

Clearly, both batch and traditional flow techniques have problems. Rate coefficients calculated using both methods are apparent since they usually are explaining not only chemical kinetics but also mass transfer or diffusion phenomena (Jardine and Sparks, 1984). Moreover, many reactions involving soil constituents such as metal adsorption on oxides and clay minerals and catalytic reactions on oxides and clay minerals occur on millisecond and microsecond time scales and cannot be measured using batch and flow techniques (Astumian et al., 1981). Anion adsorption-desorption reactions on soil constituents may also be extremely rapid. For rapid reaction kinetics, relaxation techniques such as pressure jump and electric field pulse methods are the suitable methods to be applied (Sasaki et al., 1983). The theory and application of relaxation techniques are discussed detailly in the next chapter.

## 2.3 Application of Chemical Relaxation Techniques for Studying Kinetics of Solid/Water Systems

Batch and flow techniques can only be used to obtain information for transport-controlled and diffusion-controlled reactions and to determine apparent rate laws. Relaxation techniques measure reactions with half time-$t_{1/2} < 10 - 20s$ (Sparks, 1989). Only the application of relaxation techniques in solid/water systems is discussed in this section.

### 2.3.1 Cation Adsorption and Desorption on Oxide Surfaces

Relaxation techniques have been used for determining kinetics and mechanisms of metal ion adsorption and desorption at mineral/water interfaces. Hachiya et al. (1979) studied the kinetics of $Pb^{2+}$ adsorption/desorption on a $\gamma - Al_2O_3$ surface using p-jump and electric field pulse techniques. With the p-jump study, the electric conductivity in the sample increased with pressure increase, but a very fast change in conductivity was found. The fast conductivity change then was measured with an electric field pulse technique. From both measurements, a double relaxation was obtained for the adsorption and desorption process. The value of reciprocal slow relaxation times ($\tau_s^{-1}$) was dependent on the concentration of $Pb^{2+}$ and the pH, but was independent of the ionic strength. And the value of the reciprocal fast relaxation times ($\tau_f^{-1}$) decreased with increasing concentration of $Pb^{2+}$. From the rate equation for the Langmuir-type adsorption/desorption, they derived the a linearized relationship between reciprocal relaxation times and the adsorbed Pb and free $Pb^{2-}$ in suspension. By plotting this relationship, the rate constants were obtained. The fast relaxation was attributed to adsorption/desorption of $Pb^{2-}$ on the hydrous oxide surface group Al-OH and the slow relaxation was ascribed to the deprotonation-protonation process induced by adsorbed $Pb^{2+}$. In this study, no consideration was given to the effect of surface charge on adsorption.

The p-jump technique was also applied in studying the kinetics of adsorption and desorption of divalent metal ions such as $Ca^{2-}$, $Mn^{2+}$, $Zn^{2-}$, and $Co^{2-}$ on $\gamma - Al_2O_3$. Double relaxations were observed in each of these systems (Hachiya et al., 1984). The fast relaxation was attributed to simultaneous adsorption/desorption of metal ions on surface

sites of the largest fraction on the $\gamma - Al_2O_3$ surface. The magnitude of the forward rate constant was correlated to that for release of a water molecule from a hydrated metal ion in the metal complex. Based on these results, the mechanism for metal ion adsorption/desorption was described by two steps. In the first step, hydrated metal ions lose one water molecule and form an intermediate complex with a surface site; this step was rate–limiting. The intrinsic rate constants obtained for the fast relaxation are listed in Table 2.1. In the second step, a metal ion–surface complex was formed and a proton was released from the surface of the surface. This slow relaxation step was attributed to the adsorption/desorption of metal ions on the remaining, which constituted a small portion of the surface sites. The majority of surface sites were strong attractive ones while the minority sites were weak ones (Yasunaga and Ikeda, 1986).

**Table 2.1:** Intrinsic rate constants of adsorption/desorption of metal ions on $\gamma$-$Al_2O_3$ surface at 298K

| metal ion | $k_1^{int}(mol^{-1}dm^3s^{-1})$ | $k_{-1}^{int}(mol^{-1}dm^3s^{-1})$ |
|---|---|---|
| $Pb^{2+}$ | $(6.4 \pm 1.6) \times 10^4$ | $(4.1 \pm 1.0) \times 10^6$ |
| $Cu^{2+}$ | $(7.4 \pm 2.0) \times 10^3$ | $(3.1 \pm 0.9) \times 10^5$ |
| $Zn^{2+}$ | $(5.1 \pm 0.8) \times 10^2$ | $(1.3 \pm 0.2) \times 10^5$ |
| $Mn^{2+}$ | $(3.2 \pm 0.5) \times 10$ | $(1.8 \pm 0.3) \times 10^6$ |
| $Co^{2+}$ | $(1.5 \pm 0.4) \times 10$ | $(6.9 \pm 1.9) \times 10^4$ |

Hayes and Leckie (1986) investigated lead adsorption/desorption at the goethite–water interface. The modified triple layer model, in which the adsorbed metal ion may locate either at the $\alpha$ or $\beta$ plane, was developed to obtain surface charge and potential parameters. Three types of information: 1. overall equilibrium partitioning; 2. reaction stoichiometry; and 3. rate laws that correctly related the observed product and reactant changes to the inverse of the relaxation time constant, were required to verify the reaction mechanism. A double relaxation was obtained from the p–jump measurement. Combining

the results from static and kinetic studies, a bimolecular adsorption/desorption reaction mechanism was postulated, *viz.*, a $Pb^{2+}$ ion adsorbs on a neutral surface site at the $\alpha$ plane and a proton is replaced from the surface. This analysis was based only on the fast process for the double relaxation. The rate–limiting step was the desorption step associated with breaking the surface bond of the inner–sphere lead hydroxyl complex.

The very interesting finding by Hayes and Leckie (1986) was the trend observed in the intrinsic rate constants ($k_1^{int}$ and $k_{-1}^{int}$) is contrast with that of pressure–jump change (Table 2.2). This was ascribed to the higher energy site being perturbed at higher pressure. This is reflected in the lower value of the rate constants at higher $\Delta p$, which implies a higher activation energy and a lower overall rate (Hayes and Leckie, 1986).

**Table 2.2:** Intrinsic rate constants

| $\Delta P$ | $k_1^{int}(mol^{-1}dm^3s^{-1})$ | $k_{-1}^{int}(mol^{-1}dm^3s^{-1})$ | $K_1^{int}$ |
|---|---|---|---|
| 140 | $1.7 \times 10^5$ | $4.2 \times 10^2$ | $4.0 \times 10^2$ |
| 100 | $2.4 \times 10^5$ | $6.1 \times 10^2$ | $4.0 \times 10^2$ |
| 140 | $3.6 \times 10^5$ | $8.9 \times 10^2$ | $4.0 \times 10^2$ |

### 2.3.2 Anion Adsorption and Desorption on Oxide Surfaces

The kinetics of anion adsorption/desorption on soil constituents has rarely been studied, but it is well known that a number of anions such as phosphates, sulfate, borates and/or selenite and selenate play an essential role in plant nutrition, and also the condominational source to soil and ground and surface water.

Pressure–jump relaxation has been used to study the kinetics and mechanisms of acetic acid on silica–alumina (Ikeda et al. 1982), phosphates (Mikami et al., 1983a) and chromates (Mikami et al., 1983b) on $\gamma - Al_2O_3$. Double relaxation times were

observed on the order of milleseconds for each of these three experiments. For the adsorption/desorption of acetic acid on a silica–alumina surface, the fast relaxation was attributed to the protonation–deprotonation reaction on the Si–Al surface and the slower relaxation was ascribed to the adsorption /desorption of the acetate ion, accompanied by the elimination of a water molecule from the surface (ligand exchange).

In the study of adsorption/desorption of phosphates on $\gamma - Al_2O_3$, the fast and slow relaxation times were attributed to adsorption/desorption of di- and monovalent phosphate, respectively, on protonated surface hydroxyl groups. The mechanism for the phosphate reaction was electrostatic attraction and the adsorbed phosphates locating in the same plane which contained adsorbed counterions. This mechanism was described by the triple layer model of Davis et al. (1978) and assumed that the potentionl of the surface is equal to the $\zeta$ potential.

The same conclusions and mechanisms were made for adsorption/desorption of chromate with a fast relaxation being attributed to $CrO_4^{2-}$ adsorption and a slow relaxation to $HCrO_4^-$ adsorption on the $\gamma - Al_2O_3$ surface via electrostatic attraction. The main difference in the phosphate and chromate studies reported on above is that, in the latter there was little difference in the rate constants for mono- and divalant chromate ions. However, in the phosphate study, the adsorption rate for $HPO_4^{2-}$ was much faster than for $H_2PO_4^-$. The adsorption rate constants for $HPO_4^{2-}$ and $H_2PO_4^-$ ($4.1 \times 10$ and $1.1 \times 10^7 mol^{-1}dm^3s^{-1}$, respectively) were one to two orders of magnitude larger than those for $CrO_4^{2-}$ and $HCrO_4^-$ ($5.3 \times 10^4$ and $9.9 \times 10^4 mol^{-1}dm^3s^{-1}$, respectively). The desorption rate constants for $HPO_4^{2-}$ and $H_2PO_4^-$ (2.3 and 2.7 $s^{-1}$, respectively) were one order of magnitude smaller than those for $CrO_4^{2-}$ and $HCrO_4^-$ ($1.9 \times 10$ and $5.2 \times 10 s^{-1}$, respectively). Accordingly, the authors concluded that the interaction of chromate with Al–oxide was weaker than that of phosphate (Mikami et al., 1983).

For the extremely rapid adsorption/desorption reactions of anions such as $Cl^-$ and $ClO_4^-$, reequilibrium is too rapid to be observed by the p-jump technique. For such anions, the electric field pulse technique has been employed (Sasaki et al., 1983). Two relaxations on the order of microseconds were observed in an acidified aqueous suspension

of $\alpha$–FeOOH with NaCl or $NaClO_4$. The fast relaxation was dependent on the applied electric field intensity and was attributed to physical phenomena, i.e., a diffusion process while the slower relaxation was independent of the applied electric field intensity. It was interpreted in terms of an association/dissociation reaction between counterions with the protonated surface hydroxyl group. The intrinsic equilibrium constant in the $\alpha$–FeOOH–HCl system was one order of magnitude higher than that in the $\alpha$–FeOOH–$HClO_4$ system. This fact indicated that the ion-pair formation reaction in the former system was much more stable. This finding was further supported by the finding that the stability constant for an ion pair between $Cl^-$ and metal ions is 1–2 order of magnitude larger than between $ClO_4^-$ and metal ions.

A combination of p–jump and electric field pulse relaxation techniques was employed to study the mechanisms of adsorption/desorption of $IO_3^-$ on a $TiO_2$ surface by Hachiya et al. (1980). Fast and slow relaxation times were generated by electric field pulse and p–jump techniques, respectively. The fast relaxation was attributed to the release of OH ions induced by adsorbed $IO_3^-$, and the slow relaxation was ascribed to the adsorption/desorption of $IO_3^-$ on the $TiO_2$ surface. Because of the agreement between the backward rate constants for the $OH^-$ release step ($5.8(\pm 0.2) \times 10^8 mol^{-1}dm^3s^{-1}$) and the diffusion value ($3.2 \times 10^8 mol^{-1}dm^3s^{-1}$), the association of $OH^-$ process was considered as the diffusion–controlled step. On the other hand, the value of the forward rate constant for $IO_3^-$ adsorption ( the first step) ($k_1 = 4.3 \times 10^3 mol^{-1}dm^3s^{-1}$) was five orders of magnitude smaller than for the diffusion–controlled step. This may be due to the considerably large value of the activation energy for $IO_3^-$ adsorption (Hachiya et al., 1980).

### 2.3.3 Complexation in Soil and Aqueous Environments

A detailed knowledge of the interaction of metal ions with natural organic and inorganic compounds is needed for an understanding of the essential chemical processes that occur in soil and water systems. Complexation may change the fate of a number of organic and inorganic anions and cations in the soil solution.

In most studies dealing with metal complexes in the aquatic environment only equilibrium measurements have been discussed and the kinetics involved has been neglected. However, as Pankow and Morgan (1981) pointed out, these natural systems never reach complete equilibrium and their state is controlled by kinetic processes.

As an example of how kinetic measurements may reveal the mechanism of complex formation between compounds present in soils, Lopez-Quintea et al. (1984) studied the reaction between aluminum ions and citric acid and leaf extract in aqueous solution. Citric acid or leaf abstract was mixed $Al^{3+}$ in a stopped-flow apparatus, and the progress of the reaction was monitored by observing changes in electrical conductance. To avoid a conductance change caused by inhomogeneous mixing and temperature changes, the two solutions were previously adjusted to equivalent conductance with inert reagents and at the same pH. The detected change in conductance should be caused by complex formation. At low pH range (pH=1.4-2.7), only a single relaxation was observed used stopped-flow method and p-jump experiments. The relaxation obtained using the stopped-flow method was attributed to the formation of monodentate complexes ($AlH_2Cit^{2+}$) and was the rate-determining. Using stoichoimetric information, a hypothesized reaction scheme and relaxation measurements, thermodynamic and kinetic parameters were calculated. At 293.7 K, for the monodentate complex, $AlH_2Cit^{2}-$, the bidentate complex, $AlHCit^{+}$ and the tridentate complex, AlCiT, the stability constants were $8.2(\pm 1.5) \times 10^2$, $3.6(\pm 1.6) \times 10^6$ and $5.3(\pm 2.3) \times 10^{10} dm^3 mol^{-1}$, respectively. The rate constants for the formation of the monodentate and the bidentate complexes were $5.4(0.5) \times 10^3$ and $80(\pm 10) dm^3 mol^{-1} s^{-1}$, respectively.

Complexation reactions between iron (III) and phosphate ions are important role in soil chemistry, water treatment and corrosion. Formation of various species have been postulated, depending on the experimental conditions, methods of analysis and interpretation of results. Few studies, however, have reported thermodynamic data and kinetic information on these species. Wilhelmy et al. (1985) used UV Visible and stopped-flow spectroscopies to identify the complexes which play a role in the formation of solid phases and determined the relevant thermodyanamic and kinetic constants. Wilhelmy et al. (1985) distinguished mono- and diphosphate iron species and determined their rate con-

stants of formation by stopped-flow relaxation. The mechanisms for the monophosphate iron complex were postulated as:

$$Fe^{3+} + H_2PO_4 = FeH_2PO_4^{2+}$$

or

$$FeOH^{2+} + H_3PO_4 = FeH_2PO_4^{2+}$$

or a combination of the two predominates. However,one can distinguish the mechanism(s) for complexation by evaluating the rate constants and the corresponding activation parameters $\delta H^{\neq}$ and $\delta S^{\neq}$. Also, from the kinetic study, Wilhelmy et al. (1983) found that the mechanism for formation of the biphosphate iron species ($Fe(H_2PO_4)_2^-$) consisted of a combination of several possible pathways. The respective forward and backward rate constants were calculated. These findings offer strong evidence that a static spectrophotometric procedure may not be sufficiently sensitive to detect successive complexation. In contrast, time-resolved absorbance measurements provide an effective method for identification of a series of species in solution. The detection of the ferric diphosphate complex, $Fe(H_2PO_4)_2^-$, demonstrated the value of using a kinetic technique for characterizing solution species.

Stopped-flow and temperature-jump methods as were used to investigate the kinetics of interaction of magnesium-bicarbonate in aqueous solution (Patel et al., 1974). The single relaxation times were found to be very short ($\tau \approx 5 - 20\mu$sec). The best experimental conditions were at pH$\approx$ 9, since around this pH conditions due to the formation of both $MgHCO_3^-$ and $MgCO_3$ give rise to a relatively large reaction amplitude. At lower pH's, the reaction amplitudes were much smaller and made experimental measurements very difficult. The data obtained were interpreted on the basis of a coupled reaction scheme in which the protolytic equilibria are established relatively rapidly, followed by a single relaxation process due to the formation of $MgHCO_3^-$ and $MgCO_3$. The formation rate constants were determined to be

$$k_f = 5.0 \times 10^5 mol L^{-1} s^{-1} (Mg^{2-} - HCO_3^-)$$

$$k_f = 1.5 \times 10^6 mol L^{-1} s^{-1} (Mg^{2-} - CO_3^{2-}).$$

These results, in conjunction with NMR solvent exchange rate constants ($\approx 1 \times 10^5 s^{-1}$), were analyzed in terms of a dissociative mechanism for the rate of complex formation (Patel et al., 1974).

Other kinetic studies of complexation using relaxation techniques can be found in the studies of Bridger et al. (1983) (hydroxo and chloro complexes of iron (III)); Bridger et al. (1982) (complexation of iron (III) by picolinic and dipicolinic acids); Strahm et al. (1979) (complexation of aqueous iron chloride); and Patel and Taylor (1973) (complexation of magnesium pyrophosphates).

### 2.3.4 Hydrolysis on the Mineral Sufaces

It is well known that the amphoteric properties of the hydroxyl group existing on the surface of oxide particles play an important role in adsorption and are characterized by two acidity constants, one for the protonation reaction and the other for the deprotonation reaction. These constants are functions of the surface potential created by the adsorbed ions (Davis et al., 1978; Atkinson et al., 1967).

Astumian et al. (1981) investigated the kinetics of proton adsorption/desorption on iron oxides in aqueous suspensions using p-jump relaxation. Single relaxations were observed in suspensions of $\gamma - Fe_2O_3$ (hematite) and $Fe_3O_4$ (magnetite). The reciprocal relaxation times obtained for both the hematite and magnetite suspensions showed the same parabolic dependence on pH, displaying a minimum at pH 3.4. The intrinsic rate constants for the two oxides were very similar. At $I = 2 \times 10^{-3}$ and 298K, the protonation ($k_a^{int}$) and deprotonation ($k_d^{int}$) rate constants for hematite were $2.4 \times 10^5 mol^{-1} Ls^{-1}$ and $0.16 s^{-1}$, respectively. For magnetite, they were $1.4 \times 10^5 mol^{-1} Ls^{-1}$ and $0.34 s^{-1}$ respectively. No relaxation was found in a goethite suspension. The reason for this is that the $K_a$ (acidity constant) of goethite ($10^{4.3-5.0}$) is higher than that for magnetite ($10^{3.5-4.0}$) and hematite ($10^{3.9-4.5}$). In general, upon applying a perturbation to a chemical equilibrium, the shift of the equilibrium (relaxation amplitude) is the larger the more similar the equilibrium population of the species involved. Systems with very small or very large equilibrium constants, therefore, are relatively insensitive to perturbation. So,

it is not surprising that no relaxations could be observed in the $SiO_2$ ($K_a^- < 10$) and $\gamma - Al_2O_3$ ($K_a^- = 10^{4.4-6.0}$) suspensions. The relative amplitudes were found to follow the order of $TiO_2$ ($K_a^- = 10^{2.5-3.0}$) > magnetite ($K_a^- = 10^{3.5-4.0}$) > hematite ($K_a^- = 10^{3.9-4.5}$). From these data, it would appear that relaxations can be observed in the approximate range of $2 < pK_a^- < 4$.

In a study of kinetics of hydrolysis of a zeolite surface using p-jump relaxation (Ikeda et al., 1981), a single relaxation was found above pH11.5. To prevent a relaxation possibly caused by $Na^-$ entering the cage of zeolite, tetramethylammonium hydroxide was added as the base. Even though the tetramethylammonium ion could not enter the cage structure the same single relaxation was observed. Therefore, the relaxation was due to the interaction between the hydroxide ion and the active site on the zeolite surface. With hydrolysis, a proton on the hydroxyl site was released to the bulk solution to form a water molecule with a hydroxyl ion. Based on an analysis of the equilibrium and kinetics measurements, the forward and backward rate constants for the hydrolysis process were to be $1.6 \times 10^2 mol^{-1} Ls^{-1}$ and $8.7 \times 10^{-2} s^{-1}$, respectively. Equilibrium constants obtained from kinetic and static measurements agreed with each other satisfactorily. Similar results were reported for studies of kinetics of hydrolysis on zeolites X ($Na_2O.Al_2O_3.2.5SiO_2$) and Y ($Na_2O.Al_2O_3.4.8SiO_2$) (Ikeda et al., 1982).

# CHAPTER 3
# THEORY OF CHEMICAL RELAXATION AND PRINCIPLES OF THE PRESSURE-JUMP RELAXATION TECHNIQUE

To clarify the theoretical and experimental aspects of this study, the general theory of chemical relaxation and the principles of the pressure-jump (p-jump) relaxation method are outlined in this chapter. They are taken from Bernasconi (1976), Schwarz (1986) and Sparks (1989).

## 3.1 Theoretical Considerations of Chemical Relaxation

The term "chemical relaxation" refers to effects arising from the inherent tendency toward equilibriation in the course of time when a stationary state of chemical reactions has somehow been perturbed. Under unusual circumstances such a stationary state is the ordinary chemical equilibrium determined according to thermodynamic principles. In any case a perturbation may generally be brought about by means of externally manipulated and sufficiently rapid changes in certain parameters such as temperature, pressure, or the amount of a certain reactive substance. In the course of the perturbation the system shifts to a new equilibrium position with a characteristic rate that defines the relaxation time of the system.

Let us consider a physicochemical system where a single independent variable $x$ can be observed. Equilibrium of the system is supposed to be determined by a parameter $\theta$ (e.g., temperature or pressure). Due to changes in $\theta$, the instantaneous equilibrium may vary with the time $t$. If it were actually established , the variable $x$ would assume a respective value $\bar{x}(t)$. Should, however, $x$ be different from $\bar{x}$ the inherent tendency for equilibration must give rise to a rate, $\frac{dx}{dt} = \dot{x}$, which is described as a pertinent function $f(x, \theta)$. It can be linearized if the system stays close enough to an appropriately chosen

reference state $x^0, \theta^0$ as expressed by

$$f(x,\theta) = f^0 - f_1^0(x - x^0) + f_2^0(\theta - \theta^0) \tag{3.1}$$

where $f^0, f_1^0$, and $f_2^0$ represent the values of $f(x,\theta), \frac{\partial f}{\partial x}$, and $\frac{\partial f}{\partial \theta}$ respectively, at $x = x^0, \theta = \theta^0$. Taking advantage of the equilibrium condition, that is, $f(\bar{x},\theta) = 0$, we readily arrive at

$$\dot{x} = f(x,\theta) - f(\bar{x},\theta) = f_1^0(x - \bar{x}). \tag{3.2}$$

Since the change of $x$ is necessarily directed toward $\bar{x}$, the factor $f_1^0$ must be negative. Thus a positive quantity $\tau$ (having the dimension of time) may be defined according to the relation

$$\frac{1}{\tau} = -(\frac{\partial f}{\partial x})_{x=x^0,\theta=\theta^0} \tag{3.3}$$

so that

$$\dot{x} = -(x - \bar{x})\tau. \tag{3.4}$$

The characteristic parameter $\tau$ is called the relaxation time of the process in question.

As is easily realized, the basic relaxation equation (3.4) is generally applicable in a range sufficiently close to equilibrium. There the rate can be satisfactorily linearized in using Eq. (3.2) provided $\frac{\partial f}{\partial x} \neq 0$. Then we deal with a relaxation process.

The relaxation equation (3.4) is a simple linear first-order differential equation. It can readily be solved for any practically reasonable $\bar{x}(t)$ . The procedure turns out to be especially simple when a time-independent equilibrium state is considered (i.e., $\bar{x}$ =constant). Then we immediately obtain

$$\dot{x} = \bar{x} - (x_0 - \bar{x})exp(-t/\tau) \tag{3.5}$$

($x_0$ being the value of $x$ at $t = 0$); in other words, the instantaneous deviation from equilibrium fades out gradually following an exponential function of time. The actual decay time is measured by $\tau$. So far the treatment applies to systems where only one independent variable is subject to relaxation. Frequently, however, $m(>1)$ such variables are needed to describe the relaxing properties of interest. Under these circumstances a set

of $m$ relaxation equations of the type shown in Eq. (3.4) can be established. Accordingly $m$ relaxation times are determined. In a special relaxation process each will contribute its share to the overall effect in proportion to a corresponding amplitude. The ensemble of relaxation times and amplitudes is called the relaxation spectrum of the process under consideration. It reflects the underlying molecular rate mechanism. Thus , in principle, experimental relaxation spectrometry offers a means for elusidating kinetic mechanisms.

To relate the relaxation time $\tau$ to the rate of a reaction, let us consider a reaction

$$A + B \rightleftharpoons C. \tag{3.6}$$

The overall chemical conversion rate is,

$$\nu = dc_C/dt = k_1 c_A c_B - k_{-1} c_C = k_{-1}(K c_A c_B - c_C) \tag{3.7}$$

where $c_A, c_B$ and $c_C$ represent the concentrations for $A, B$ and $C$, respectively, $k_1$ and $k_{-1}$ are the rate constants for the forward and backward reactions and $K$ is the equilibrium constant of the reaction. According to the conservation of mass, the change in concentration must conform to the stoichiometry of the given reaction step. An appropriate concentration variable $x$ may be defined as the difference between $c_C$ and an optional reference value $c_C^0$. Accordingly, we have

$$c_C = c_C^0 + x; \quad c_A = c_A^0 - x; \quad c_B = c_B^0 - x \tag{3.8}$$

provided $c_A^0$, and $c_B^0$ are the corresponding reference concentrations of $A$ and $B$, respectively. Chemical turnover can therefore be described by the single variable $x$.

Employing Eq. (3.8), we find that the concentration variable $x$ is subject to the differential equation

$$\dot{x} = k_1(c_A^0 - x)(c_B^0 - x) - k_{-1}(c_C^0 + x). \tag{3.9}$$

This must be equal to zero if $x$ takes the value $\bar{x}$ corresponding to the instantaneous equilibrium condition. Accordingly, we can transform the rate expression to

$$\dot{x} = -[k_1(c_A^0 + c_B^0) + k_{-1}](x - \bar{x}) + k_1(x^2 - \bar{x}^2). \tag{3.10}$$

In general the instantaneous equilibrium could vary with $t$, too, due to changes in the temperature of the system. Then $k_1, k_{-1}$ and/or $\bar{x}$ may be a complicated function of $t$, giving rise to substantial mathematical difficulties when a solution of the differential equation (3.10) is attempted.

A quite general solution can be achieved, however, if the instantaneous equilibrium remains unaltered. In such a case the $k_1$, and $k_{-1}$ are independent of time and the equilibrium concentrations may be chosen for reference so that $\bar{x} = 0$. Under these circumstances $x = c_C - \bar{c}_C = -(c_A - \bar{c}_A) = -(c_B - \bar{c}_B)$. The above rate equation (3.10) now takes the simplified form

$$\dot{x} = k_1(x^2 - \bar{u}x) \Rightarrow \frac{dx}{x(\bar{u} - x)} = -k_1 dt \tag{3.11}$$

with $\bar{u} = \bar{c}_A + \bar{c}_B + K^{-1}$. Integration readily leads to

$$ln[(\bar{u} - x)/ \mid x \mid] = ln[(\bar{u} - x_0) \mid x \mid] + k_1 \bar{u} t \tag{3.12}$$

where $x_0$ is the initial value of $x$ at $t = 0$ (note that always $\bar{u} - x = c_A + c_B + K^{-1} > 0$). This can be rewritten as

$$x = \frac{\bar{u}}{(\bar{u} - x_0)exp(t/\tau) + x_0} x_0 \tag{3.13}$$

when a characteristic time constant $\tau$ is defined according to

$$1/\tau = k_1(\bar{c}_A + \bar{c}_B) + k_{-1}. \tag{3.14}$$

The situation proves to even simpler if the initial concentrations differ only slightly from their equilibrium values as expressed by an amount

$$\mid x_0 \mid \ll \bar{c}_A + \bar{c}_B \leq \bar{u}. \tag{3.15}$$

Then, in good appoximation it follows from Eq. (3.10) that

$$x = x_0 exp(-t/\tau) \tag{3.16}$$

that is, deviations from the equilibrium concentrations die away as a single exponential function of time. This reflects the typical behavior of a relaxation process.

In fact, the mathematical problems associated with the general equation (3.10) are largely eliminated if the actual concentrations and their equilibrium values deviate only slightly from some appropriate reference. We note that Eq. (3.10) can also be written as

$$\dot{x} = -[k_1(c_A + c_B) + k_{-1}](x - \bar{x}). \tag{3.17}$$

The possible time dependences of the quantities in the brackets are negligible, provided

$$x, \bar{x} \ll c_A^0 \approx c_A, \qquad c_B^0 \approx c_B.$$

Then, a (practically) constant relaxation time $\tau$ may be introduced by defining

$$1/\tau = k_1(c_A + c_B) + k_{-1} \tag{3.18}$$

Accordingly, the basic relaxation equation

$$\dot{x} = -(1/\tau)(x - \bar{x}) \tag{3.19}$$

is obtained . This applies to any perturbation function $\bar{x}(t)$ which is brought about by some modification of external forcing parameters (e.g., induced variations in temperature and/or pressure).

Let first assume that at $t = 0$, a slight step-wise change of a forcing parameter (for instance a pressure jump) is generated in an equilibrium system. The initial concentrations are to serve as the references. Therefore

$$\bar{x} = 0 \qquad \text{for} \qquad t < 0, \quad \bar{x} = \bar{x}_0 \neq 0 \qquad \text{for} \qquad t \geq 0$$

where the amplitude of the step $\bar{x}_0 = \partial\bar{x}$ is given as pointed out in the preceding section. In this case the relaxation Eq. (3.19) readily yields,

$$x = x_0[1 - exp(-t/\tau)] \qquad \text{at} \qquad t \geq 0. \tag{3.20}$$

The apparent difference in Eq. (3.20) relative to Eq. (3.18) only arises from the different choice of reference concentrations. Another convenient method of perturbing an existing equilibrium involves harmonic oscillations of the forcing parameters (viz., due to an ultrasonic wave). With the original equilibrium being the reference and an angular frequence $\omega$ one may then write,

$$\bar{x} = \bar{x}_0 cos(\omega t) \qquad \text{or} \qquad \bar{x} = \bar{x}_0 exp(i\omega t), \quad \text{respectively}$$

($i = \sqrt{-1}$) where $\bar{x}_0$ stands for the amplitude of the oscillations. An appropriate solution of the relaxation equation can more readily be obtained when the complex version of $\bar{x}$ is used. Reformulating Eq.(3.19) as

$$\tau \dot{x} + x = \bar{x}_0 esp(i\omega t)$$

and inserting $x = x_0 exp(i\omega t)$ immediately results in

$$x = \frac{\bar{x}_0}{1 + i\omega\tau} exp(i\omega t)$$

Its real part describes the actual oscillations of the concentration variable. One can find that

$$x = \frac{\bar{x}_0}{\sqrt{1 + \omega^2\tau^2}} cos(\omega t - \psi) \tag{3.21}$$

with $\psi = tan^{-1}(\omega\tau)$.

## 3.2 General Features of Relaxation Techniques

Relaxation methods can be classfied as either transient or stationary depending on the approaches that are employed to perturb the chemical systems (Bernasconi, 1976). The transient methods involve a single perturbation of a chemical system at equilibrium, brought about by a sudden change in an external parameter such as temperature, pressure or concentration. With the stationary techniques, the chemical system is subject to an oscillating forcing function or oscillating perturbation such as a sound wave which produces temperature and pressure fluctations in the solution, or an oscillating electrical field. Each individual method has its own advantages and disadvantages. Some of the basic features of the commonly used techniques are summarized in Table 3.1.

Table 3.1: Relaxation methods*

| Method | Time range (s) | Method of detection |
|---|---|---|
| A. Transient Methods | | |
| 1. Temperature jump | $1 - 10^{-6}(10^{-8})$ | spectrophotometric<br>fluorimentric |
| 2. Pressure jump | $10 - 5 \times 10^{-5}$(mechanical)<br>pressure release)<br>$5 \times 10^{-4} - 5 \times 10^{-7}$<br>(liquid shock wave) | conductometric<br>spectrophotometric |
| 3. Electrical field pulse | $10^{-4} - 10^{-8}$ | conductometric<br>spectrophotometric |
| 4. Concentration jump | $10^{8} - 10^{2}$(conventional)<br>$10^{3} - 10^{-3}$(stopped flow) | spectrophotometric<br>flurorimetric<br>and many others |
| B. Stationary methods | | |
| 5. Sound absorption and dispersion | $10^{-5} - 10^{-11}$(overall time range for different acoustical techniques) | power loss or<br>frequency change:<br>Resonance or<br>reverberation<br>($10^{4} - 10^{6}$Hz): light diffraction<br>($10^{6} - 10^{8}$Hz): impulse echo<br>($10^{6} - 5 \times 10^{8}$Hz);<br>Brillouin scattering |
| 6. Dielectric dispersion | $10^{-3} - 10^{-12}$ | power loss,<br>capacitance change |

* From Bernasconi (1976)

### 3.3 Pressure-Jump Apparatus with Conductivity Detection

The p-jump method is based on the fact that chemical equilibria display a more or less marked pressure dependence (Bernasconi, 1976). The dependence is given by the well-known thermodynamic relationship

$$\left(\frac{\partial ln K}{\partial p}\right)_T = -\frac{\Delta V^{\circ}}{RT} \tag{3.22}$$

where $\Delta V^{\circ}$ is the standard molar volume change of the reaction, $p$ is the pressure, $R$ is the gas constant and $T$ is the absolute temperature. A pressure perturbation results in the shifting of the equilibrium. The return of the system to the original equilibrium is related to the rates of all the elementary reaction steps. The determination of relaxation time may be used to describe the mechanism of a reaction. Analogous to Eq.(3.22), for a

small perturbation, one can write,

$$\frac{\Delta K}{K} = -\frac{\Delta V}{RT}\Delta p. \tag{3.23}$$

Fig. 3.1 shows the p-jump apparatus (DIA-RPC) used in this study. The main components include the autoclave, pressure pump, two cells and a vacuum pump. The pressure is built up by the pump with water as the pressure transmitter. The sample and reference cell are covered with a plastic membrane which effectively transmits the pressure. A piece of brass membrane is clamped on one wall of the autoclave with the bayonet socket. When the pressure in the autoclave gets high enough that the brass membrane cannot bear, the brass membrane bursts and the pressure in the autoclave returns to ambient pressure within 70$\mu$s. After the membrane bursts, the sample suspension having equilibrium at a higher pressure is out of equilibrium due to the 'instantaneous' pressure jump. The time required to approach equilibrium at the ambient pressure is then monitored by conductivity detection. The cell filled with the nonrelaxed background electrolyte (e.g., $NaNO_3$) solution is used as a reference which removes the effect of physics such as mechanical and temperature disturbances. Water was circulated in the autoclave to maintain a constant temperature at 298±0.1 K.

Since the equilibrium displacement following a p-jump is usually quite small, the very sensitive conductometric detection method was used in this study (Fig. 3.1). The specific conductivity, $\sigma$ (in S $m^{-1}$), of an electrolyte solution is given by

$$\sigma = \frac{F}{1000}\sum C_j|z_j|\mu_j = \frac{F}{1000}\rho\sum m_j|z_j|\mu_j \tag{3.24}$$

where $F$ is the Faraday constant, $z_j$ the valence of ion j, $C_j$ the molar and $m_j$ the molality concentrations of ion j, $\mu_j$ is the electrical mobility, and $\rho$ is the density of the solution. One can write an equation for a small perturbation as

$$\Delta\sigma = \frac{F}{1000}\left(\rho\sum z_j\mu_j\Delta m_j - \rho\sum|z_j|m_j\Delta\mu_j - \sum|z_j|m_j\mu_j\Delta\rho\right). \tag{3.25}$$

The first term on the right hand side of Eq. (3.25) corresponds to chemical relaxation. The other terms are "physical effects", i.e., the change in ionic mobility and density as a

consequence of pressure and temperature changes. However, problems caused by physical effects were eliminated by using a reference cell filled with a nonrelaxed solution (e.g., $NaNO_3$) which had the same temperature dependence on conductivity as the sample cell. The change in conductivity in this case corresponds only to the change in concentration of reactants or products. A Wheatstone bridge was set up to measure the change in conductivity in sample and reference cells which are the two arms of the bridge (Fig. 3.1). The bridge was operated at a frequency of 40 kHz which was greater than the $\tau^{-1}$ values that were measured.

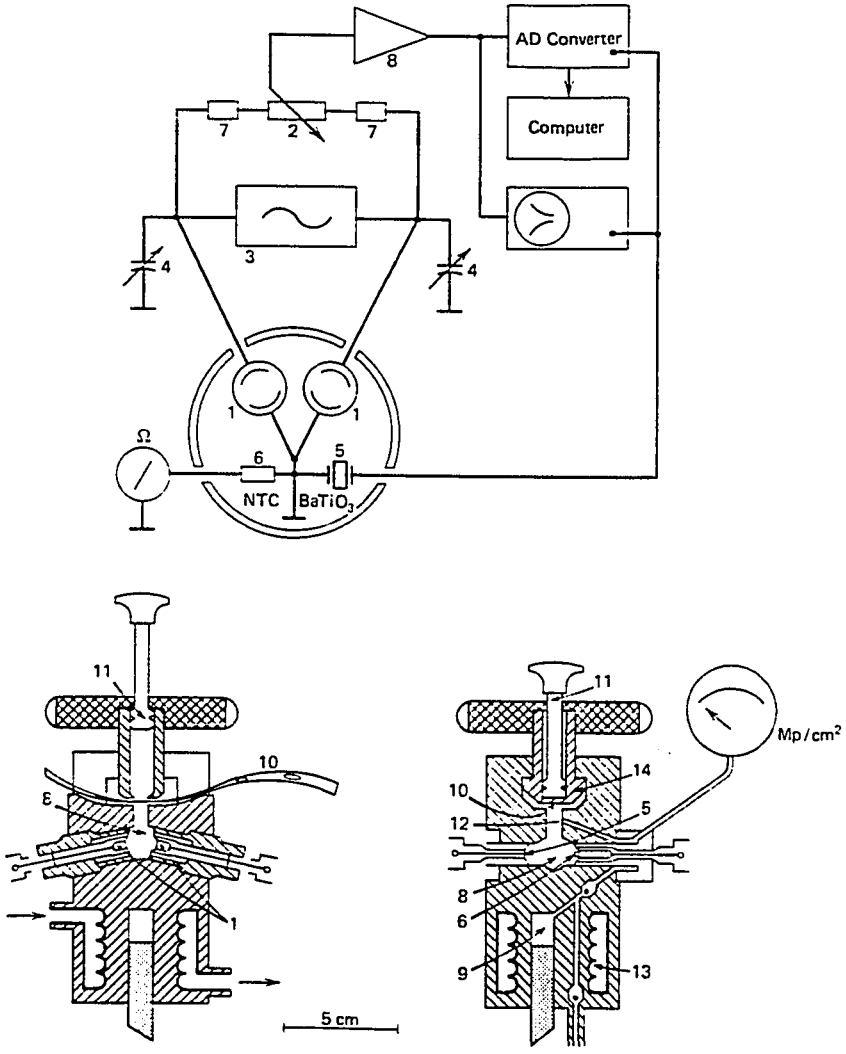


**Figure 3.1:** Schematic diagram and sectional views of the pressure–jump apparatus: 1, conductivity cells; 2, potentiometer; 3, 40-kHz generator for Wheatstone bridge; 4, tunable capacitors; 5, piezoelectric capacitor; 6, thermistor; 7, 10–turn helipot for turning bridge; 8, experimental chamber; 9, pressure pump; 10, rupture diaphragm; 11, vacuum pump; 12, pressure inlet; 13, heat exchanger; 14, bayonet socket. From Knoche and Wiese (1974), with permission.

# CHAPTER 4
# KINETICS AND MECHANISMS OF MOLYBDATE ADSORPTION/DESORPTION AT THE GOETHITE/WATER INTERFACE

## 4.1 Introduction

Molybdenum is an essential element for plant and animal life: however, excessive amounts can have deleterious effects on various organisms. Molybdenum largely occurs in the soil as an oxycomplex - $MoO_4^{2-}$ (Mengel and Kirkby, 1982). The adsorption of molybdate by soil colloids may be expected to have an important influence on its mobility and avilability to plants (Barrow, 1977).

It was widely known that the adsorption of molybdate in soils occurs through anion exchange, primarily with surface hydroxyl groups of soil minerals. The adsorption reaction is dependent on the pH and iron oxide concentration in the soil and is accompanied by an increase in pH upon the addition of molybdate solutions to soil suspensions (Barshad, 1951: Evans et al., 1951: Johns, 1957: Stout et al., 1951: Reisenauer et al., 1962: Reyes and Jurinak, 1967). Molybdate can be desorbed from soil by phosphate or sulfate (Stout et al., 1951: Barrow, 1973). Phosphates also reduce molybdate adsorption from solution, but sulfate has no effect. The effects with phosphate decrease with time, which shows that molybdate is more strongly adsorbed after initial adsorption (Parfitt, 1978).

The studies of adsorption of molybdate on oxides indicate that molybdate is adsorbed on goethite and gibbsite by a ligand exchange reaction (Hingston et al., 1972), which suggests that molybdate will react with exposed FeOH and AlOH groups. A stoichiometric release of two hydroxyl ions and one molecule of water by an adsorbed molybdate ion on $Fe_2O_3.xH_2O$ was observed by Reisenauer et al. (1961). Accordingly, the

formation of $Fe_2(MoO_4)_3$ or chemisorption of molybdate on complex iron water–hydroxyl solid phase materials might occur. This assumption was drawn from equilibrium studies and no reports were found in the literature on spectroscopic and kinetic studies.

The adsorption isotherms of molybdate by soils or soil minerals are usually of the L type (Giles et al., 1974). Adsorption has been described using the Bemmelen-Freundlich (Reisenauer et al., 1962; Jarrel and Dowson, 1978; Karimia and Cox, 1978) and Langmuir equations (Phelan and Mattigod, 1984). These equations suffer from the disadvantage that their parameters are unknown functions of both the pH and the ionic strength of the suspension containing the adsorbate (Motta and Miranda, 1989). The fact that good fits are frequently obtained with such equations is due to the insensitivity of the linear forms of these equations to adsorbate concentrations in suspension (Barrow, 1978; Bohn et al., 1979).

Mackenzie (1983) measured the adsorption of molybdate on 12 oxides with zpc (zero point of charg) ranging from pH 2 to 7.6. The four layer model (Bowden et al., 1980a,b) was used to successfully describe the data obtained from the molybdate–goethite system assuming specific adsorption of molybdate. Oxides with a low zpc, however, showed adsorption maxima below the the predicted value of pH 3.3. It was postulated that a positively charged polycationic form of molybdenum was adsorbed at low pH by oxides with low zpc (Mackenzie, 1983).

Motta and Miranda (1989) reported that the constant capacitance model (Stumm et al., 1980) was successfully applied to predicate the adsorption of molybdate on kaolinite, montomorillonite and illite. According to the assumptions of this model, the adsorbed ion should locate on the surface where potential determining ions such as protons are found.

Unfortunately, kinetic studies on molybdate adsorption on soils and soil minerals are scarce.

## 4.2 Materials and Methods

### 4.2.1 Sample Preparation

The goethite that was used in this study was synthesized according to the procedure described by Atkinson et al. (1967). After freeze–drying, it was examined by X–ray diffraction and the characteristic 0.418 nm peak for goethite was observed. The goethite was then placed in a dialysis tube and dialyzed in deionized water. The water was changed daily until the conductivity in the goethite suspension equaled that of the deionized water. The dialyzed goethite was then dispersed using an ultrasonic disperser. The particle size of the dispersed goethite was $< 2$ $\mu$m.

Specific surface area of the goethite which was determined using the EGME method of Carter et al. (1986), was $70.1 \times 10^3$ $m^2$ $kg^{-1}$. A potentiometric titration technique was employed to determine the surface site density of the goethite which was 6.4 site $nm^{-2}$ and the intrinsic constants for protonation ($K_{a1}^{int}$) and deprotonation ($K_{a2}^{int}$) and the intrinsic constants for background electrolyte reactions on the surfaces ($K_{NO_3}^{int}$ and $K_{Na}^{int}$) which are defined in Eqs. (4.1) to (4.4) were determined using the nonlinear least squares optimization program FITEQL (Westall, 1982). The constants used in this investigation are given in Table 4.1.

Sodium nitrate and $HNO_3$ were used to adjust the ionic strength and pH, respectively, of the oxide suspension. Sodium molybdate was the adsorptive. All the chemicals that were used were analytical reagents and no further purification was made.

### 4.2.2 Static Studies

The adsorption studies were carried out by placing a goethite suspension containing a $4.5x10^{-3}$mol $L^{-1}$ $Na_2MoO_4$ solution, and $NaNO_3$ as the background electrolyte, such that the concentration of $NaNO_3$ in the suspension was 0.01, 0.05, or 0.1 mol $L^{-1}$ , into polypropylene centrifuge tubes. The final particle concentration was 15.8 g $L^{-1}$. The tubes were shaken end–to–end on a reciprocating shaker overnight, centrifuged using a super speed centrifuge (Sorvall RC–5B, Du Pont Instrument) at 34550 g for 30 min., and

**Table 4.1:** Intrinsic equilibrium constants for the oxide suspension as determined from the modified TLM

| |
|---|
| $logK_{a1}^{int} = -5.80$ |
| $logK_{a2}^{int} = -11.1$ |
| $logK_{Na}^{int} = -8.80$ |
| $logK_{NO_3}^{int} = 7.6$ |

the supernatant solution was then filtered through 0.2 $\mu$m matric membrane filter paper. Molybdate and Na concentrations were determined using a Perkin–Elmer 5000 atomic absorption spectrophotometer, $NO_3$ was measured using ion chromatography, and the pH of the supernatant was determined.

### 4.2.3 Kinetic Studies

In the kinetic studies, relaxation times ($\tau$ values) were measured for the molybdate–oxide suspension at a 0.01 M ionic strength using a p–jump apparatus (DIA–RPC, produced by Dia–log Co., distributed by Inrad Interactive Radiation Inc., Northvale, NJ) and conductivity detector (DIA–RPM, Dia–log Co.). Before analyzing a given $MoO_4$–goethite suspension kinetically, part of the suspension was separated and analyzed for pH and $NO_3$, Na, and $MoO_4$ concentrations using the procedures given previously. During the p–jump relaxation measurement, 9.595 MPa of pressure was established on a cell containing the goethite and molybdate suspension; then the pressure was released within 70 $\mu$s by bursting a brass membrane of 0.03 mm thickness. A digitizer (DIA–RRC, Dia–log Co.) was then triggered and the changes in conductivity of the suspension were caught. The signals were digitized and then sent to a microcomputer(AIM 65, Rockwell International Co., Anaheim, CA). The results of the relaxation could be read from the computer print out and displayed on an oscilloscope. The p–jump relaxation and electrical conductivity detection devices are described in Chapter 3.

### 4.2.4 Application of Modified Triple Layer Model

A modified triple layer adsorption model (TLM)), which was used by Hayes and Leckie (1986) to study Pb adsorption on goethite, was employed in this study. The modified TLM differs from the original model (Davis and Leckie, 1980) in two ways: 1) the adsorbed ion can be located at both the $\alpha$ layer and $\beta$ layer rather than only at the $\beta$ layer, i.e., the adsorbed ion can form an inner- and/or outer-sphere surface complex, not just an outer-sphere complex: and 2) the chemical potential and standard and reference states are defined equivalently for both solution and surface species, leading to a different relationship between the activity coeffcients and the interfacial potential than previously used. Further details about the TLM and modifications to it can be found in Hayes and Leckie (1986, 1987).

The following chemical reactions can be defined for the application of the TLM to molybdate adsorption on goethite,

$$\mathrm{XOH_2^+ \rightleftharpoons XOH + H^+} \tag{4.1}$$

$$\mathrm{XOH \rightleftharpoons XO^- + H^+} \tag{4.2}$$

$$\mathrm{XOH_2^+ + NO_3^- \rightleftharpoons XOH_2^+ - NO_3^-} \tag{4.3}$$

$$\mathrm{XO^- + Na^+ \rightleftharpoons XO^- - Na^+} \tag{4.4}$$

$$\mathrm{XOH_2^+ + MoO_4^{2-} \rightleftharpoons XOH_2^+ - MoO_4^{2-}} \tag{4.5}$$

$$\mathrm{XOH_2^+ + HMoO_4^- \rightleftharpoons XOH_2^+ - HMoO_4^-} \tag{4.6}$$

where XOH represents one mol of reactive surface hydroxyls bound to a Fe ion in goethite. Equations (4.5) and (4.6) represent the formation of an outer-sphere surface complex in which molybdate ions are located at the $\beta$ layer. The intrinsic conditional equilibrium constants are defined using Eqs. (4.7)-(4.12):

$$K_{a1}^{int} = \frac{[\mathrm{XOH}][\mathrm{H^+}]}{[\mathrm{XOH_2^+}]} exp(-F\dot{\psi}_\alpha/RT) \tag{4.7}$$

$$K_{a2}^{int} = \frac{[\mathrm{XO^-}][\mathrm{H^+}]}{[\mathrm{XOH}]} exp(-F\psi_\alpha/RT) \tag{4.8}$$

$$K_{\mathrm{NO_3^-}}^{int} = \frac{[\mathrm{XOH_2^+ - NO_3^-}]}{[\mathrm{XOH_2^+}][\mathrm{NO_3^-}]} exp(-F\psi_\beta/RT) \tag{4.9}$$

$$K_{Na^+}^{int} = \frac{[\mathrm{XO^- - Na^+}]}{[\mathrm{XO^-}][\mathrm{Na^+}]} exp(F\psi_\beta/RT) \tag{4.10}$$

$$K_{\mathrm{MoO_4^{2-}}}^{int} = \frac{[\mathrm{XOH_2^+ - MoO_4^{2-}}]}{[\mathrm{XOH_2^+}][\mathrm{MoO_4^{2-}}]} exp(-2F\psi_\beta/RT) \tag{4.11}$$

$$K_{\mathrm{HMoO_4^-}}^{int} = \frac{[\mathrm{XOH_2^+ - HMoO_4^-}]}{[\mathrm{XOH_2^+}][\mathrm{HMoO_4^-}]} exp(-F\psi_\beta/RT) \tag{4.12}$$

where $F$ is the Faraday constant, $R$ is the universal gas constant and $T$ is the absolute temperature. Square brackets indicate concentration and the exponential terms represent the activity coefficients for a charged surface where $\psi_\alpha$ and $\psi_\beta$ are the electrical potentials at the $\alpha$ and $\beta$ layer, respectively.

The surface charge balance equations based on the above reactions are:

$$\sigma_\alpha = [\mathrm{XOH_2^+}] + [\mathrm{XOH_2^+ - NO_3^-}] + [\mathrm{XOH_2^+ - HMoO_4^-}] + [\mathrm{XOH_2^+ - MoO_4^{2-}}] - [\mathrm{XO^-}] - [\mathrm{XO^- - Na^+}] \tag{4.13}$$

$$\sigma_\beta = [\mathrm{XO^- - Na^+}] - [\mathrm{XOH_2^+ - HMoO_4^-}] - 2[\mathrm{XOH_2^+ - MoO_4^{2-}}] - [\mathrm{XOH_2^+ - NO_3^-}]. \tag{4.14}$$

From the electroneutrality condition,

$$\sigma_\alpha + \sigma_\beta + \sigma_d = 0 \tag{4.15}$$

where $\sigma_d$ is the charge at the diffusion layer; it can be calculated using Gouy–Chapman theory and the relationship,

$$\sigma_d = -11.74 C_s^{1/2} sinh(\frac{F\psi_d}{2RT}) \tag{4.16}$$

where $C_s$ is the concentration of a symmetrical monovalent electrolyte. The relation between charge and potential are derived assuming that the planes can be treated as plates of two parallel plate capacitors with

$$\sigma_\alpha = C_1(\psi_\alpha - \psi_\beta) \text{ and,} \tag{4.17}$$

$$-\sigma_d = C_2(\psi_\beta - \psi_d) \tag{4.18}$$

where $C_1$ and $C_2$ are the capacitance constants for the $\alpha$ and $\beta$ plane layers, respectively which cannot be measured experimentally. The values of $C_1$ and $C_2$ in this study are 1.2 and 0.2 F $m^{-2}$ respectively, and they were determined based on the goodness of fit to the TLM.

In the modified TLM, the molybdate ions are allowed to form an inner-sphere surface coordination complex by placement of the molybdate ions in the $\alpha$ layer such that,

$$XOH_2^+ + MoO_4^{2-} = SMoO_4^- + H_2O \tag{4.19}$$

$$XOH_2^+ + HMoO_4^- = SHMoO_4 + H_2O. \tag{4.20}$$

The charge balance for the reactions is then,

$$\sigma_\alpha = [XOH_2^+] + [XOH_2^+ - NO_3^-] - [SMoO_4^-] - [XO^-] - [XO^- - Na^+] \tag{4.21}$$

$$\sigma_\beta = [XO^- - Na^+] - [XOH_2^+ - NO_3^-]. \tag{4.22}$$

The intrinsic conditional constants for adsorption of molybdate ions in this case would be:

$$K^{int}_{MoO_4^{2-}} = \frac{[SMoO_4^-]}{[XOH_2^+][MoO_4^{2-}]} exp(-2F\psi_\alpha/RT) \tag{4.23}$$

$$K^{int}_{HMoO_4^-} = \frac{[SHMoO_4]}{[XOH_2^+][HMoO_4^-]} exp(-F\psi_\alpha/RT). \tag{4.24}$$

In the present study, parameters from both the computed results when the adsorbed molybdate ions are treated as an ion-pair (outer-sphere) surface complex or as a surface

coordination (inner-sphere) complex were used to model the reactions thermodynamically and kinetically. It should be mentioned that other equilibrium-based models were tested in this study; however, only the modified TLM fit the observed experimental data well.

## 4.3 Results and Discussion

### 4.3.1 Static Studies

Results of molybdate ($4.5 \times 10^{-3}$ mol $L^{-1}$) adsorption on goethite (15.8 g $L^{-1}$) as a function of pH in three different $NaNO_3$ background electrolyte concentrations (0.01, 0.05, and 0.1 mol $L^{-1}$) are shown in Fig. 4.1. There was a small effect of background electrolyte concentration on adsorption at a given pH. The modified TLM was used to model molybdate adsorption for both inner- (Fig. 4.1) and outer-sphere surface (Fig. 4.2) complexation at the three ionic strengths. For the inner-sphere case, the simulations agree quite well with the experimental data (Fig. 4.1). On the other hand, the observed data are not described well assuming that outer-sphere complexation is operational (Fig. 4.2). In both cases, the constants listed in Table 4.1 were used in the computations.

Hingston et al. (1972) reported that molybdate adsorption on goethite involves a ligand exchange process which they referred to as specific adsorption. The $NO_3$ anion, which was present in the background electrolyte solution ($NaNO_3$) that was used in this study, is adsorbed very weakly on colloidal surfaces through electrostatic attractive forces (Parfitt, 1978; Mott, 1981). This type of adsorption is termed nonspecific adsorption . The TLM applied in this chapter places ions adsorbed by electrostatic forces at the $\beta$ layer; thus, little or no competition occurs between the molybdate and $NO_3$ anions.

A previous assumption was that only one molybdate ion reacts with one protonated surface site. The goodness of fit of the experimental data to the modified TLM indicates that only one mol of ligand was replaced by one mol of adsorbed molybdate. Based on this, the stoichiometry of the overall molybdate adsorption on goethite can be established. Furthermore, while modeling molybdate adsorption, the speciation of molybdate ions was considered. In the pH range of 4-7 that was employed in this study, the molybdate

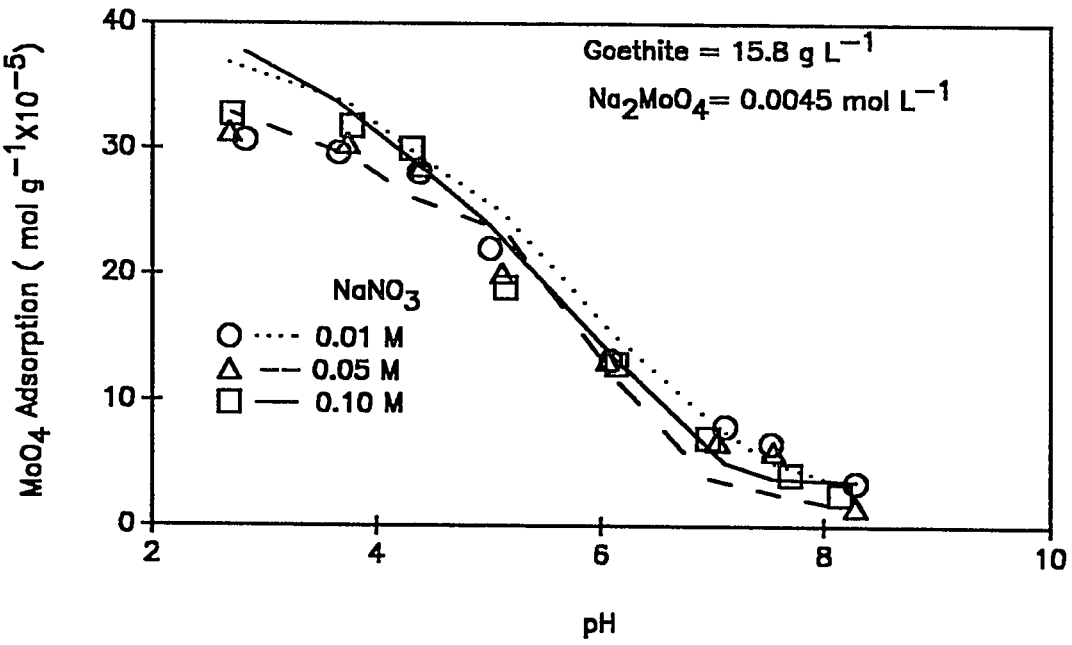


**Figure 4.1:** Adsorption of $MoO_4$ on goethite vs. pH at three $NaNO_3$ background electrolyte concentrations. Experimental data are applied to the modified TLM assuming inner–sphere surface complexation; symbols represent experimental data and lines represent TLM prediction.

ion can exist as two species, $HMoO_4^-$ and $MoO_4^{2-}$, with an association constant ($K_2$) of $10^{-4}$. However, the dominant form of the molybdate anion is $MoO_4^{2-}$ when the pH of the suspension is > 4. Based on the modeling of the data, it was found that the major fraction of the goethite–molybdate suspension is $SMoO_4^-$, with the $SHMoO_4$ species existing in a very trace amount (about $10^{-23} - 10^{-26}$ mol $L^{-1}$). Thus, this latter species can be ignored in this study.

Additionally, by using the modified TLM, we checked the form of the functional group that was directly reacting with molybdate. It was found that the molybdate anions reacted primarily with the protonated site, $XOH_2^+$ and not with the neutral one, XOH. For the reactions carried out over a pH range of 4–7, the goethite surface is positively charged since the pzc of the goethite is about 8.4. Neutral sites were used in the calculation, but the results obtained were not reasonable.

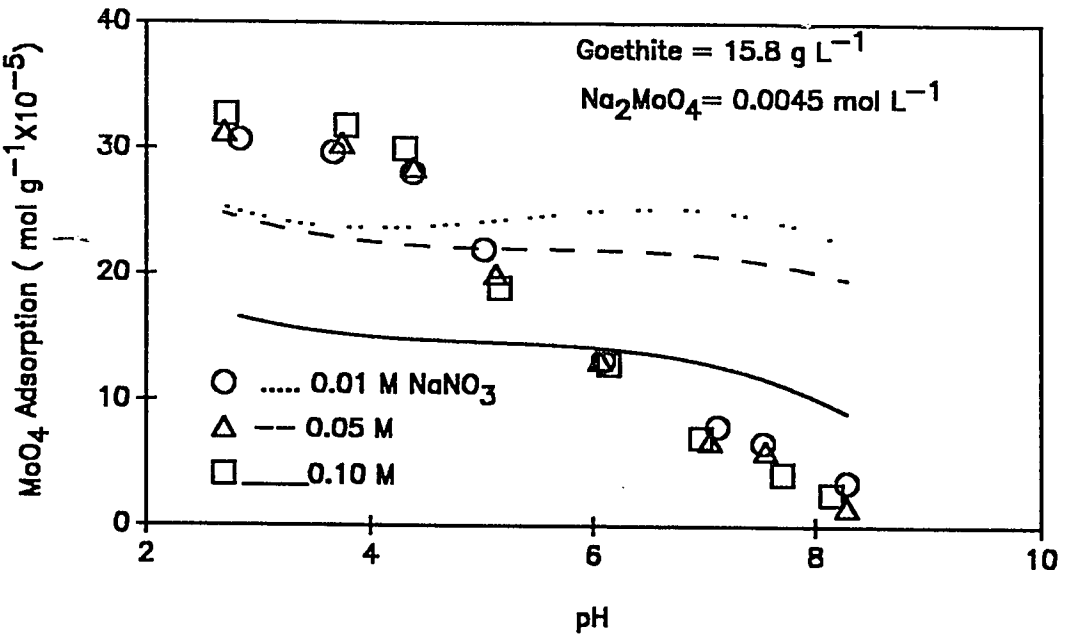


**Figure 4.2:** Adsorption of $MoO_4$ on goethite vs. pH at three $NaNO_3$ background electrolyte concentrations. Experimental data are applied to the modified TLM assuming outer-sphere surface complexation; symbols represent experimental data and lines represent TLM prediction.

### 4.3.2 Kinetic Studies

Kinetics of $MoO_4$ adsorption on goethite using the p-jump technique with electrical conductivity detection revealed a double relaxation (Fig. 4.3). The directions of both of the relaxation signals indicate a decrease in conductivity of the suspension during the relaxation. Relaxations were not obtained when a goethite-$NaNO_3$ suspension, the supernatant solution of a goethite-molybdate suspension and only a goethite suspension were examined using p-jump relaxation. However, the concentration of molybdate in suspension significantly decreased after it was equilibrated with goethite. These findings indicate that the relaxations were caused by adsorption/desorption of molybdate at the goethite/water interface.

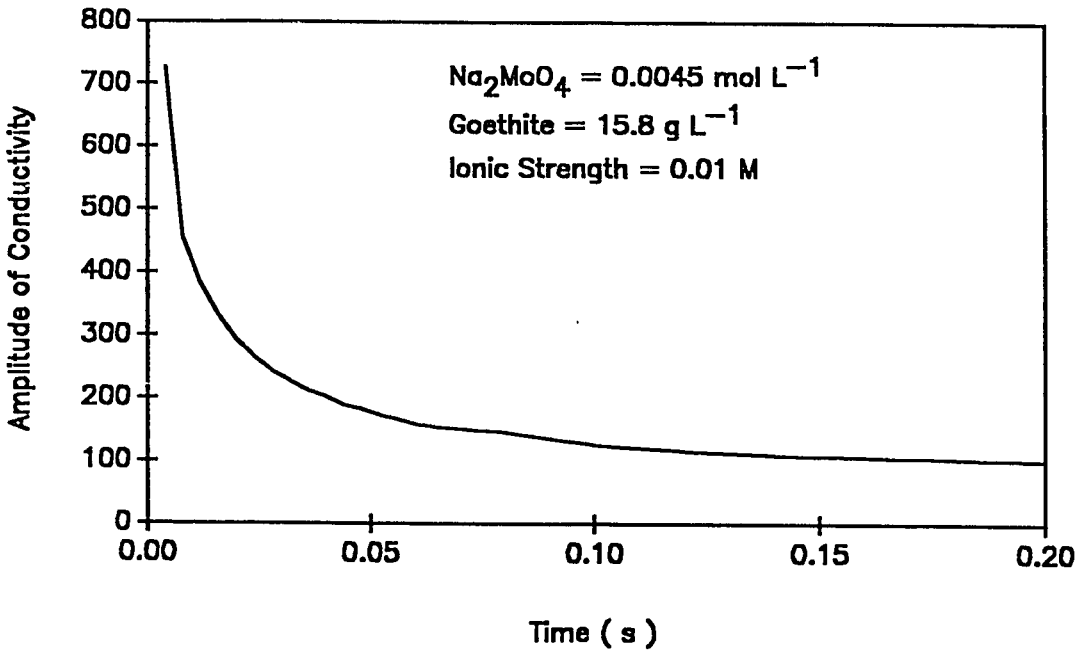


**Figure 4.3:** Typical pressure–jump relaxation curve showing change in conductivity vs. time for the goethite suspension.

Determination of reciprocal relaxation time constants ($\tau_1^{-1}$ and $\tau_2^{-1}$) were made from semi–log plots of the relaxation curves as shown in Fig. 4.4. A fast reciprocal relaxation time, $\tau_1^{-1}$, can be separated from a slow one, $\tau_2^{-1}$, based on the significantly different rates of conductivity change as a function of time. Both $\tau_1^{-1}$ and $\tau_2^{-1}$ increased with increases in pH of the goethite suspensions (Fig. 4.5).

The double relaxation curve that was observed (Fig. 4.3) following pressure perturbation would indicate that two reactions are operational. Combining the information from the p–jump relaxation studies and from the overall equilibrium partitioning and the reaction stoichiometry, a two step reaction is postulated to describe the mechanism of molybdate adsorption on goethite:

$$\underset{\text{step 1}}{XOH_2^+ + MoO_4^{2-} = XOH_2^+ - MoO_4^{2-}} \underset{\text{step 2}}{= SMoO_4^- + H_2O.} \qquad (4.25)$$

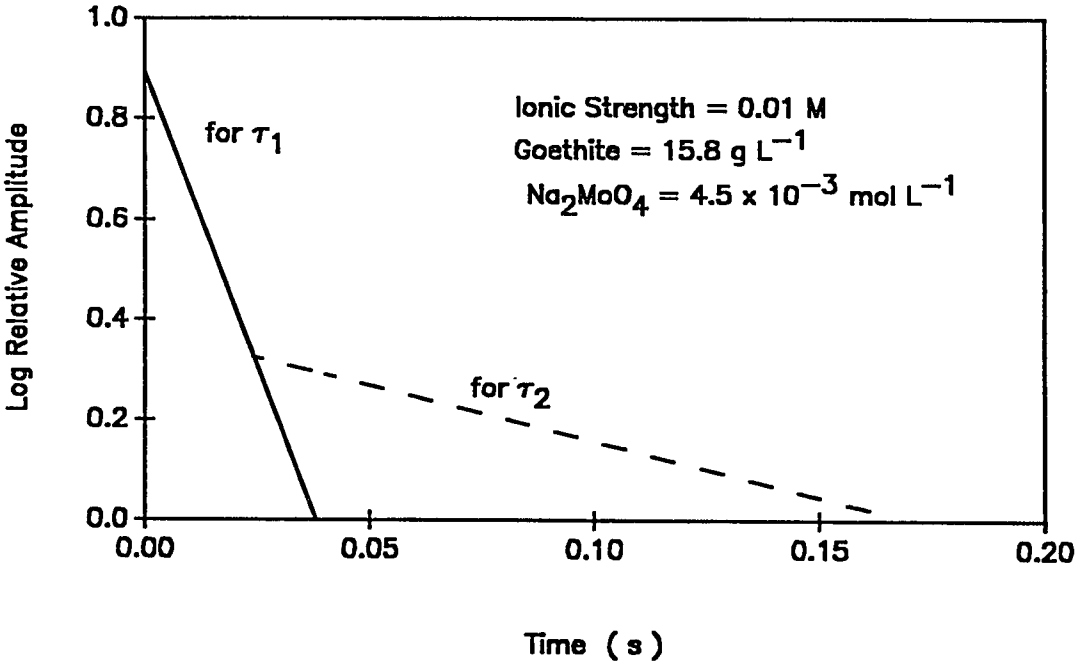


**Figure 4.4:** Semi-log relaxation curves for the goethite suspension.

In the first step, $MoO_4$ is attracted to the $\beta$ layer by electrostatic interaction, and forms an ion-pair complex with a protonated surface site. Then, through the second step, $MoO_4$ replaces a ligand from the surface site to form an inner-sphere surface complex at the $\alpha$ layer . The $MoO_4$ now occupies the position of the replaced ligand, in this case, the $H_2O$ molecule. The second step in Eq. (4.25) includes processes of bond breaking and bond formation. The intrinsic equilibrium constants $K_1^{int}$ and $K_2^{int}$ for step 1 and step 2, respectively, are defined as,

$$K_1^{int} = \frac{[XOH_2^- - MoO_4^{2-}]}{[XOH_2^+][MoO_4^{2-}]} exp(\frac{-2F\psi_\beta}{RT}) \tag{4.26}$$

$$K_1^{int} = \frac{k_1^{int}}{k_{-1}^{int}} = K_1 exp(\frac{-2F\psi_\beta}{RT}) \tag{4.27}$$

$$K_2^{int} = \frac{[SMoO_4^-]}{[XOH_2^- - MoO_4^{2-}]} exp(\frac{-2F(\psi_\alpha - \psi_\beta)}{RT}) \tag{4.28}$$

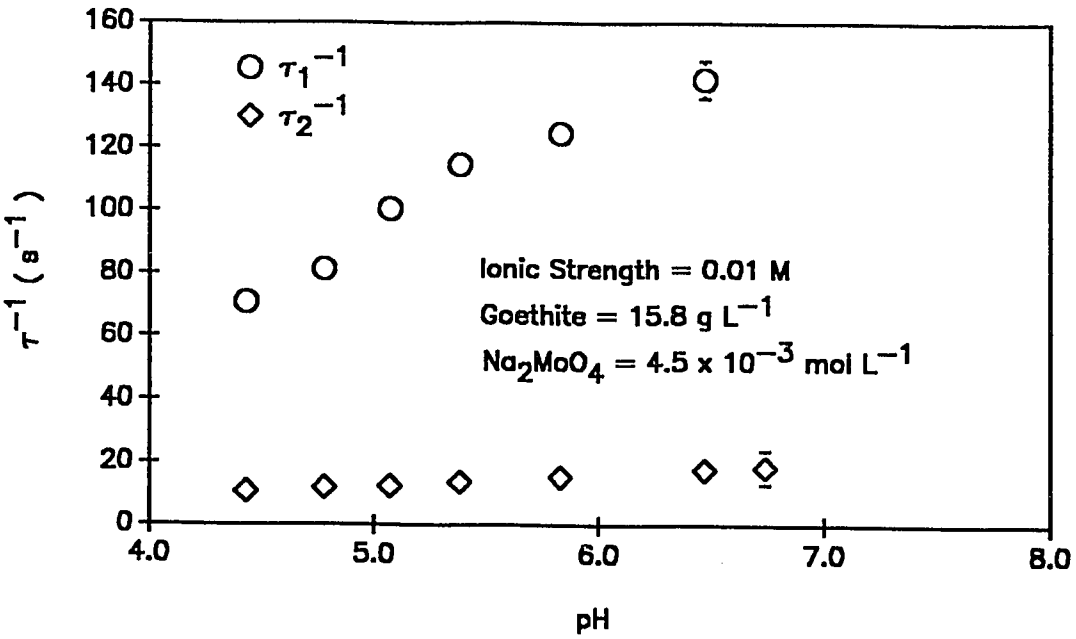


**Figure 4.5:** Relationship between pH and fast ($\tau_1^{-1}$) and slow ($\tau_2^{-1}$) reciprocal relaxation times for step two of the reaction given in Eq. (4.25).

$$K_2^{int} = \frac{k_2^{int}}{k_{-2}^{int}} = K_2 exp(\frac{-2F(\psi_\alpha - \psi_\beta)}{RT}) \tag{4.29}$$

where the $k_1^{int}, k_{-1}^{int}, k_2^{int}$ and $k_{-2}^{int}$ are the intrinsic foward ($k_1^{int}$ and $k_2^{int}$) and backward ($k_{-1}^{int}$ and $k_{-2}^{int}$) rate constants for steps 1 and 2 in Eq. (4.25). The electrical potential term used to describe step 1 is associated with the $\beta$ layer, and that used to describe step 2 is associated with the $\alpha$ layer. The reason for this is that the two steps create different effects at the two layers.

Using the kinetic model described in Eq. (4.25) and the stoichiometry of the overall reactions, i.e., one molybdate ion replaces one ligand from the protonated surface, the following relationships between $\tau_1^{-1}, \tau_2^{-1}$ and the reactant concentrations can be derived (see Appendix A for details):

$$\tau_1^{-1} = k_1^{int}\{exp(\frac{F\psi_\beta}{RT})([XOH_2^+] + [MoO_4^{2-}])\} + k_{-1}^{int} exp(\frac{-F\psi_\beta}{RT}) \tag{4.30}$$

$$\tau_2^{-1} = k_2^{int}\Big\{exp(\frac{F(\psi_\alpha - \psi_\beta)}{RT})\frac{k_1^{int}exp(\frac{F\psi_\beta}{RT})([XOH_2^+] + [MoO_4^{2-}])}{k_1^{int}exp(\frac{\psi_\beta}{RT})([XOH_2^+] + [MoO_4^{2-}]) + k_{-1}^{int}exp(\frac{-F\psi_\beta}{RT})}\Big\}$$
$$+ k_{-2}^{int}exp(\frac{-F(\psi_\alpha - \psi_\beta)}{RT}). \tag{4.31}$$

Rearranging Eqs. (4.30) and (4.31),

$$\tau_1^{-1}exp(\frac{F\psi_\beta}{RT}) = k_1^{int}\{exp(\frac{2F\psi_\beta}{RT})([XOH_2^+] + [MoO_4^{2-}])\} + k_{-1}^{int}$$
$$= k_1^{int}F_1 + k_{-1}^{int} \tag{4.32}$$

$$\tau_2^{-1}exp(\frac{F(\psi_\alpha - \psi_\beta)}{RT}) = k_2^{int}\Big\{exp(\frac{2F(\psi_\alpha - \psi_\beta)}{RT})$$
$$\frac{k_1^{int}exp(\frac{F\psi_\beta}{RT})([XOH_2^+] + [MoO_4^{2-}])}{k_1^{int}exp(\frac{F\psi_\beta}{RT})([XOH_2^+] + [MoO_4^{2-}]) + k_{-1}^{int}exp(\frac{-F\psi_\beta}{RT})}\Big\} + k_{-2}^{int}$$
$$= k_2^{int}F_2 + k_{-2}^{int}. \tag{4.33}$$

If the mechanism proposed in Eq. (4.25) is consistent with the experimental relaxation data, then plots of $\tau_1^{-1}$ and $\tau_2^{-1}$ with the exponential terms on the left hand side of Eqs. (4.32) and (4.33) versus the concentration terms ($F_1$ and $F_2$) on the right hand sides of Eqs. (4.32) and (4.33) will generate two straight lines, and the slopes and intercepts will give the forward and backward intrinsic rate constants ($k_1^{int}$, $k_{-1}^{int}$, $k_2^{int}$ and $k_{-2}^{int}$), respectively, for the two steps. As shown in Figs. (4.6) and (4.7), two linear relationships are obtained from the plots. Thus, intrinsic rate constants and equilibrium constants for the two steps can be calculated from the two linear relationships and these are listed in Table 4.2. One can see that step 1 has the highest forward rate constant ($k_1^{int}$), which is about 10 times higher than its backward rate constant ($k_{-1}^{int}$). Contrastingly, the backward rate constant for step 2 ($k_{-2}^{int}$) is much higher than the forward rate constant ($k_2^{int}$).

The rate constants describe the reaction process postulated earlier. Firstly, the $MoO_4$ anion which has already diffused close to the goethite surface is attracted to the surface because of the protonated and positively charged surface site; an ion-pair complex is thus formed very rapidly. Secondly, the $MoO_4$ anion reaches the oxide surface to break the bond between Fe and the hydroxyls, and the $H_2O$ molecule is released to the bulk

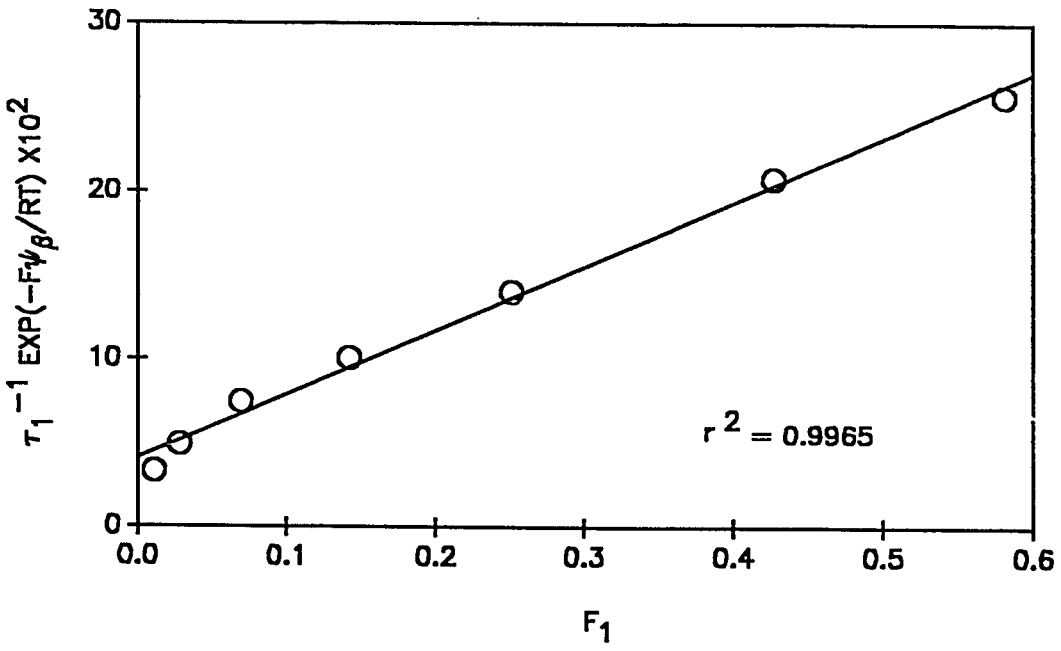


**Figure 4.6:** Plot of $\tau_1^{-1} exp(\frac{F\psi_\beta}{RT})$ vs. $F_1$ in Eq. (4.32) to test the mechanism for step 1 as proposed in Eq. (4.25).

solution. Over time, a new bond is established between $MoO_4$ and Fe at the oxide surface. The latter ligand exchange process (step 2) is slow compared to step 1. Accordingly, step 2 in Eq. (4.25) is the rate-controlling step in the reaction between $MoO_4$ and goethite.

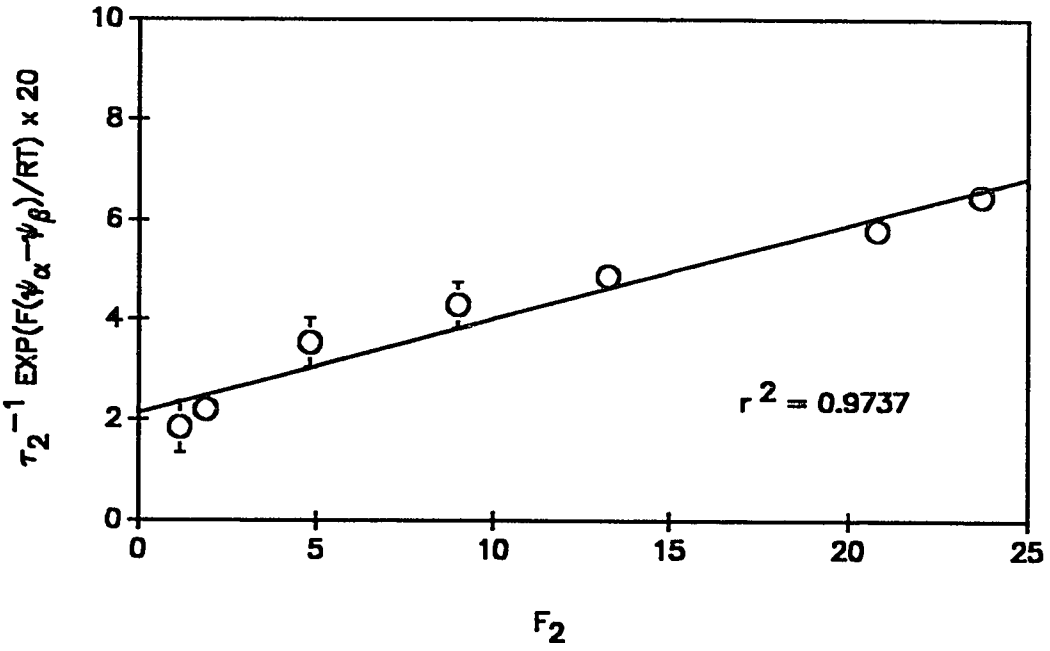


**Figure 4.7:** Plot of $\tau_2^{-1} exp(\frac{F(\psi_\alpha - \psi_\beta)}{RT})$ vs. $F_2$ in Eq. (4.33) to test the mechanism for step 2 as proposed in Eq. (4.25).

**Table 4.2:** Intrinsic rate and equilibrium constants determined from kinetic measurements

| $k_1^{int}$ | $k_{-1}^{int}$ | $k_2^{int}$ | $k_{-2}^{int}$ | $K_1^{int}$ | $K_2^{int}$ |
|---|---|---|---|---|---|
| $mol^{-1}Ls^{-1}$ | $s^{-1}$ | $mol^{-1}Ls^{-1}$ | $s^{-1}$ | $mol^{-1}L$ | $mol^{-1}L$ |
| 4019.2 | 391.5 | 1.89 | 42.34 | 10.28 | 0.045 |

# CHAPTER 5
# KINETICS AND MECHANISMS OF SULFATE ADSORPTION/DESORPTION ON GOETHITE

## 5.1 Introduction

Adsorption of $SO_4^{2-}$ on soils and soil constituents has been extensively studied particularly as it affects various aspects of plant nutrition, soil acidity, soil salinity and water quality. Many soils retain $SO_4^{2-}$, particularly those with high contents of Al- and Fe-oxides (Freney et al., 1962; Harward and Reisenauer, 1966). Hingston et al. (1972) showed that $SO_4^{2-}$ adsorption on goethite and gibbsite decreased with an increase in pH up to 8, beyond which no further adsorption occurred. Similar results were found with soils (Harward and Reisenauer, 1966; Scott, 1976). Marsh et al. (1987) investigated the relationship between soil surface charge and $SO_4^{2-}$ adsorption and found that a direct and very close relationship existed between surface positive charge and $SO_4^{2-}$ adsorption. When postive surface charge was low, little or no $SO_4^{2-}$ was sorbed by soils where the background electrolyte was NaCl or $CaCl_2$.

Sulfate leaching in soils has been reported by a number of investigators, and is more extensive in soils that are low in Al- and Fe-oxides, particularly in the A horizons (Parfitt, 1978). Swoboda and Thomas (1965) found that $SO_4^{2-}$ leaching occurred even in highly weathered soils that contained large amounts of Fe-oxides, particularly if large volumes of water were applied to the soils. Sulfate leaching also can occur if positive sites on soils and soil constituents are blocked by organic ligands (for example, in highly organic soils), in part due to $SO_4^{2-}$ having a lower binding constant than polycarboxylic acids (Haque and Walmsley, 1974). Thus, Gillman (1974) found more phosphate-extractable $SO_4^{2-}$ in lower horizons where the pzc was higher and where there were more positive sites.

One of the possible mechanisms for $SO_4^{2-}$ adsorption on soils and soil constituents is ligand exchange whereby $SO_4^{2-}$ replaces $H_2O$ and/or OH groups from $XOH_2$ and XOH sites, where $XOH_2$ and XOH represent protonated and nonprotonated surface sites, respectively (Parfitt, 1978). Bornemesza and Llanos (1967) have also shown that OH ions are released during $SO_4^{2-}$ adsorption. Parfitt and Russell (1977), Parfitt and Smart (1977) and Rajan (1978) showed that $SO_4^{2-}$ is adsorbed by forming binuclear bridged complexes on Al– and Fe–oxides. Further evidence to support this mechanism was found by Martin and Smart (1987) who used X-ray photoelectron spectroscopy (XPS) to study $SO_4^{2-}$ adsorption. Their results are consistent with those observed from infrared spectroscopy (IRS) studies by Parfitt and Smart (1977) who showed that an adsorbed $SO_4^{2-}$ ion replaces two A-type OH groups (singly coordinated to $Fe^{3-}$ ions) on (100) and (010) goethite surface sites.

However, Hansmann and Anderson (1985) developed a relationship for net adsorption energy ($E_{net}$) that is equal to the sum of an intrinsic energy term ($E_{int}$) and an electrostatic term ($E_{elect}$). They showed that the $E_{int}$ for $SO_4^{2-}$ adsorption on goethite was low, and that the electrostatic energy term predominated. They also showed that electrostatic repulsion cannot decrease the amount adsorbed in any meaningful sense. Therefore, $SO_4^{2-}$ should only be bound at low pH values, and free energy data are difficult to obtain above pH 6 because the concentration of adsorptive sites becomes exceedingly small. The adsorption behavior of $SO_4^{2-}$ is different from phosphates and from $SeO_3$ which are generally assumed to be adsorbed on oxides by ligand exchange.

Ryden et al. (1987) reported that $SO_4^{2-}$ did not have a detectable effect on $PO_4$ adsorption on hydrous ferric oxide gel, but other anions such as $AsO_3$, $SeO_3$, $SiO_3$ and $MoO_4$ decreased $PO_4$ adsorption. Yates and Healy (1975) found that the rate and extent of $SO_4^{2-}$ adsorption on ferric and chromic oxide/water interfaces were different from $PO_4$, but similar to $NO_3$, and concluded that $SO_4^{2-}$ adsorption did not occur by a ligand exchange process. However, the PZSE (point of zero salt effect) is shifted upward in a $SO_4^{2-}$ background solution. These results illustrate, as Sposito (1984) pointed out, the "intermediate" surface complexation behavior of $SO_4^{2-}$. Arnold (1978) has reported that adsorption of $SO_4^{2-}$ on a tropical soil resulted in an increase in the pzc of the soil. This

would indicate that $SO_4^{2-}$ is not located in the inner Helmholtz plane and so is not adsorbed by a ligand exchange phenomenon. However, $SO_4^{2-}$ is more strongly attracted to the surface than, say, Cl under similar experimental conditions (Mott, 1981). Marsh et al. (1987) noted that the adsorption of $SO_4^{2-}$ is not entirely nonspecific for there is a strong selectivity of $SO_4^{2-}$ over Cl. However, they considered that electrostatic forces predominated for $SO_4^{2-}$/solid interactions.

Thus, the mechanism(s) of sulfate adsorption on soils and soil constituents is not definitively understood. It is clear that macroscopic equilibrium studies are not suitable for determining adsorption mechanism(s) . Spectroscopic studies provide direct information about adsorption mechanisms. However, previous $SO_4^{2-}$ adsorption studies employing spectroscopic techniques such as XPS and IRS are not appropriate since the samples must first be subjected to desiccation and high vacuum techniques. Johnston and Sposito (1987) have noted that harsh sampling techniques often eliminate or inreversibly alter the surface species of interest. Molecular level information gleaned about the mechanisms, orientation, and dynamics of adsorbed species that is obtained from experiments involving dessication and high vaccum treatments may not be relevant to systems in a hydrated environment.

Few reports appear in the literature on the kinetics of $SO_4^{2-}$ adsorption on soils and soil constituents (Sparks, 1989). Chang and Thomas (1963) studied $SO_4^{2-}$ adsorption kinetics on soils and minerals on a time scale of weeks. They suggested that the mechanism for $SO_4^{2-}$ adsorption was ligand exchange. Rajan (1978) measured the rate of $SO_4^{2-}$ adsorption on an Al-oxide and the rate and amount of OH groups being released. He found that 90% of the reaction was complete in 10 min. Zhang et al. (1987) also studied $SO_4^{2-}$ adsorption on soils using the same procedure as Rajan (1978) and they found a smaller ratio of $OH^-/SO_4^{2-}$ as compared to that observed by Rajan (1978) for oxides. Zhang et al. (1987) also found that the amount of OH released to the aqueous solution was much lower when $SO_4^{2-}$ was adsorbed than when F was adsorbed. They concluded that the mechanism for $SO_4^{2-}$ adsorption on soils is different than that on oxides.

Hodges and Johnson (1987) studied the kinetics of $SO_4^{2-}$ adsorption and desorption on a Cecil soil using miscible displacement and rapidly stirred batch procedures. They

fitted data to a number of kinetic models to hypothesize the possible mechanism and the rate–controlling steps for the adsorption/desorption process. The rate coefficients were affected by the degree of mixing and by flow rate which led Hodges and Johnson (1987) to conclude that diffusion was the overall rate–limiting step. However, the authors concluded that the mechanism of $SO_4^{2-}$ adsorption was not clear.

It would appear that lack of a suitable technique to measure the rate of $SO_4^{2-}$ adsorption/desorption may be a major obstacle in understanding the mechanism of $SO_4$ retention on soils and soil constituents. Accordingly, in this study a pressure jump (p–jump) relaxation technique was used to determine the kinetics of $SO_4^{2-}$ adsorption/desorption at the goethite/water interface. This technique, which can make measurements at millisecond and microsecond time scales, was previously used to ascertain the kinetics and mechanisms of molybdate adsorption/desorption on goethite in Chapter 4. Results from both thermodynamic and kinetic studies were used to ascertain the mechanism(s) for $SO_4^{2-}$ adsorption/desorption.

## 5.2 Materials and Methods

### 5.2.1 Sample Preparation

The goethite used in the study was synthesized in our laboratory following the procedure described by Atkinson et al. (1967). The freeze–dried sample was examined by X–ray diffraction and the characteristic 0.418 nm peak for goethite was observed. The goethite then was dialyzed in dialysis tubing until the conductivity of the suspension equaled that of deionized water. The particle size was $< 2\mu$m after dispersion with an ultrasonic disperser.

The specific surface area of the goethite which was measured using the ethylene glycol monoethyl ether adsorption method (Carter et al., 1986) was $70.1 \times 10^3 m^2 kg^{-1}$. A potentiometric titration technique was employed to determine the surface site density of the goethite which was 6.4 site $nm^{-2}$. The intrinsic constants for protonation ($K_{a1}^{int}$) and deprotonation ($K_{a2}^{int}$) and the intrinsic constants for background electrolyte reactions on

the surface ($K_{Na}^{int}$) and ($K_{NO_3}^{int}$), which are defined in Eq.(5.1) to (5.4), were determined using the nonlinear least squares optimization program FITEQL (Westall, 1982). The constants used in this investigation are given in Table 5.1.

Sodium nitrate and $HNO_3$ were used to adjust the ionic strength and pH, respectively, of the goethite suspension. Sodium sulfate was the adsorptive. All chemicals that were used were analytical reagent grade and no further purification was made.

### 5.2.2 Static Studies

The adsorption study was carried out by placing a goethite suspension containing a 2 x $10^{-3}$ mol $L^{-1}$ $Na_2SO_4$ solution, and $NaNO_3$ as the background electrolyte, into polypropylene centrifuge tubes. The final goethite particle concentration was 11.58 g $L^{-1}$ and the ionic strength was 0.01 M. The tubes were shaken end-to-end on a reciprocating shaker overnight, centrifuged using a super-speed centrifuger (Sorvall RC-5B, Du Pont Instrument) at 34550 $\times$g for 30 min., and the supernatant solution was then filtered through 0.2-$\mu$m matric membrane filter paper. Sulfate concentration was determined using ion chromatography, and the pH of the supernatant was measured.

### 5.2.3 Kinetic Studies

In the kinetic studies, relaxation times ($\tau$ values) were measured for the sulfate-goethite suspension at a 0.01 $M$ ionic strength using a Dia-Log p-jump apparatus (Dia-RPC, Dia-Log Co.) and conductivity detector (Dia-RPM, Dig-Log Co.). During the p-jump relaxation measurement, 13.5 MPa of pressure was established on a cell containing the goethite and sulfate suspension; then the pressure was released within 70 $\mu$s by bursting a brass membrane of 0.05-mm thickness. The reaction system was perturbated and a new equilibrium was established. The time required to reach the new equilibrium from the sudden pressure release is related to the relaxation time ($\tau$). In this study, the change in the reaction system was recorded as the change in conductivity which reflected the concentration change in the reaction system during relaxation (Zhang, Sparks, 1989) A digitizer (DIA-RRC, Dia-log Co.) was then triggered and the relative changes in

conductivity between the suspension and the reference solution were recorded. The signals were then converted and transferred to a microcomputer for analysis. The final results of the relaxation could be read from the computer print out and displayed on an oscilloscope. The p-jump apparatus and the electrical conductivity detector were described previously in Chapter 4.

### 5.2.4 Application of Surface Complexation Models

The constant capacitance and modified triple layer models were used to describe $SO_4$ adsorption on goethite. The constant capacitance model assumes that all adsorbed ions form inner-sphere complexes (Sposito, 1984). It has been successfully used to describe the adsorption of arsenate, borates, and phosphates on oxides and soils (Goldberg, 1986; Goldberg and Glaubig, 1986; Goldberg and Sposito, 1984a,b). In this study, the constant capacitance model did not successfully describe $SO_4$ adsorption on goethite.

The triple layer model (TLM) assumes that all adsorbed ions, except for H and OH, stay in the *3* plane and are adsorbed as outer-sphere complexes (Sposito, 1984). The following chemical reactions can be defined for the application of the TLM to $SO_4$ adsorption on goethite using the experimental conditions given earlier:

$$XOH_2^+ = XOH + H^+ \tag{5.1}$$

$$XOH = XO^- + H^+ \tag{5.2}$$

$$XOH_2^+ - NO_3^- = XOH_2^+ - NO_3^- \tag{5.3}$$

$$XO^- - Na^+ = XO^- - Na^+ \tag{5.4}$$

$$XOH_2^+ - SO_4^{2-} = XOH_2^+ - SO_4^{2-} \tag{5.5}$$

where XOH represents 1 mol of reactive surface hydroxyl bound to a Fe ion in goethite. Equation (5.5) is the formation of an outer-sphere surface complex in which $SO_4$ ions are located at the *3* plane. The intrinsic conditional equilibrium constants for the previous

reactions can be defined using Eq. (5.6) to (5.10):

$$K_{a1}^{int} = \frac{[XOH][H^+]}{[XOH_2^+]} exp(-F\psi_\alpha/RT) \tag{5.6}$$

$$K_{a2}^{int} = \frac{[XO^-][H^+]}{[XOH]} exp(-F\psi_\alpha/RT) \tag{5.7}$$

$$K_{NO_3^-}^{int} = \frac{[XOH_2^+ - NO_3^-]}{[XOH_2^+][NO_3^-]} exp(-F\psi_\beta/RT) \tag{5.8}$$

$$K_{Na^+}^{int} = \frac{[XO^- - Na^+]}{[XO^-][Na^+]} exp(F\psi_\beta/RT) \tag{5.9}$$

$$K^{int} = \frac{[XOH_2^+ - SO_4^{2-}]}{[XOH_2^+][SO_4^{2-}]} exp(-2F\psi_\beta/RT) \tag{5.10}$$

where $F$ is the Faraday constant, $R$ is the universal gas constant and $T$ is the absolute temperature. Square brackets indicate concentration and the exponential terms represent the activity coefficients for a charged surface where $\psi_\alpha$ and $\psi_\beta$ are the electrical potentials at the $\alpha$ and $\beta$ layer, respectively. The intrinsic constants of Eqs. (5.6) to (5.9) were determined by potentiometric titration and are presented in Table (5.1).

**Table 5.1:** Intrinsic equilibrium constants for the oxide suspension as determined from the modified TLM

| |
|---|
| $logK_{a1}^{int} = -5.80$ |
| $logK_{a2}^{int} = -11.1$ |
| $logK_{Na}^{int} = -8.80$ |
| $logK_{NO_3}^{int} = 7.6$ |
| $C_1 = 1.2$ |
| $C_2 = 0.2$ |

The surface charge balance equations based on the above reactions are:

$$\sigma_\alpha = [XOH_2^+] + [XOH_2^+ - NO_3^-] + [XOH_2^+ - SO_4^{2-}]$$

$$- [XO^-] - [XO^- - Na^+] \tag{5.11}$$

$$\sigma_\beta = [XO^- - Na^+] - 2[XOH_2^+ - SO_4^{2-}] - [XOH_2^+ - NO_3^-]. \tag{5.12}$$

From the electroneutrality condition,

$$\sigma_\alpha + \sigma_\beta + \sigma_d = 0 \tag{5.13}$$

where $\sigma_d$ is the charge at the diffusion layer; it can be calculated using Gouy–Chapman theory and the relationship,

$$\sigma_d = -11.74 C_s^{1/2} sinh(\frac{F\psi_d}{2RT}) \tag{5.14}$$

where $C_s$ is the concentration of a symmetrical monovalent electrolyte. The relation between charge and potential are derived assuming that the planes can be treated as plates of two parallel plate capacitors with

$$\sigma_\alpha = C_1(\psi_\alpha - \psi_\beta) \tag{5.15}$$

$$-\sigma_d = C_2(\psi_\beta - \psi_d) \tag{5.16}$$

where $C_1$ and $C_2$ are the capacitance constants for the $\alpha$ and $\beta$ plane layers, respectively, which cannot be measured experimentally. The values of $C_1$ and $C_2$ in this study are 1.2 and 0.2 F $m^{-2}$ respectively, and they were determined based on the goodness of the data fit to the TLM.

The TLM used in this study is modified from the original. A theoretical discussion and application of the modified TLM can be found in Hayes and Leckie (1986), Hayes and Leckie (1987) and Zhang and Sparks (1989). In the modified TLM, $SO_4$ ions are allowed to form an inner-sphere surface coordination complex by placing them in the $\alpha$ layer such that,

$$XOH_2^+ - SO_4^{2-} = XSO_4^- - H_2O \tag{5.17}$$

where $XSO_4^-$ is the inner-sphere surface complex. The charge balance for the reactions in the $\alpha$ and $\beta$ layer are then.

$$\sigma_\alpha = [XOH_2^+] - [XOH_2^+ - NO_3^-] - [XSO_4^-] - [XO^-] - [XO^- - Na^+] \quad (5.18)$$

$$\sigma_\beta = [XO^- - Na^+] - [XOH_2^+ - NO_3^-]. \quad (5.19)$$

In the case of $SO_4$ being adsorbed through an inner-sphere complex, the intrinsic conditional constant would be:

$$K^{int} = \frac{[XSO_4^-]}{[XOH_2^+][SO_4^{2-}]} exp(-2F\psi_\alpha/RT) \quad (5.20)$$

In the present study, parameters from both the computed results when the adsorbed sulfate ions are treated as an ion-pair (outer-sphere) surface complex or as a surface coordination (inner-sphere) complex were used to model the reactions thermodynamically and kinetically.

## 5.3 Results and Discussion

### 5.3.1 Static Study

The isotherm for $SO_4$ adsorption on goethite is shown in Fig.5.1. The adsorption of $SO_4$ was based on the difference between sulfate concentration in the initial suspension and that in the supernatant solution after equilibrium. As pH increased, $SO_4$ adsorption decreased rapidly. The modified TLM was used to describe $SO_4$ adsorption on goethite for both inner- and outer-sphere complexation. For the outer-sphere case, (Fig.5.1), the predicted line agrees well with the experimental data. Although not shown, the data were not satisfactorily described when inner-sphere complexation was assumed to be operational. These findings would suggest that outer-sphere complexation or electrostatic attractions between $SO_4$ and the goethite surface predominate. This mechanism will be confirmed using p-jump relaxation studies.

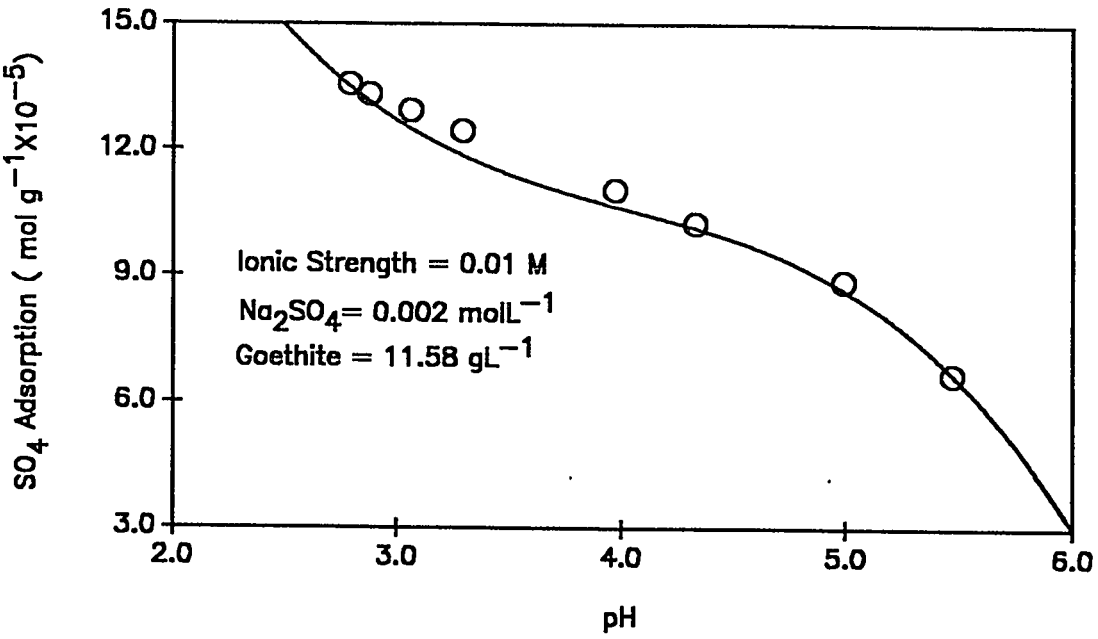


**Figure 5.1:** Adsorption of $SO_4$ on goethite vs. pH. Experimental data are applied to the TLM assuming outer–sphere complexation. Symbols represent experimental data and the line represents the predicted relationship based on the TLM.

### 5.3.2 p–jump Relaxation Studies

A single relaxation was observed with the direction of the relaxation signals indicating a decrease in the suspension conductivity of the suspensions during relaxation (Fig. 5.2). The reciprocal relaxation times ($\tau^{-1}$) increased with increasing pH (Fig. 5.3), which may indicate that the relaxation was related to the proton concentration in the suspension. In preliminary experiments, relaxations were not observed in goethite–$NaNO_3$, goethite–$HNO_3$, $HNO_3 - NaNO_3$, $HNO_3 - Na_2SO_4$, and $HNO_3 - NaNO_3 - Na_2SO_4$ systems. These findings indicate that the relaxation observed was attributable to adsorption/desorption of $SO_4$ on the goethite surface.

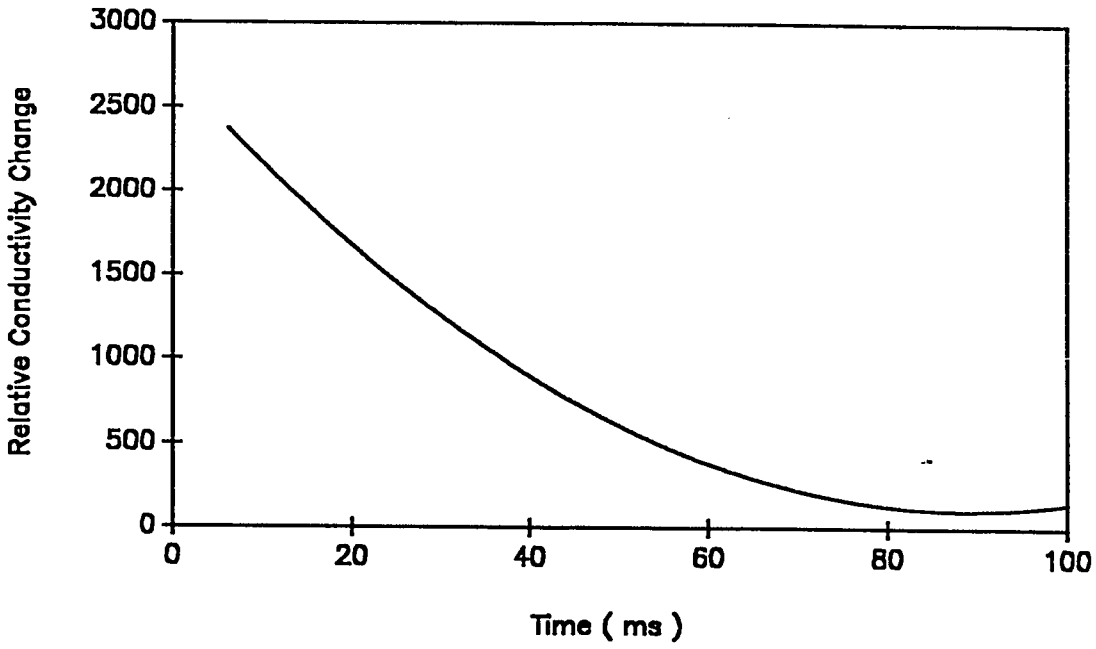


**Figure 5.2:** Typical p-jump relaxation curve for the goethite suspension showing change in conductivity vs. time during the relaxation.

If $SO_4$ adsorption on goethite occurs by electrostatic attraction or by outer-sphere complexation, one can propose two possible reaction mechanisms:

$$XOH_2^+ + SO_4^{2-} \rightleftharpoons XOH_2^+ - SO_4^{2-} \qquad \text{(Reaction 1)}$$

$$XOH + H^+ + SO_4^{2-} \rightleftharpoons XOH_2^+ - SO_4^{2-} \qquad \text{(Reaction 2)}$$

where $XOH_2^+ - SO_4^{2-}$ represents a surface complex between a positively charged surface site and adsorbed $SO_4$ via electrostatic attraction. In Reaction 1, $SO_4$ is adsorbed on a protonated surface site which is positively charged. In Reaction 2, protonation and $SO_4$ adsorption on a neutral site occur simultaneously. The products of the two reactions are the same; thus it is impossible from equilibrium studies to determine which of them is the correct mechanism. One way to ascertain the correct mechanism is to determine the consistency between kinetic and equilibrium results for each reaction. The intrinsic

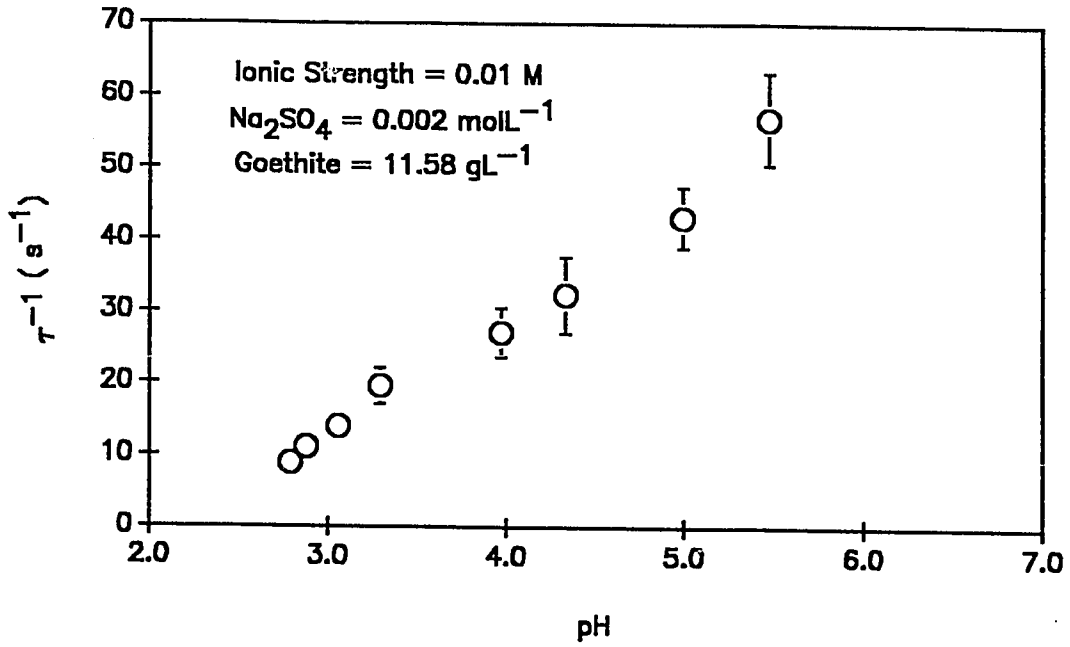


**Figure 5.3:** Relationship between reciprocal relaxation times ($\tau^{-1}$) and pH in the goethite suspension.

equilibrium constants for the two reactions ($K_1^{int}$ and $K_2^{int}$, respectively) can be written as:

For Reaction 1:

$$K_1^{int} = \frac{[XOH_2^+ - SO_4^{2-}]}{[XOH_2^+][SO_4^{2-}]} exp(\frac{-2F\psi_\beta}{RT}) \tag{5.21}$$

and for Reaction 2:

$$K_2^{int} = \frac{[XOH_2^+ - SO_4^{2-}]}{[XOH][H^+][SO_4^{2-}]} exp[\frac{F(\psi_\alpha - 2\psi_\beta)}{RT}] \tag{5.22}$$

where the exponential terms in Eqs. (5.21) and (5.22) represent the influence of surface potential on the conditional equilibrium constants, and are called the "activity coefficient" for the species in the suspension. The subscripts 1 and 2 refer to Reaction 1 and 2, respectively. One must also relate the surface potential to activation potentials for both the adsorption and desorption reactions. Defining the activation potentials as $\psi_f^\#$ and $\psi_b^\#$ for

those required to overcome the electrical double layer (EDL) potential for the adsorption (forward) and desorption (backward) steps, respectively, and relating the intrinsic rate constants directly to the rate constants, one obtains,

$$k_f^{int} = k_f exp[\frac{F\psi_f^{\#}}{RT}] \tag{5.23}$$

$$k_b^{int} = k_b exp[\frac{F\psi_b^{\#}}{RT}] \tag{5.24}$$

where $k_f$ and $k_b$ are the rate constants for the forward and backward reactions, respectively. The overall reaction constant is

$$K^{int} = \frac{k_f^{int}}{k_b^{int}} = \frac{k_f exp[\frac{F\psi_f^{\#}}{RT}]}{k_b exp[\frac{F\psi_b^{\#}}{RT}]} = K_1 exp[\frac{F\psi_o}{RT}] \tag{5.25}$$

and

$$\frac{exp[\frac{F\psi_f^{\#}}{RT}]}{exp[\frac{F\psi_b^{\#}}{RT}]} = exp[\frac{F\psi_o}{RT}] \tag{5.26}$$

where $\psi_o$ is the EDL potential for a specific reaction. In this study,

$$\psi_f^{\#} = -\psi_b^{\#} = \psi_o/2 = (\psi_\alpha - 2\psi_\beta)/2. \tag{5.27}$$

In arriving at Eq.(5.27), it is assumed that the magnitude of the activation potentials for adsorption and desorption are equal and opposite in sign. In this manner, the EDL properties are developed consistently for both equilibrium and kinetic analyses based on the TLM.

In the neighborhood of equilibrium, linearized relaxation rate equations can be obtained (see derivations in Appendix B):

For Reaction 1:

$$\tau^{-1} = k_1^{int} exp(\frac{F\psi_\beta}{RT})([XOH_2^+] + [SO_4^{2-}]) + k_{-1}^{int} exp(\frac{-F\psi_\beta}{RT}). \tag{5.28}$$

For Reaction 2:

$$\tau^{-1} = k_2^{int} exp[\frac{-F(\psi_\alpha - 2\psi_\beta)}{2RT}]([XOH][H^+] + [XOH][SO_4^{2-}] + [H^+][SO_4]) + k_{-2}^{int} exp[\frac{F(\psi_\alpha - 2\psi_\beta)}{2RT}] \quad (5.29)$$

where $k_1^{int}, k_{-1}^{int}, k_2^{int}$, and $k_{-2}^{int}$ are the intrinsic forward and backward rate constants for Reaction 1 and 2, respectively. Rearranging Eq.(5.28) and (5.29), one obtains Eqs.(5.30) and (5.31),

$$\tau^{-1} exp(\frac{F\psi_\beta}{RT}) = k_1^{int}\Big\{exp(\frac{2F\psi_\beta}{RT})([XOH_2^+] + [SO_4^{2-}])\Big\} + k_{-1}^{int} \quad (5.30)$$

$$\tau^{-1} exp\Big(\frac{-F(\psi_\alpha - \psi_\beta)}{2RT}\Big) = k_2^{int}\Big\{exp[\frac{-F(\psi_\alpha - 2\psi_\beta)}{RT}]([XOH][H^+] + [XOH][SO_4^{2-}] + [SO_4^{2-}][H^+])\Big\} + k_{-2}^{int}. \quad (5.31)$$

Equations (5.30) and (5.31) represent the linearized relationships between the reciprocal relaxation times, the exponential terms, and the concentration terms. If a suggested mechanism is consistent with the experimental relaxation data, than a plot of $\tau^{-1}$ with the exponential term versus the the expression in the brackets of Eq.(5.30) or Eq.(5.31) will give a straight line with a slope of $k_1^{int}$ and an intercept of $k_{-1}^{int}$ if Reaction 1 is operational or $k_2^{int}$ and $k_{-2}^{int}$ if Reaction 2 is applicable. For each pH at which the kinetic experiments were run, values for $\psi_\alpha$, $\psi_\beta$, and reactant and product concentrations as determined from the equilibrium studies were inserted into Eqs.(5.30) and (5.31). As shown in Figs.5.4 and 5.5, Eqs.(5.30) and (5.31) both produce straight lines indicating that both Reaction 1 and 2 are operational. Intrinsic equilibrium constants for both reactions were calculated using the ratios of $k_1^{int}/k_{-1}^{int}$ ($4.239 \times 10^7 mol^{-1}Ls^{-1}/3.157s^{-1}$), and $k_2^{int}/k_{-2}^{int}$ (see Table 5.2). The forward and backward intrinsic rate constants were calculated from the slope and intercept, respectively, of Figs. 5.4 and 5.5. The values of Reaction 2 are listed in Table 5.2. The values obtained were $K_1^{int} = 10^{7.13}$ and $K_2^{int} = 10^{9.14}$. The $K_{eq}^{int}$ obtained from the static study was $10^{9.6}$. Thus $K_2^{int}$ is of similar magnitude to $K_{eq}^{int}$, the data are

presented in Table 5.2. Based on the consistency between equilibrium and kinetic results, one can conclude that Reaction 2 is the most plausible mechanism for $SO_4$ adsorption on goethite.

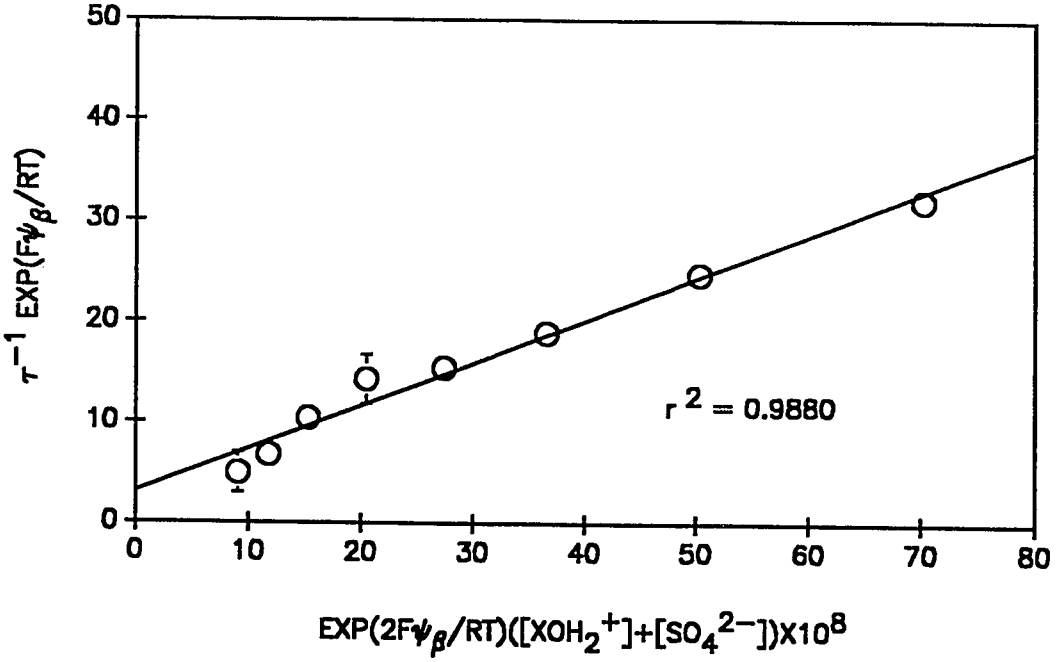


**Figure 5.4:** Plot of the relationship between $\tau_1^{-1}$ with exponential and concentration terms as proposed in Eq.(5.30)

It has often been observed that the pH of an oxide suspension increases when $SO_4$ is added, or that a certain amount of acid must be added to maintain the pH. This finding led some investigators to conclude that $SO_4$ is adsorbed via ligand exchange (Rajan, 1978; Parfitt, 1978). As was mentioned earlier, there has not been direct evidence that OH is released from the hydrated surface site. The increase in OH concentration during adsorption may be caused by dissociation of $H_2O$. $H^+$ can then be consumed by two processes. One way is through the reaction given in Eq. (5.31). The other possible mechanism is the protonation of the anion itself, especially at high anion concentrations

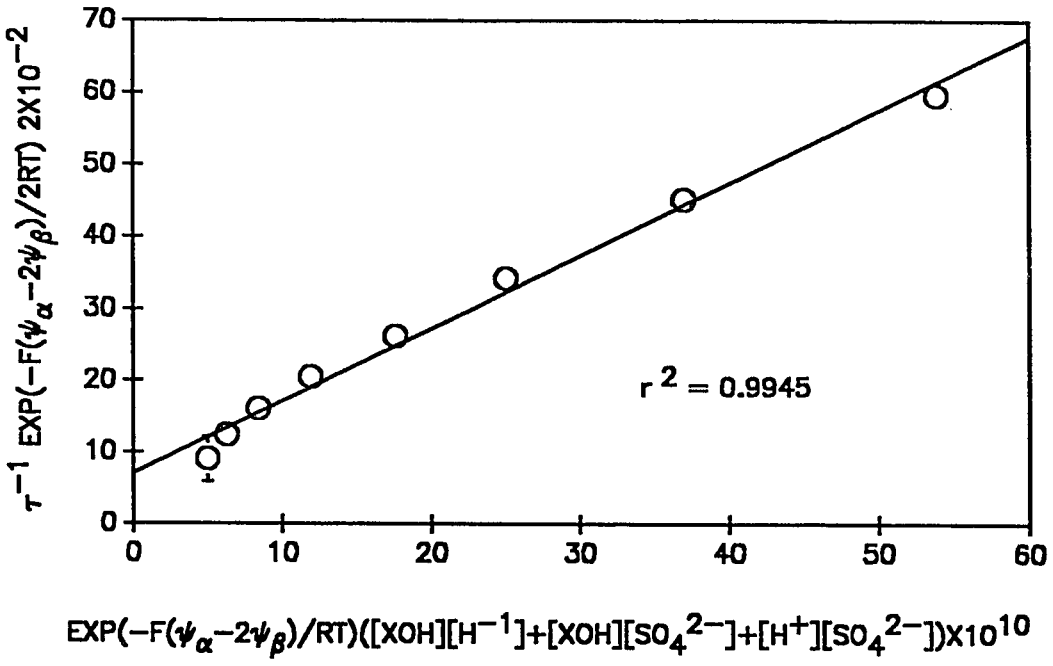


**Figure 5.5:** Plot of the relationship between $\tau_2^{-1}$ with exponential and concentration terms as proposed in Eq.(5.31)

**Table 5.2:** Intrinsic rate and equilibrium constants for Reaction 2 determined from kinetic and equilibrium measurements

| $k_2^{int}$ | $k_{-2}^{int}$ | $\mathrm{Log}K_2^{int*}$ | $\mathrm{Log}K_{eq}^{int*}$ |
|---|---|---|---|
| $mol^{-1}Ls^{-1}$ | $s^{-1}$ | | |
| $2.02 \times 10^8$ | 0.144 | 9.15 | 9.60 |

*$K_2^{int}$ is the intrinsic equilibrium constant determined from the ratio of the rate constants i.e., $k_2^{int}/k_{-2}^{int}$ and $K_{eq}^{int}$ is the intrinsic equilibrium constant determined from equilibrium (static) measurements.

(Davis and Leckie, 1980). Both of these processes would yield $OH^-$ causing an increase in pH.

Based on the finding of this study, the mechanism of $SO_4$ adsorption on goethite is adsorption of $SO_4$ on a neutral site that is simultaneously protonated. Adsorption on goethite results in the formation of an outer-sphere surface complex via electrostatic attraction. The adsorption process occurs very raplidly and desorption is the rate-limiting step.

# CHAPTER 6
# KINETICS AND MECHANISMS OF SELENATE AND SELENITE ADSORPTION/DESORPTION ON GOETHITE

## 6.1 Introduction

The role of selenium in animal and human health is not entirely clear. From the observations of experiments done so far, Se is both a micronutrient and a toxin in animal and human nutrition (Kabatapendias and Pendias, 1984). Selenium may occur in soils in a number of forms including elemental selenium, selenides, selenites, selenates and organic selenium. Selenites represent the most abundant sources of selenium in many areas and their association with oxides determines to a large extent the availability of selenium to plants (Fleming, 1980). Selenates frequently occur in association with sulfates in soils of arid regions and, being soluble, are often responsible for vegetation that contains level harmful to animals (Olsen et al., 1942).

The behavior of selenium interaction with soils and soil constituents has been studied with most of experiments focusing on selenite retention by soils. Cary et al. (1967) found that selenium is immobilized by sesquioxides in acid soils and later Geering et al. (1968) reported that the concentration of selenium in soil solution is governed primarily by a ferric oxide-selenite adsorption complex, which forms rapidly when selenite is added to soils. However, Levesque (1974) found that selenite was also associated with aluminum and organic matters in Canadian podzols. Johns and Belling (1967) showed that selenite but not selenate was retained by calcareous soils. Brown and Carter (1969) found that selenite leaching was increased by addition of sulfate. When the concentration of $SO_4$ was sufficiently high, it competed with selenite ions for surface sites. Neal et al. (1987a, b) studied the pH dependence of selenite adsorption on five alluvial soils suspended in a NaCl background solution. The adsorption of selenite was a function of pH, no

effect was observed for selenite adsorption when sulfate was present in the suspension. Approximately equal competition between o-phosphate and selenite for adsorption sites was observed when both were added at the same initial concentration (2 mmol $M^{-3}$). These results led Neal et al. (1987b) to hypothesize that selenite and o-phosphate were adsorbed by the same mechanism, viz., ligand exchange. This mechanism was previously suggested by Hingston et al. (1971).

Selenite adsorption on oxides such as gibbsite and goethite is a function of pH (Hingston et al., 1967; Hingston el al., 1971; Balistrieri and Chao, 1987). Adsorption vs. pH reaches a maximum level and the maximum is insensitive to changes in the ionic strength, so that the adsorption is not determined by the properties of the diffuse double layer of the outer Helmholtz layer (Hingston et al., 1967). In other words, selenite adsorption does not occur by electrostatic attraction; rather, a new bond forms between the adsorbed ion and adsorbent.

Competitive adsorption studies of phosphate–selenite on goethite and gibbsite indicate that selenite and phosphate are adsorbed on the same type of sites on oxide surfaces. The maximum anion adsorption from a mixture of phosphate and selenite species is approximately equal to the sum of the maximum adsorption for each anion in the absence of competition (Hingston et al., 1971).

Hingston et al. (1974) studied the reversibility of selenite adsorption on goethite and gibbsite. Little of the selenite adsorbed on goethite could be desorbed by washing, whereas selenite adsorption on gibbsite was easily reversible by washing at a constant pH in 0.1 M NaCl. The irreversibility observed for gibbsite may be due to bridging or multidentate ligand formation and to the formation of ring structures at the surface.

To obtain direct evidence for mechanisms of selenite and selenate adsorption on colloidal surfaces, the extended X-ray absorption fine structure (EXAFS) technique was employed to study the interactions of selenite and selenate with goethite in aqueous suspensions (Hayes et al., 1987). Measurements showed that selenate forms a weakly bonded, outer-sphere surface complex and that selenite forms a strongly bonded, inner-sphere complex. The adsorbed selenite ion is directly bonded to the goethite surface in a

bidentate fashion with two Fe atoms 3.38 nm from the selenium atom. Adsorbed selenate has no iron atom in the second coordination shell of selenium, which indicates retention of its hydration sphere upon adsorption (Hayes et al., 1987).

Very few reports have appeared on the adsorption of selenate on soils and soil constituents. Davis and Leckie (1980) showed that for ionic concentrations of $10^{-5}M$ the percent of selenate and sulfate adsorbed on amorphous Fe–oxyhydroxide as a function of pH is essentially the same. Balistrieri and Chao (1987) and Merrill et al. (1986) also observed that at the same pH, selenate adsorption on goethite and Fe oxyhydroxide is much lower than selenite adsorption. Merrill et al. (1986) attributed the lower selenate adsorption to competition with sulfate in solution. However, the differences in adsorption of the two selenium species can also be explained by the difference in the affinity of the two oxidation states of selenium for the surface (Balistrieri and Chao, 1987).

The constant capacitance model has been employed to describe the adsorption of selenite on goethite (Goldberg, 1985), alluvial soils (Sposito et al., 1988) and a calcareous, montmorillonitic soil (Goldberg and Glaubig, 1988), assuming ligand exchange. In a single anion system, the constant capacitance model was able to describe selenite adsorption on goethite quantitatively over the pH range 3 to 11, but could describe only qualitatively adsorption in a mixed phosphate–selenite anion system (Goldberg, 1985). In modeling the adsorption of selenite on soils, Sposito et al., (1988) found that by adapting the assumption of $XHSeO_3$ and $XSeO_3^-$ as the "major" set of soil adsorbents and $X_2SeO_3^-$ as an independent, "minor" set of soil adsorbent as suggested by adsorption studies on specimen minerals by Rajan (1979) and Hayes et al. (1987), and in the pH range 4 to 9 and an initial selenite concentration of 2 to 8 mmol $M^{-3}$, the constant capacitance model predicted the adsorption envelopes qualitatively satisfactory, but the quantitative agreements ranged from excellent to poor. Goldberg and Glaubig (1988) found that the constant capacitance model is able to describe selenite sorption on soil satisfactorily up to pH 7, but is unable to fit the sorption plateau occurring in the pH range 8 to 11. They attributed the inability of the model to describe sorption over the entire pH range to two types of surface sites competing for the adsorption of selenite. The constant capacitance model satisfactorily described selenite sorption on Ca–montmorillonite and kaolinite up to

pH 9. Goldberg and Glaubig (1988) ascribed the mechanism to a ligand exchange process occurring at the reactive surface aluminal groups (AlOH) located at the particle edges.

Kinetic studies of selenium adsorption/desorption on soils and soil constituents are rarely found. In this study, the mechanisms of selenate and selenite adsorption and desorption on goethite in aqueous suspension will be studied kinetically. Intrinsic rate constants and kinetic models for selenate and selenite reactions on goethite will be determined.

## 6.2 Materials and Methods

### 6.2.1 Experimental Procedures

The goethite concentration used in the selenate studies was 27.01 g $L^{-1}$. The original selenate (as $Na_2SeO_4$) concentration was 0.003 mol $L^{-1}$, and the ionic strength of the selenate solution which included the added $Na_2SeO_3$, NaCl, and HCl was 0.015 M. In the selenite studies, the goethite concentration was 20.1 g $L^{-1}$, the initial $SeO_3^{2-}$ concentration was 0.0045 mol $L^{-1}$ and the ionic strength was 0.02 M.

Adsorption isotherms were determined for the selenate and selenite. After a 24 h shaking peroid, the selenate–goethite and selenite–goethite suspensions were centrifuged under 34500g for 30 min. The supernatants were filtered through 0.2 $\mu$m pore membrane filters and the concentrations of selenate and selenite in the filtrate were determined using a Waters Model 430 ion chromatograph The adsorption of selenate and selenite was the difference between the added selenium species and that remaining in filtrate.

In the selenium adsorption and kinetics studies, NaCl and HCl were used to adjust the ionic strength and pH of the suspension instead of using $NaNO_3$ and $HNO_3$ as were employed in the molybdate and sulfate studies. The reason for this is that when the concentrations of $SeO_3^{2-}$ and $SeO_4^{2-}$ are determined by ion chromatography, the peak for $NO_3^-$ appears very close to that for $SeO_3^{2-}$ (about 4.5 min.). In order to avoid the possible interaction between $SeO_3^{2-}$ and $NO_3^-$, NaCl and HCl were used, chloride has a peak appearing at 2 min. which is easily separated from that of $SeO_3^{2-}$.

Kinetic studies were carried out to determine the relaxation times in the suspensions containing goethite and $HSeO_3^-$ or $SeO_3^{2-}$ at different pH using the p-jump relaxation apparatus described previously. The thickness of brass membrane used in this study was 0.05 mm. The pressure required to burst the membrane is 13.5 MPa.

### 6.2.2 Model Application

The modified triple layer model (TLM) was employed to model selenate and selenite adsorption on goethite. Theoretical discussions and aspects of the application of the TLM can be found in Chapter 4 and 5 of this dissertation. The following reactions can be defined for the application of the TLM to selenate and selenite adsorption on goethite using the experimental conditions given earlier:

$$XOH_2^+ = XOH + H^+ \tag{6.1}$$

$$XOH = XO^- + H^+ \tag{6.2}$$

$$XOH_2^+ + Cl^- = XOH_2^+ - Cl^- \tag{6.3}$$

$$XO^- + Na^+ = XO^- - Na^+ \tag{6.4}.$$

For selenate adsorption, it is assumed that the adsorption is nonspecific and the reaction product is an outer-sphere surface complex,

$$XOH + H^+ - SeO_4^{2-} = XOH_2^+ - SeO_4^{2-}. \tag{6.5}$$

If $SeO_4^{2-}$ adsorption is assumed to be specific, viz., a ligand exchange process occurs, then the reaction can be written as,

$$XOH + H^+ + SeO_4^{2-} = XSeO_4^- + H_2O. \tag{6.6}$$

For selenite adsorption assuming formation of outer-sphere surface complexes, one can write,

$$XOH + 2H^+ + SeO_3^{2-} = XOH_2^+ - HSeO_3^- \tag{6.7}$$

$$XOH + H^+ + SeO_3^{2-} = XOH_2^+ - SeO_3^{2-}, \tag{6.8}$$

or, if the adsorption of selenite involves ligand exchange and forms inner–sphere surface complexes then,

$$XOH + 2H^+ + SeO_3^{2-} = XHSeO_3^0 + H_2O \tag{6.9}$$

$$XOH + H^+ + SeO_3^{2-} = XSeO_3^- + H_2O \tag{6.10}$$

where XOH represents 1 mol of reactive surface hydroxyl bound to a Fe ion in goethite. Eq. (6.1) and (6.2) are the protonation and deprotonation reactions for which their intrinsic equilibrium constants are defined as two acidic constants $K_{a1}^{int}$ and $K_{a2}^{int}$, respectively. The intrinsic equilibrium constants for the reactions represented by Eqs.(6.1) to (6.10) are expressed as Eq.(6.11) to (6.20):

$$K_{a1}^{int} = \frac{[XOH][H^+]}{[XOH_2^+]} exp(-F\psi_\alpha/RT) \tag{6.11}$$

$$K_{a2}^{int} = \frac{[XO^-][H^+]}{[XOH]} exp(-F\psi_\alpha/RT) \tag{6.12}$$

$$K_{Cl^-}^{int} = \frac{[XOH_2^+ - Cl^-]}{[XOH_2^+][Cl^-]} exp(-F\psi_\beta/RT) \tag{6.13}$$

$$K_{Na^+}^{int} = \frac{[XO^- - Na^+]}{[XO^-][Na^+]} exp(F\psi_\beta/RT) \tag{6.14}$$

$$K_{XOH_2^+ - SeO_4^{2-}}^{int} = \frac{[XOH_2^+ - SeO_4^{2-}]}{[XOH][H^+][SeO_4^{2-}]} exp(F(\psi_\alpha - 2\psi_\beta)/RT) \tag{6.15}$$

$$K_{XSeO_4^-}^{int} = \frac{[XSeO_4^-]}{[XOH][H^+][SeO_4^{2-}]} exp(-F\psi_\alpha/RT) \tag{6.16}$$

$$K_{XOH_2^+ - HSeO_3^-}^{int} = \frac{[XOH_2^+ - HSeO_3^-]}{[XOH][H^+]^2[SeO_3^{2-}]} exp(F(\psi_\alpha - \psi_\beta)/RT) \tag{6.17}$$

$$K_{XOH_2^+ - SeO_3^{2-}}^{int} = \frac{[XOH_2^+ - SeO_3^{2-}]}{[XOH][H^+][SeO_3^{2-}]} exp(F(\psi_\alpha - 2\psi_\beta)/RT) \tag{6.18}$$

$$K_{XHSeO_3^0}^{int} = \frac{[XHSeO_3^0]}{[XOH][H^+]^2[SeO_3^{2-}]} \tag{6.19}$$

$$K^{int}_{XSeO_3^-} = \frac{[XSeO_3^-]}{[XOH][H^+][SeO_3^{2-}]} exp(-F\psi_\alpha/RT). \qquad (6.20)$$

The intrinsic equilibrium constants for Eq.(6.11) to (6.14) which were obtained by separate potentometric titration experiments, are given in Table 6.1. Also, the two capacitance constants ($C_1$ and $C_2$) which are adopted by the TLM to relate surface charge to surface potential, are listed in Table 6.1. When modeling the adsorption of selenate and selenite on goethite, the computer program FITEQL (Westall, 1982) was used to calculate the intrinsic equilibrium constants for the individual reactions represented in Eq.(6.15) to (6.20), the surface charge and potential at every layer, and the exponential terms for every layer. In addition, the FITEQL program is able to compute the species concentration in the reaction system based on the titration data. The intrinsic constants $K^{int}_{a1}$, $K^{int}_{a2}$, $K^{int}_{Cl^-}$ and $K^{int}_{Na^+}$ were fixed when adsorption of selenite and selenate were modeled.

The methodology and equations used to calculate the mass balance, charge balance, the relationships between surface charge and potential are presented in Chapter 4 of this dissertation and they are not discussed in detail here.

**Table 6.1:** Intrinsic constants for protonation and deprotonation and NaCl adsorption and desorption on goethite

| | |
|---|---|
| $\mathrm{Log}K^{int}_{a1}$ | −4.3 |
| $\mathrm{Log}K^{int}_{a2}$ | −9.8 |
| $\mathrm{Log}K^{int}_{Na^+}$ | −9.3 |
| $\mathrm{Log}K^{int}_{Cl^-}$ | 5.4 |
| $C_1$ | 1.2 |
| $C_2$ | 0.13 |

## 6.3 Results and Discussion

### 6.3.1 Kinetics and Mechanism of Selenate Adsorption on Goethite

Selenate adsorption mostly occurs under acidic conditions as shown in Fig. 6.1. Selenic acid ($H_2SeO_4$) is a strong acid with a $pK_2 = 2.0$, the dominate species of selenate anion in the suspension is $SeO_4^{2-}$ in the pH range studied. With an increase in pH, $SeO_4^{2-}$ adsorption rapidly decreased. At pH 2.98, the total percent of adsorption was 93. When pH is higher than 7.2, no adsorption was recorded. Because too much acid was required to reduce the pH lower than 2.98 and to maintain a constant ionic strength of 0.015 M, lower pH experiments were not conducted. Selenate adsorption was described very well by the TLM. with this model it is assumed that the adsorption of $SeO_4^{2-}$ occurs at the $\beta$ layer via electrostatic attraction to form outer-sphere surface complexes.

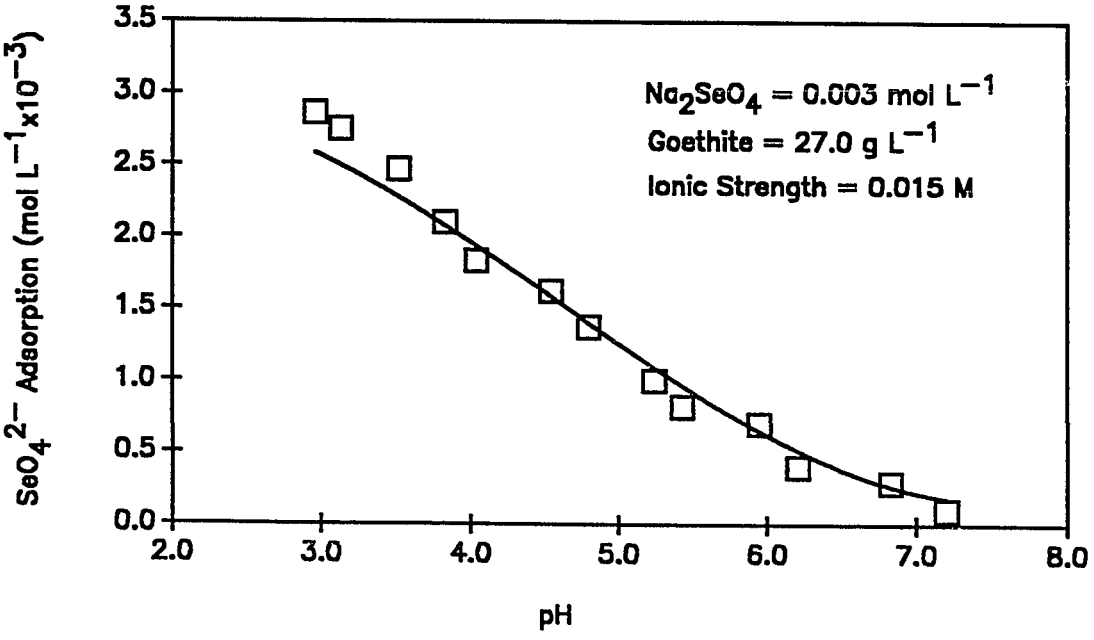


**Figure 6.1:** Adsorption of $SeO_4^{2-}$ on goethite vs. pH. The symbols represent the experimental data and the solid line represents TLM conformity assuming nonspecific adsorption

Single relaxations were found in selenate–goethite suspensions in the pH range 2.98 to 7.20 that was studied. The reciprocal relaxation times ($\tau^{-1}$) increased with an increase in pH or an decrease in adsorption (Fig. 6.2). The systems NaCl–HCl–goethite, Na–HCl–goethite supernatant, NaCl–HCl–selenate–goethite supernatant, and NaCl–HCl–$Na_2SeO_4$ mixed solutions were examined by p–jump analysis using the same procedure as for the selenate–goethite system, but no relaxation was observed. This finding indicates that the relaxation observed for the $SeO_4^{2-}$–goethite system must be caused by $SeO_4^{2-}$ adsorption/desorption on the goethite surface. A possible mechanism for $SeO_4^{2-}$ adsorption on goethite assuming outer–sphere complexation and adsorption of $SeO_4^{2-}$ in the $\beta$ layer is,

$$XOH + H^+ + SeO_4^{2-} \rightleftharpoons XOH_2^+ - SeO_4^{2-}. \qquad (6.21)$$

This mechanism assumes that a $SeO_4^{2-}$ anion adsorbs on a protonated surface site. The protonation and adsorption phenomena occur simultaneously.

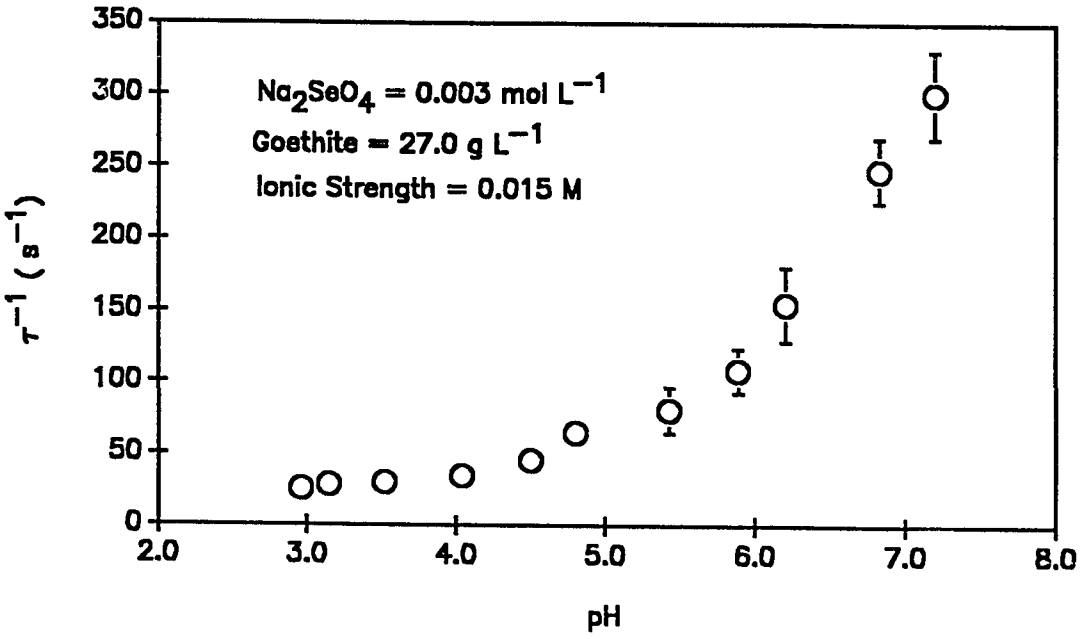


**Figure 6.2:** Relationship between pH and reciprocal relaxation times ($\tau^{-1}$) of selenate–goethite system

The linearized relationship between the reciprocal relaxation time and the concentration of species in suspension is (the derivation of the equation is same as described in Chapter 5 for $SO_4^{2-}$ adsorption on goethite),

$$\tau^{-1} = k_1([XOH][SeO_4^{2-}] - [XOH][H^+] - [SeO_4^{2-}][H^-]) - k_{-1}, \tag{6.22}$$

where $k_1$ and $k_{-1}$ are the forward and backward rate constants for reaction (6.21), respectively. Considering the reaction is carried out at the solid/water interface, the electrostatic effect has to be considered in calculating intrinsic rate constants, as was mwntioned before, using the TLM to obtain the necessary parameters. Eq.(6.22) becomes

$$\tau^{-1} = k_1^{int} exp(\frac{-F(\psi_\alpha - 2\psi_\beta)}{2RT})([XOH][SeO_4^{2-}] - [XOH][H^-] - [SeO_4^{2-}][H^+]) - k_{-1}^{int} exp(\frac{F(\psi_\alpha - 2\psi_\beta)}{2RT}). \tag{6.23}$$

In order to obtain a simple first-order equation, Eq.(6.23) can be rearranged as,

$$\tau^{-1} exp(\frac{-F(\psi_\alpha - 2\psi_\beta)}{2RT}) = k_1^{int}\left\{ exp(\frac{-F(\psi_\alpha - 2\psi_\beta)}{RT})([XOH][SeO_4^{2-}] - [XOH][H^+] + [SeO_4^{2-}][H^-])\right\} - k_{-1}^{int}. \tag{6.24}$$

If a plot of the reciprocal relaxation time with the exponential terms versus the terms in the brackets of Eq. (6.24) results in a linear relationship, then the forward and backward intrinsic rate constants ($k_1^{int}$ and $k_{-1}^{int}$, respectively), can be determined from the slope and intercept, respectively of the straight line. It is very clear from Fig. (6.3) that the relationship given in Eq. (6.24) is correct. Morever, the computation of the intrinsic equilibrium constant ($K^{int}$) for the reaction expressed in Eq. (6.21) using the kinetic data ptovide more evidence that the outer-sphere complexation mechanism is correct. In Table 6.2, the intrinsic rate constants, $k_1^{int}$ and $k_{-1}^{int}$, the intrinsic equilibrium constant from TLM modeling, ($K_{model}$), and the intrinsic equilibrium constant from the kinetic study ($K_{kinetic}^{int} = k_1^{int}/k_{-1}^{int}$), are presented. Based on the agreement between the results from both the equilibrium the kinetic studies, the conclusion can be drawn that the assumed reaction mechanism is correct. The mechanism is the same as that for sulfate intracting with goethite.

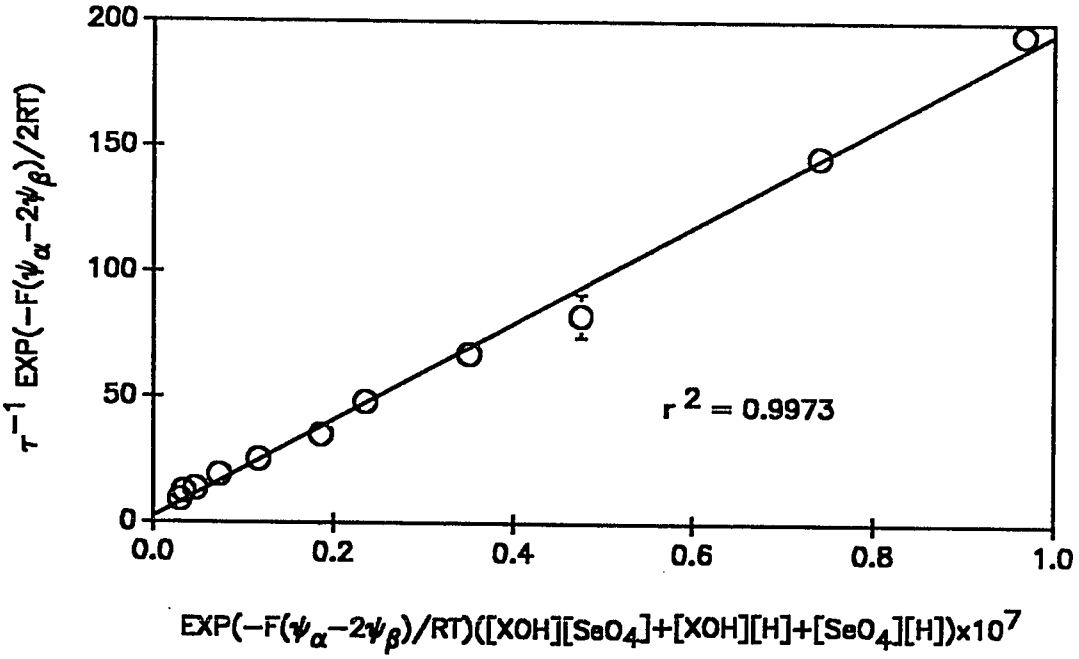


**Figure 6.3:** Plot of the relationship between $\tau^{-1}$ with exponential and concentration terms as proposed in Eq.(6.1).

In addition, from the data shown in Table 6.2, one can can see that the $k_1^{int}$ is eight orders of magnitude higher than the $k_{-1}^{int}$, which means that the rate of the forward reaction, or adsorption, is much higher than the rate of the backward reaction, or desorption. The latter process is thus rate–limiting.

**Table 6.2:** Intrinsic rate constants and constants for $SeO_4^{2-}$ adsorption and desorption on goethite

| $k_1^{int}$ | $k_{-1}^{int}$ | $\mathrm{Log}K_{kinetic}^{int}$ | $\mathrm{Log}K_{model}^{int}$ |
|---|---|---|---|
| $mol^{-2}L^2s^{-1}$ | $s^{-1}$ | | |
| $3.52 \times 10^8$ | 3.34 | 8.02 | 8.64 |

### 6.3.2 Kinetics and Mechanisms of Selenite Adsorption on Goethite

Total selenite adsorption on goethite decreased with an increase in pH as illustrated in Fig. 6.4. Data from the modified TLM indicated that in the pH range studied, selenite adsorbed on the goethite surface to form monovalent and bivalent selenite–Fe complexes, since selenite exists as both $SeO_3^{2-}$ and $HSeO_3^-$ in suspension over the pH range studied. The amount of both complexes, $XHSeO_3^0$ and $XSeO_3^-$, as shown in the Fig.6.4, is significant in the suspension. This finding implies that neither of them can be ignored nor considered as the dominant species in the suspension. This fact, as will be seen later, makes the derivation of rate equations complicated. As shown in Fig.6.4, the amount of $XHSeO_3^0$ dropped sharply at pH 8.3 ($pK_2^{SeO_3^{2-}}$ =8.24); meanwhile, the amount of $XSeO_3^-$ increased with pH until pH 8.3 and then dropped with the total adsorption decreased. The solid line in Fig.(6.4) represents the total adsorption as predicted by the TLM, it matches the experimental data very well. Adsorption of $HSeO_3^-$ and $SeO_3^{2-}$ predicated from the TLM are also shown in Fig. 6.4. Using the FITEQL algorithm, the intrinsic equilibrium constants for the formation of $XHSeO_3^0$ and $XSeO_3^-$, electrostatic parameters such as surface charge and potential at the $\alpha$ and $\beta$ layers ($\sigma_\alpha$, $\sigma_\beta$, $\psi_\alpha$ and $\psi_\beta$), and the concentrations of XOH, $XOH_2^+$, $XO^-$, $XHSeO_3^0$ and $XSeO_3^-$ were calculated. It should be pointed out that the intrinsic constants for reactions involving protonation/deprotonation and adsorption of counterion ions are fixed in the program since they are determined in separate proton isotherm titration experiments.

The p-jump relaxation studies were carried out over the pH range of 6 to 10. Double relaxations were observed for the goethite–selenite suspension. Both reciprocal relaxation times, as shown in Fig.6.5, increased as the pH of the suspensions increased. The procedure for determining the relaxation times from the changes in the amplitude of conductivity versus time after a sudden pressure change applied can be found in Chapter 4 of this dissertation. In order to ascertain the reactions which caused relaxation, each of the following systems was examined: NaCl–HCl–$Na_2SeO_3$ mixed solution, $Na_2SeO_3$–goethite supernatant, NaCl–goethite suspension and its supernatant. No relaxation was observed with any of these systems. Thus the relaxation that was observed in the selenite–goethite suspension was caused by the adsorption and desorption of selenite on goethite.

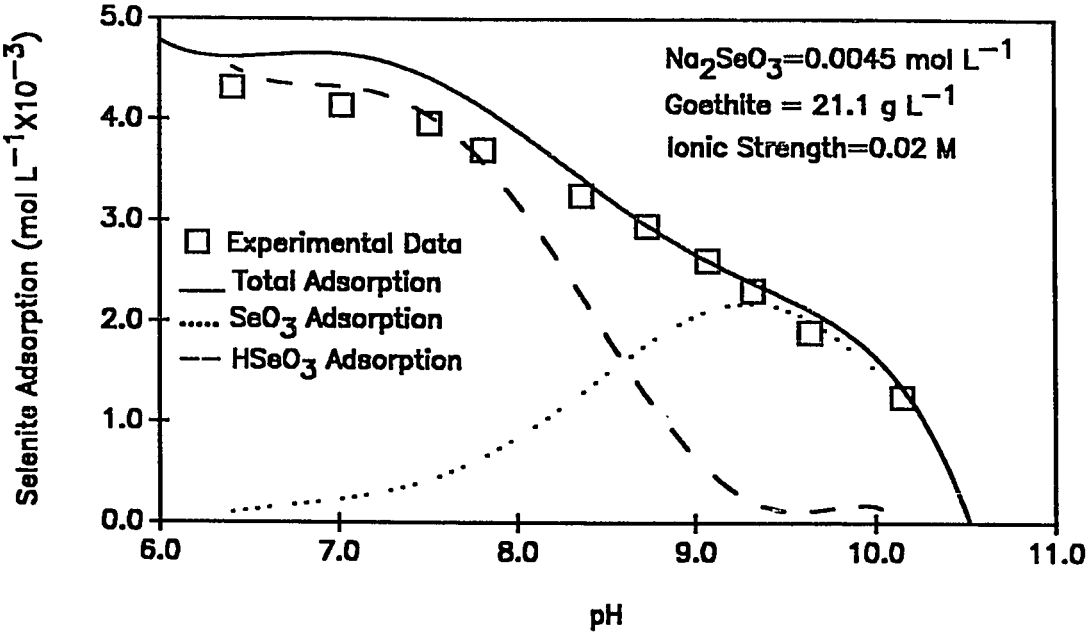


**Figure 6.4:** Selenite adsorption vs. pH in selenite–goethite system. The lines represent the predication of TLM when the assumption of formation of inner–sphere surface complexes

Based on the findings from the adsorption isotherm and p–jump experiments, one may hypothesize that the mechanism(s) involved in the adsorption and desorption reactions involves the two complexes, $XHSeO_3^0$ and $XSeO_3^-$, and possibly multiple reaction steps. With this in mind, a comprehensive two step adsorption mechanism was assumed to be operational,

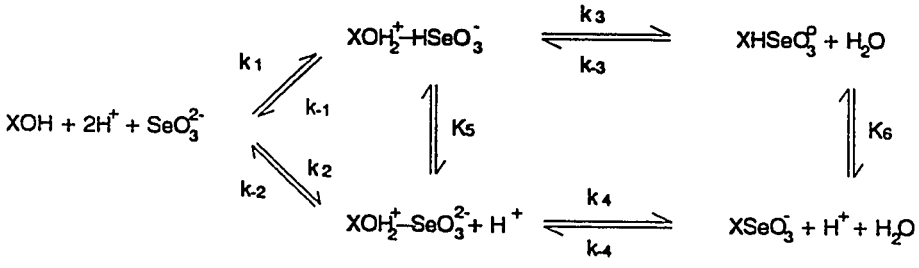


(6.25)

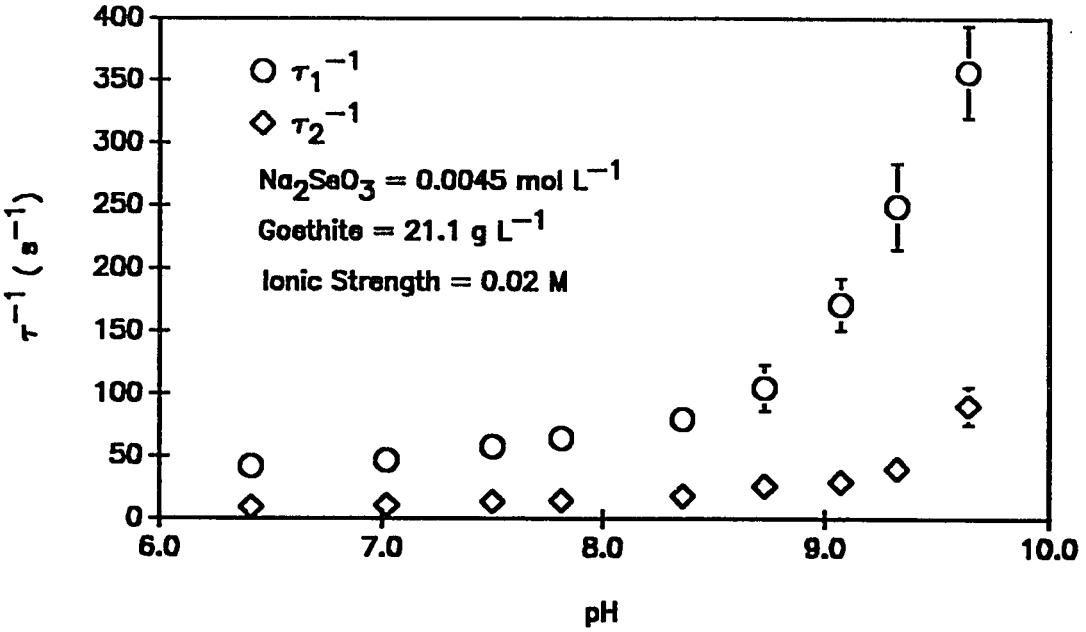


**Figure 6.5:** Relationship between pH and fast ($\tau_1^{-1}$) and slow ($\tau_2^{-1}$) reciprocal relaxation times

The first step is the formation of outer-sphere surface complexes ($XOH_2^+ - HSeO_3^-$ and $XOH_2^+ - SeO_3^{2-}$) in the $\beta$ layer. The second step involves a ligand exchange process, whereby the adsorbed selenites enter the $\alpha$ layer and replace a ligand from the goethite surface to form the inner-sphere surface complexes ($XHSeO_3^0$ and $XSeO_3^-$). The two protolytic equilibrium (represented by $K_5$ and $K_6$ and shown by vertical arrows between the complexes in Eq. (6.25)) are established rapidly by compared with the complexation reactions (Eigen and DeMaeyer, 1963; Patel and Taylor, 1973; Patel et al., 1974).

To confirm the assumed mechanism in Eq. (6.25), one has to: 1) derive equations to show the relationships between the reciprocal relaxation times and the concentrations of species involved in the reactions and the rate constants for each individual elementary reaction; 2) solve the equations so that rate constants can be obtained for the expected mechanism; and 3) use the equation, $\tau_{observed}^{-1}$ values, and other concentration terms in the equation to calculate intrinsic rate constants for a series of the pH levels studied. These

rate constants are then inserted into the equation for other pH levels studied to calculated $\tau^{-1}_{calculated}$ values. If the assumed mechanism is acceptable, the $\tau^{-1}_{calculated}$ values will match the $\tau^{-1}_{observed}$. Moreover, the intrinsic equilibrium constants for formation of $XHSeO_3^0$ and $XSeO_3^-$ from the intrinsic rate constants which are calculated from the linearized equations should be consistent with these obtained from equilibrium studies.

The fast relaxation time, $\tau_1$ observed from the selenite–goethite system, is attributed to step 1 and the slower relaxation, $\tau_2$, to the second step. Two equations relating the $\tau$ values to the concentrations of the species in the suspensions should be established to calculate the intrinsic rate constant ($k$) for each step in Eq. (6.25). Because the derivation processes for the equations are long and tedious, each step will be discussed separately.

### 6.3.2.1 Step One

In step one, $HSeO_3^-$, $SeO_3^{2-}$ and $H^+$ react with the surface site to form the outer-sphere surface complexes $XOH_2^+ - HSeO_3^-$ and $XOH_2^+ - SeO_3^{2-}$, respectively, at the $\beta$ layer. The conditional constants for these reactions are:

$$K_1' = \frac{k_1}{k_{-1}} = \frac{[XOH_2^+ - HSeO_3^-]}{[XOH][H^+]^2[SeO_3^{2-}]} \tag{6.26}$$

$$K_2' = \frac{k_2}{k_{-2}} = \frac{[XOH_2^- - SeO_3^{2-}]}{[XOH][H^+][SeO_3^{2-}]} \tag{6.27}$$

where the square bracket represents the concentration of species at equilibrium, $k_1$, $k_{-1}$, $k_2$, and $k_{-2}$ are the rate constants. For simplicity, the following symbols are adopted to represent the concentration terms in Eq. (6.26) and (6.27).

$$x_1 = [XOH] \qquad S = [SeO_3^{2-}]$$

$$x_2 = [XOH_2^+ - HSeO_3^-] \qquad H = [H^+]$$

$$x_3 = [XOH_2^+ - SeO_3^{2-}]$$

The rate law derived for step 1 covering the pH range that was studied is,

$$-\frac{dx_1}{dt} = (k_1 + k_2)x_1H^2S - K_{-1}x_2 - k_{-2}x_3H = 0 \tag{6.28}$$

For a small perturbation caused by a sudden pressure change, the small amount of change $\Delta$ resulting from deviation of the equilibrium concentration, the rate law becomes,

$$-\frac{d\Delta x_1}{dt} = (k_1 + k_2)(x_1 - \Delta x_1)(H - \Delta H)^2(S + \Delta S) - k_1(x_2 + \Delta x_2) - k_{-2}(x_3 + \Delta x_3)(H + \Delta H). \quad (6.29)$$

Rearranging Eq. (6.29), one obtains,

$$-\frac{d\Delta x_1}{dt} = (k_1 + k_2)(x_1H^2S - 2x_1HS\Delta H + x_1S\Delta H^2 - H^2S\Delta x_1 + 2HS\Delta H^2 + S\Delta x_1\Delta H^2 + x_1H^2\Delta S - 2H\Delta x_1\Delta H\Delta S - \Delta x_1\Delta S\Delta H^2) - k_1(x_2 - \Delta x_2) - k_{-2}(x_3H + \Delta x_3\Delta H - H\Delta x_3 - x_3\Delta H). \quad (6.30)$$

Since the perturbation in the equilibrium of the selenite–goethite system is small, the change of species ($\Delta$s) is very small. All of the terms that contain more than one $\Delta$ are deleted because they are extremely small compared with the other terms (Bernasconi, 1976; Sparks, 1989). Equation (6.30) can now be written as,

$$-\frac{d\Delta x_1}{dt} = (k_1 + k_2)(x_1H^2S) - k_{-1}x_2 - k_{-2}(x_3H) - (k_1 + k_2)(2x_1HS\Delta S - H^2S\Delta x_1 - x_1H^2\Delta S) - k_{-1}\Delta x_2 - k_{-2}(H\Delta x_3 - x_3\Delta H). \quad (6.31)$$

According to Eq.(6.28), the first three terms in Eq.(6.31) can be canceled, and thus Eq.(6.31) becomes

$$-\frac{d\Delta x_1}{dt} = (k_1 - k_2)(2x_1HS\Delta S - H^2S\Delta x_1 - x_1H^2\Delta S) - k_{-1}\Delta x_2 - k_{-2}(H\Delta x_3 - x_3\Delta H). \quad (6.32)$$

The definition for relaxation time is

$$-\frac{d\Delta x}{dt} = \frac{1}{\tau}\Delta x \quad (6.33)$$

Accordingly, $\tau_1^{-1}$ can be defined as

$$\tau_1^{-1} = (k_1 + k_2)(2x_1HS\frac{\Delta S}{\Delta x_1} + H^2S\frac{\Delta x_1}{\Delta x_1} + x_1H^2\frac{\Delta S}{\Delta x_1}) - k_{-1}\frac{\Delta x_2}{\Delta x_1} - k_{-2}(H\frac{\Delta x_3}{\Delta x_1} + x_3\frac{\Delta H}{\Delta x_1}) \tag{6.34}$$

From mass balance,

$$\Delta x_1 + \Delta x_2 + \Delta x_3 = 0 \qquad \Delta x_1 = \Delta S$$

and Eq.(6.26) and (6.27), one can derive the two equations below,

$$\frac{\Delta x_2}{x_2} = \frac{\Delta x_1}{x_1} + \frac{\Delta S}{S} + \frac{2\Delta H}{H} \tag{6.35}$$

$$\frac{\Delta x_3}{x_3} = \frac{\Delta x_1}{x_1} + \frac{\Delta S}{S} + \frac{\Delta H}{H} \tag{6.36}$$

Let

$$\frac{\Delta x_3}{\Delta x_1} = m, \qquad \Delta x_3 = m\Delta x_1 \tag{6.37}$$

and

$$\frac{\Delta H}{\Delta x_1} = n, \qquad \Delta H = n\Delta x_1 \tag{6.38}$$

then Eq.(6.34) can be rewritten as

$$\tau_1^{-1} = (k_1 + k_2)(H^2(x_1 - S) + 2HSx_1n) + k_{-1}(1 + m) - k_{-2}(x_1n + mH). \tag{6.39}$$

By substituting Eq.(6.37) and (6.38) into Eq. (6.35) and (6.36), the latter two equations become

$$\frac{m}{x_3} = \frac{1}{x_1} + \frac{1}{S} + \frac{n}{H} \tag{6.40}$$

$$-\frac{1+m}{x_2} = \frac{1}{x_1} + \frac{1}{S} - \frac{2n}{H}. \tag{6.41}$$

Using the program MACSYMA (Rand, 1984) to solve for $m$ and $n$, and then using it to substitute to $m$ and $n$ to Eq.(6.39), one can obtain a complete relationship between the reciprocal relaxation time and the equilibrium concentrations and the rate constants. Since $XOH_2^- - HSeO_3^-$ and $XOH_2^+ - SeO_3^{2-}$ are the intermediate products and their concentrations cannot be determined directly, only the concentrations of reactants are

used in linearized rate equation. This makes the equation very long and nonlinear, but it is solvable with the help of a computer. The following equations give the solutions for $m$ and $n$ in which all $\Delta$ terms and $XOH_2^+ - HSeO_3^-$ and $XOH_2^+ - SeO_3^{2-}$ are expressed with the equilibrium concentrations of reactants and the rate constants:

$$m = \frac{H^2 k_1 k_2 (x_1 + S) - k_2 k_{-1}}{2H k_1 k_{-2} + k_2 k_{-1}} \tag{6.42}$$

$$n = -\frac{(H^2 k_1 k_{-2} + H k_2 k_{-1})(x_1 + S) + k_{-1} k_{-2}}{(2H k_1 k_{-2} + k_2 k_{-1}) S x_1}. \tag{6.43}$$

Substituting Eq. (6.42) and (6.43) into Eq. (6.39), the right side of the equation is expressed with the function of equilibrium concentrations of XOH, $SeO_3^{2-}$ and $H^+$ and the rate constants $k_1, k_2, k_{-1}$, and $k_{-2}$ instead of the function of $\Delta$s. Thus,

$$\begin{aligned}\tau_1^{-1} =& (k_1 + k_2)\left\{H^2(x_1 + S) - \frac{2H[(H^2 k_1 k_{-2} + H k_2 k_{-1})(x_1 + S) + k_{-1} k_{-2}]}{(2H k_1 k_{-2} + k_2 k_{-1}) S}\right\} \\ & - k_{-2}\left\{\frac{H[H^2 k_1 k_2 (x_1 + 1) - k_2 k_{-1}]}{2H k_1 k_{-2} + k_2 k_{-1}} - \frac{(H^2 k_1 k_{-2} + H k_2 k_{-1})(x_1 + S) + k_{-1} k_{-2}}{(2H k_1 k_{-2} + k_2 k_{-1}) S}\right\} \\ & + k_{-1}\left[\frac{H^2 k_1 k_2 (x_1 + 1) - k_2 k_{-1}}{2H k_1 k_{-2} + k_2 k_{-1}} + 1\right]\end{aligned} \tag{6.44}$$

Since the selenite reactions are carried out at the solid/water interface, the effects of the charged surface have to be considered. The intrinsic constants and rate constants can be related to the conditional constants as follows:

$$K_1^{int} = \frac{[XOH_2^+ - HSeO_3^-]}{[XOH][H^+]^2[SeO_3^{2-}]} exp\left(\frac{F(\psi_\alpha - \psi_\beta)}{RT}\right) = K_1' exp\left(\frac{F(\psi_\alpha - \psi_\beta)}{RT}\right) \tag{6.45}$$

$$K_2^{int} = \frac{[XOH_2^+ - SeO_3^{2-}]}{[XOH][H^+][SeO_3^{2-}]} exp\left(\frac{F(\psi_\alpha - 2\psi_\beta)}{RT}\right) = k_2' exp\left(\frac{F(\psi_\alpha - 2\psi_\beta)}{RT}\right). \tag{6.46}$$

Relating these to the rate constants, on obtains,

$$K_1' = \frac{k_1}{k_{-1}} = \frac{k_1^{int}}{k_{-1}^{int}} exp\left(\frac{-F(\psi_\alpha - \psi_\beta)}{RT}\right) = \frac{k_1^{int} exp\left(\frac{-F(\psi_\alpha - \psi_\beta)}{2RT}\right)}{k_{-1}^{int} exp\left(\frac{F(\psi_\alpha - \psi_\beta)}{2RT}\right)} \tag{6.47}$$

$$K_2' = \frac{k_2}{k_{-2}} = \frac{k_2^{int}}{k_{-2}^{int}} exp\left(\frac{-F(\psi_\alpha - 2\psi_\beta)}{RT}\right) = \frac{k_2^{int} exp\left(\frac{-F(\psi_\alpha - 2\psi_\alpha)}{2RT}\right)}{k_{-2}^{int} exp\left(\frac{F(\psi_\alpha - 2\psi_\alpha)}{2RT}\right)} \tag{6.48}.$$

In Eq.(6.44), all of the rate constants ($k$) will be substituted by the intrinsic rate constants ($k^{int}$) and their exponential terms and the final solutions are obtained by solving four of the nonlinear equations simultaneously. The computer program NAG Fortran Library, Mark II, (Numerical Algorithms Group Ltd.) was employed to solve the simultaneous equations. The exponential terms are calculated from the results of TLM at pH levels that were studied. For a group of four dimensional nonlinear equations, the distribution of solution may vary from none to infinity. To obtain the correct solution for the specific case, one must: 1) choose the reasonable range for each of $k^{int}$; and, 2) minimize the allowed error in the program, since the constants in the equations vary from $10^{2}$ to $10^{-20}$, and some terms will be easily shaded by errors. Double precision was adopted in the program that was employed and the estimated values for the $k^{int}$ were very slowly increased or decreased during the looping procedure. To do this, a huge amount of computing time was required. The intrinsic rate constants ($k_1^{int}$, $k_{-1}^{int}$, $k_2^{int}$, and $k_{-2}^{int}$) for the first step of the selenite–goethite reaction mechanism are listed in Table 6.4 and 6.5.

To examine the plausibility of the mechanism in Eq.(6.25), the similarity in results from the thermodynamic and kinetic studies must be compared. This involves two tests: 1) inserting the values of $\tau_1^{-1}$, concentration and electrostatic parameters of four pH levels that were studied in to Eq.(6.44) to calculate intrinsic rate constants $k^{int}$. And then, inserting the concentration and electrostatic parameters at other pH levels into Eq.(6.44) in which the $k^{int}$ were known now, the equation would provide the values of $\tau_{1,calculated}^{-1}$. If the intrinsic rate constants ($k^{int}$) were correct, then the values of $\tau_{1,calculated}^{-1}$ would agree with the values of reciprocal relaxation times from experiments ($\tau_{1,observed}^{-1}$) at each pH level that was studied; and 2) the overall intrinsic constants for the reactions of formation of $XHSeO_3^0$ and $XSeO_3^-$ should be of the same order of magnitude. Table 6.3 lists the fast reciprocal relaxation times ($\tau_1^{-1}$) obtained experimentally ($\tau_{1,observed}^{-1}$) and those calculated from Eq.(6.44) at the various pH values that were studied ($\tau_{1,calculated}^{-1}$). One can see that these values are quite similar.

**Table 6.3:** Relaxation data for selenite adsorption and desorption on goethite as a function of pH at 298K and 0.02 M ionic strength

| pH | $\tau^{-1}_{1,observed}(s^{-1})$ | $\tau^{-1}_{1,calculated}(s^{-1})$ | $\tau^{-1}_{2,observed}(s^{-1})$ | $\tau^{-1}_{2,calculated}(s^{-1})$ |
|---|---|---|---|---|
| 6.41 | 41.6 | 41.6 | 9.12 | 8.54 |
| 7.02 | 46.5 | 45.1 | 10.64 | 9.84 |
| 7.50 | 57.7 | 58.7 | 13.62 | 13.03 |
| 7.81 | 64.1 | 65.2 | 14.64 | 15.21 |
| 8.36 | 79.6 | 80.3 | 18.20 | 19.89 |
| 8.73 | 105.0 | 105.9 | 26.19 | 27.55 |
| 9.07 | 171.5 | 171.8 | 29.57 | 31.68 |
| 9.32 | 249.4 | 269.7 | 39.98 | 42.58 |
| 9.64 | 357.1 | 357.3 | 90.50 | 91.69 |

#### 6.3.2.2 Step Two

In this step, divalent and monovalent selenite anions enter the $\alpha$ layer, to replace a molecule of water from the active site, and form inner–sphere surface complexes $XSeO_3^-$ and $XHSeO_3^0$, respectively. The following nomenclature is adopted to simplify the terms in the equation derivation,

$$x_2 = [XOH_2^+ - HSeO_3^-] \qquad x_4 = [XSeO_3^-]$$

$$x_3 = [XOH_2^+ - SeO_3^{2-}] \qquad x_5 = [XHSeO_3^0].$$

In the second step the rate law for the change in concentration of the species after a small perturbation is,

$$-\frac{d(\Delta x_2 + \Delta x_3)}{dt} = k_3\Delta x_2 - k_{-3}\Delta x_5 + k_4\Delta x_3 - k_{-4}\Delta x_4. \tag{6.49}$$

If one lets $(\Delta x_2 + \Delta x_3) = x$, Eq. (6.49) becomes

$$-\frac{dx}{dt} = \left[\frac{k_3}{1+\frac{\Delta x_1}{\Delta x_2}} + \frac{k_{-3}}{1+\frac{\Delta x_4}{\Delta x_5}} + \frac{k_4}{1+\frac{\Delta x_2}{\Delta x_3}} + \frac{k_{-4}}{1+\frac{\Delta x_5}{\Delta x_4}}\right] x \tag{6.50}$$

so

$$\tau_2^{-1} = \frac{k_3}{1+\frac{\Delta x_1}{\Delta x_2}} + \frac{k_{-3}}{1+\frac{\Delta x_4}{\Delta x_5}} + \frac{k_4}{1+\frac{\Delta x_2}{\Delta x_3}} + \frac{k_{-4}}{1+\frac{\Delta x_5}{\Delta x_4}} \tag{6.51}$$

From the mass balance existing in step 2

$$\Delta x_2 + \Delta x_3 + \Delta x_4 + \Delta x_5 = 0 \tag{6.52}$$

$$\Delta x_2 + \Delta x_5 + \Delta H = 0 \tag{6.53}$$

and the relationships

$$K_5 = \frac{x_3 H}{x_2}. \qquad K_6 = \frac{x_4 H}{x_5}.$$

Two equations result,

$$\frac{\Delta x_3}{x_3} + \frac{\Delta H}{H} - \frac{\Delta x_2}{x_2} = 0 \tag{6.54}$$

$$\frac{\Delta x_4}{x_4} + \frac{\Delta H}{H} - \frac{\Delta x_5}{x_5} = 0. \tag{6.55}$$

Let $\frac{\Delta x_2}{\Delta x_3} = i$ and $\frac{\Delta x_4}{\Delta x_5} = j$. Then, from Eq.(6.52) and (6.53), one can express $\Delta x_3$ and $\Delta x_5$ as,

$$\Delta x_3 = \frac{-\Delta x_5(j+1)}{(i+1)}. \qquad \Delta x_5 = \frac{-\Delta x_3(i+1)}{(j_1)}.$$

Subsitituting them in Eq. (6.54) and (6.55), one obtains,

$$\frac{1}{x_3} + \frac{1}{H} - \frac{j(i+1)}{H(j+1)} - \frac{i}{x_2} = 0 \tag{6.56}$$

$$j\left(\frac{1}{x_4} + \frac{1}{H}\right) - \frac{(j+1)}{(i+1)H} - \frac{1}{x_5} = 0. \tag{6.57}$$

As was mentioned before, $XOH_2^+ - HSeO_3^-$ and $XOH_2^+ - SeO_3^{2-}$ are the intermediate products and their concentrations cannot be directly determined. Therefore, it is necessary to express the relaxation times as a function of the concentrations of the final products, $XHSeO_3^0$ and $XSeO_3^-$. In order to do this, $i$ and $j$ should be first derived as functions

of $XHSeO_3^0$, $XSeO_3^-$ and $H^+$. Use MACSYMA to solve Eq.(6.56) and (6.57), $i$ and $j$ are given as,

$$i = \frac{x_4x_5^2k_2k_{-2} + [(x_5^2 + x_4x - 5)H + x_4x_5^2]k_2k_{-1}}{(x_4^2x - 5k_2 + ((x_4x_5 + x_4^2)H + x_4^2x_5)k_1)k_{-2}}$$

$$j = \frac{[x_4^2x_5k_2 + (x_4^2H + x_4^2x_5)k_1]k_{-2} + x_4x_5Hk_2k_{-1}}{(x_4x_5^2k_2 + x_4x - 5Hk_1)k_{-2} + (x_5^2H + x_4x_5^2)k_2k_{-1}}$$

Equation (6.50) now is changed as a function of $i$ and $j$ such that,

$$\tau_2^{-1} = \frac{k_3}{1 + i^{-1}} + \frac{k_{-3}}{1 + j} + \frac{k_4}{1 + i} + \frac{k_{-4}}{1 + j^{-1}}. \tag{6.58}$$

Subsitituting $i$ and $j$ for Eq.(6.58), the relationship between $\tau_2^{-1}$ and $XHSeO_3^0$ and $XSeO_3^-$ is obtained.

$$\begin{aligned}\tau_2^{-1} =& k_{-3}/\Big[\frac{(f_7k_{-3} + f_4k_3)k_{-4} + f_5k_{-3}k_4}{(f_1k_{-3} + f_5k_3)k_{-4} + f_6k_{-3}k_4} + 1\Big] \\ &+ k_{-4}/\Big[\frac{(f_1k_{-3} + f_5k_3)k_{-4} + f_6k_{-3}k_4}{(f_7k_{-3} + f_4k_3)k_{-4} + f_5k_{-3}k_4} + 1\Big] \\ &+ k_4/\Big[\frac{f_1k_{-3}k_{-4} + f_2k_{-3}k_4}{(f_7k_{-3} + f_3k_3)k_{-4}} + 1\Big] \\ &+ k_3/\Big[\frac{(f_7k_{-3} + f_3k_3)k_{-4}}{f_1k_{-3}k_{-4} + f_2k_{-3}k_4} + 1\Big].\end{aligned} \tag{6.59}$$

where

$$f_1 = x_4x_5^2 \qquad f_5 = x_4x_5x_5$$

$$f_2 = (x_5^2 + x_4x_5)H + x_4x_5^2 \qquad f_6 = x_5^2(H + x_4)$$

$$f_3 = (x_4x_5 + x_4^2)H + x_3^2x_4 \qquad f_7 = x_4^2x_5$$

$$f_4 = x_4^2(H + x_5)$$

As for the final equation in step 1, the rate constants ($k$) in Eq.(6.59) are expressed as their intrinsic forms ($k^{int}$) and the exponential terms indicate the effect of the electric double layer. The relationships between the intrinsic constants ($K^{int}$) and the conditional constants ($K'$) are,

$$K_3^{int} = \frac{[XHSeO_3^0]}{[XOH_2^+ - HSeO_3^-]}exp(\frac{-F(\psi_\alpha - \psi_\beta)}{RT}) = K_3'exp(\frac{-F(\psi_\alpha - \psi_\beta)}{RT}) \tag{6.60}$$

$$K_4^{int} = \frac{[XSeO_3^-]exp(\frac{-F\psi_\alpha}{RT})}{[XOH_2^+ - SeO_3^{2-}]exp(\frac{F(\psi_\alpha - 2\psi_\beta)}{RT})} = K_4' exp(\frac{-2F(\psi_\alpha - \psi_\beta)}{RT}). \quad (6.61)$$

Coorespondingly, the rate constants have the relationships,

$$K_3' = k_3^{int} exp(\frac{F(\psi_\alpha - \psi_\beta)}{RT}) = \frac{k_3^{int} exp(\frac{F(\psi_\alpha - \psi_\beta)}{2RT})}{k_{-3}^{int} exp(\frac{-F(\psi_\alpha - \psi_\beta)}{2RT})} \quad (6.62)$$

$$K_4' = K_4^{int} exp(\frac{2F(\psi_\alpha - \psi_\beta)}{RT}) = \frac{k_4^{int} exp(\frac{F(\psi_\alpha - \psi_\beta)}{RT})}{k_{-4}^{int} exp(\frac{-F(\psi_\alpha - \psi_\beta)}{RT})}. \quad (6.63)$$

Substituting the exponential terms into Eq. (6.59), a very complicated nonlinear equation with four unknown variables, which covers all over the second steps, was established. Again, the NAG program was employed to solve the four simultaneous equations to obtain the four $k^{int}$ in the equation. The solution is listed in Table 6.4 and 6.5. The intrinsic equilibrium constant obtained from static study in Table 6.4 agrees with that from the kinetic study; the latter one is calculated from the intrinsic rate constants of step 1 and step 2 of $HSeO_3^-$ adsorption on goethite. The calculation can be expressed as,

$$K_{XHSeO_3^0}^{int} = \frac{k_1^{int}}{k_{-1}^{int}} \frac{k_3^{int}}{k_{-3}^{int}} \quad (6.64)$$

. Also, one can see from Table 6.5 that for adsorption of $SeO_3^{2-}$ on goethite, both values of intrinsic equilibrium constants obtained from static and kinetic studies are at the same order of magnitude. The following equation is for calculation of $K_{XSeO_3^-}^{int}$ using intirinsic rate constants of step 1 and step 2.

$$K_{XSeO_3^-}^{int} = \frac{k_2^{int}}{k_{-2}^{int}} \frac{k_4^{int}}{k_{-4}^{int}}. \quad (6.65)$$

Moreover, as was done for the first reaction step, the $k^{int}$ values were used in Eq (6.59) to calculate the other $\tau_2^{-1}$ values at which the p-jump experiment was conducted. The results, $\tau_{2,observed}^{-1}$ and $\tau_{2,calculated}^{-1}$, are listed in Table 6.3, and the are in close agreement.

**Table 6.4:** Intrinsic rate constants and equilibrium constants for $HSeO_3^-$ adsorption and desorption on goethite

| | $k_1^{int}$ | $k_{-1}^{int}$ | $k_3^{int}$ | $k_{-3}^{int}$ | $logK_{XHSeO_3^0}^{int}$ |
|---|---|---|---|---|---|
| | $mol^{-3}L^3s^{-1}$ | $s^{-1}$ | $s^{-1}$ | $s^{-1}$ | |
| Static Study | | | | | 20.42 |
| Kinetic Study | $3.82 \times 10^{14}$ | 4.07 | 101.0 | $9.7 \times 10^{-5}$ | 19.99 |

**Table 6.5:** Intrinsic rate constants and equilibrium constants of $SeO_3^{2-}$ adsorption and desorption on goethite

| | $k_2^{int}$ | $k_{-2}^{int}$ | $k_4^{int}$ | $k_{-4}^{int}$ | $logK_{XSeO_3^-}^{int}$ |
|---|---|---|---|---|---|
| | $mol^{-2}L^2s^{-1}$ | $s^{-1}$ | $s^{-1}$ | $s^{-1}$ | |
| Static Study | | | | | 15.48 |
| Kinetic Study | $2.18 \times 10^{13}$ | $3.26 \times 10^{-3}$ | 0.13 | 0.05 | 16.24 |

#### 6.3.2.3 Summary

Adsorption of selenite on goethite produces two types of complexes: the protonated selenite anion ($HSeO_3^-$) with the active site on the goethite surface; and the bivalent selenite anion ($SeO_3^{2-}$) reacting with the surface site. The proportion of each complex depends on the pH of the suspension. Both of them are inner-sphere surface complexes. The formation of the inner-sphere surface complexes involves two steps: selenite first forms an outer-sphere surface complexes at the $\beta$ layer and then, a ligand is replaced from the surface site by either adsorbed $HSeO_3^-$ or $SeO_3^{2-}$ from the surface. The adsorbed selenite binds directly to the surface site to form an inner-sphere surface complex. The second step is much slower than the first step and thus is rate-limiting.

# APPENDIX A
# DERIVATION OF EQUATIONS FOR RELATIONSHIP BETWEEN $\tau^{-1}$ AND CONCENTRATION TERMS FOR MOLYBDATE ADSORPTION

For the adsorption–desorption reaction,

$$XOH_2^+ + MoO_4^{2-} = XOH_2^+ - MoO_4^{2-} = XMoO_4^- + H_2O \tag{A.1}$$

the general forms for relationships between reciprocal relaxation times ($\tau^{-1}$) and other terms associated with the reaction in Eq. (A.1) can be derived as (Bernasconi, 1976):

$$\tau_1^{-1} = 1/2(a_{11} + a_{22}) + \{[1/2(a_{11} + a_{22})]^2 + a_{12}a_{21} - a_{11}a_{22}\}^{1/2} \tag{A.2}$$

$$\tau_2^{-1} = 1/2(a_{11} + a_{22}) - \{[1/2(a_{11} + a_{22})]^2 + a_{12}a_{21} - a_{11}a_{22}\}^{1/2} \tag{A.3}$$

where

$$a_{11} = k_1([XOH_2^+] + [MoO_4^{2-}]) + k_{-1} \tag{A.4}$$

$$a_{12} = k_{-1} \tag{A.5}$$

$$a_{21} = k_2 \tag{A.6}$$

$$a_{22} = k_2 + k_{-2}. \tag{A.7}$$

In the case when $k_1([XOH_2^+] + [MoO_4^{2-}]) + k_{-1} \gg k_2,\ k_{-2},\ \tau_1^{-1}$ and $\tau_2^{-1}$ are derived as,

$$\tau_1^{-1} = k_1([XOH_2^+] + [MoO_4^{2-}]) + k_{-1} \tag{A.8}$$

$$\tau_2^{-1} = k_2 \frac{k_1([XOH_2^+] + [MoO_4^{2-}])}{k_1([XOH_2^+] + [MoO_4^{2-}]) + k_{-1}} + k_{-2} \qquad (A.9)$$

# APPENDIX B
# DERIVATION OF EQUATION FOR RELATIONSHIP BETWEEN $\tau^{-1}$ AND CONCENTRATION TERMS FOR $SO_4$ ADSORPTION ON GOETHITE

The relationship between the inverse of the relaxation time constant, $\tau$, and the concentration of the reacting species shown in Eq. (5.29) can be developed as follows. The same procedure can be used to derive the relationship in Eq. (5.28). For the reaction

$$XOH + H^+ + SO_4^{2-} = XOH_2 - SO_4^{2-} \tag{B.1}$$

the rate is defined as

$$r = -\frac{d[XOH]}{dt} = -\frac{d[SO_4^{2-}]}{dt} = -\frac{d[H^+]}{dt} = \frac{d[XOH_2 - SO_4^{2-}]}{dt} \tag{B.2}$$

or

$$r = -k_f[XOH][SO_4^{2-}][H^+] + k_b[XOH_2 - SO_4^{2-}] \tag{B.3}$$

where $k_f$ and $k_b$ are the rate constants for the forward and backward reactions, respectively, and the terms in the brackets are the time-dependent concentrations. At equilibrium, $r = 0$ and Eq. (B.3) becomes

$$0 = -k_f[\overline{XOH}][\overline{SO_4^{2-}}][\overline{H^+}] + k_b[\overline{XOH_2^+ - SO_4^{2-}}] \tag{B.4}$$

where the overbar denotes the equilibrium concentration. Relating this to the law of mass action

$$\frac{[\overline{XOH_2^+ - SO_4^{2-}}]}{[\overline{XOH}][\overline{SO_4^{2-}}][\overline{H^+}]} = \frac{k_f}{k_b} = K_1 \tag{B.5}$$

Following a small perturbation, e.g., a pressure-jump, equilibrium concentrations are shifted a small amount, x. According to the conservation of mass law, the time-dependent

concentrations are

$$[XOH] = [\overline{XOH}] + x \tag{B.6.1}$$

$$[SO_4^{2-}] = [\overline{SO_4^{2-}}] + x \tag{B.6.2}$$

$$[H^+] = [\overline{H^+}] + x \tag{B.6.3}$$

$$[XOH_2 - SO_4^{2-}] = [\overline{XOH_2^+ - SO_4^{2-}}] - x \tag{B.6.4}$$

Substituting Eq. (B.6)s into Eq. (B.3)

$$\begin{aligned} r = \frac{dx}{dt} &= -k_f([\overline{XOH}] + x)([\overline{SO_4^{2-}}] + x)([\overline{H^+}] + x) \\ &\quad + k_b([\overline{XOH_2^+ - SO_4^{2-}}] - x) \\ &= -k_f[\overline{XOH}][\overline{SO_4^{2-}}][\overline{H^+}] + k_b[\overline{XOH_2^+ - SO_4^{2-}}] \\ &\quad - k_f([\overline{XOH}][\overline{SO_4^{2-}}] + [\overline{XOH}][\overline{H^+}] + [\overline{SO_4^{2-}}][\overline{H^+}])x \\ &\quad - k_f([\overline{XOH}] + [\overline{SO_4^{2-}}] + [\overline{H^+}])x^2 - k_f x^3 - k_b x \end{aligned} \tag{B.7}$$

The first two terms vanish because of Eq. (B.4). One then obtains

$$\begin{aligned} \frac{dx}{dt} &= -(k_f[\overline{XOH}][\overline{SO_4^{2-}}] + [\overline{XOH}][\overline{H^+}] + [\overline{SO_4^{2-}}][\overline{H^+}] + k_b)x \\ &\quad - k_f([\overline{XOH}] + [\overline{SO_4^{2-}}] + [\overline{H^+}])x^2 - k_f x^3 \end{aligned} \tag{B.8}$$

which can be further simplified if only small equilibrium perturbations are considered, i.e., small x. Then the last two terms become vanishingly small leading to

$$\frac{dx}{dt} = -(k_f[\overline{XOH}][\overline{SO_4^{2-}}] + [\overline{XOH}][\overline{H^+}] + [\overline{SO_4^{2-}}][\overline{H^+}] + k_b)x \tag{B.9}$$

One can define

$$\frac{dx}{dt} = -\frac{1}{\tau}x \tag{B.10}$$

where

$$\tau^{-1} = k_f([\overline{XOH}][\overline{SO_4^{2-}}] + [\overline{XOH}][\overline{H^+}] + [\overline{SO_4^{2-}}][\overline{H^+}]) + k_b \tag{B.11}$$

## REFERENCES


Alvarez, R., and D. L. Sparks. 1985. Polymerization of silicate anions in solutions at low concentrations. Nature. 318:649–651.

Anderson, M. A., J. F. Ferguson, and J. Gavis. 1976. Arsenate adsorption on amorphous aluminum hydroxide. J. Colloid. Sci. 54:391–399.

Anderson, M. A., and D. T. Malotky. 1979. The adsorption of protolyzable anions on hydrous oxides at the isoelectric pH. J. Colloid. Interf. Sci. 72:413–427.

Arnold, P. W. 1978. Surface-electrolyte interfactions. p.355–404. *In* D. J. Greenland and M. H. Hayes (eds) The chemistry of soil constituents. John Wiley, Chichester and New York.

Ashida, M., M. Sasaki, H. Kan, T.Yasunaga, K. Hachiya, and T. Inoue. 1978. Kinetics of proton adsorption-desorption at $TiO_2 - H_2O$ interface by means of pressure-jump technique. J. Colloid Interf. Sci. 67:219–225.

Astumian, R. D., M. Sasaki, T. Yasunaga, and Z. A. Schelly. 1981. Proton adsorption-desorption kinetics on iron oxides in aqueous suspensions, using the pressure-jump method. J. Phys. Chem. 85:3832–3835.

Atkinson, R. J., A. M. Posner, and J. P. Quirk. 1967. Adsorption of potential determining ions at the ferric oxide-aqueous electrolyte interface. J. Phys. Chem. 71:550–558.

Balistrieri, L. S., and T. T. Chao. 1987. Selenium adsorption by goethite. Soil Sci. Soc. Am. J. 51:1145–1151.

Barshad, I. 1951. Factors affecting molybdenum content of pasture plants: I. Nature of soil molybdenum, growth of plants, and soil pH. Soil Sci. 81:209–223.

Barrow, N. J. 1973. On the displacement of adsorbed anions from soil: 1. Desplacement of molybdate by phosphate and by hydroxde. Soil Sci. 116:423–431.

Barrow, N. J. 1977. Factors affecting the molybdenum status of soils. p. 583–595. *In* W. R. Chappell and K. K. Peterson (ed.) Molybdenum in the environment. Marcel Dekker, New Yoork.

Barrow, N. J. 1978. The description of phosphate adsorption curves. J. Soil Sci. 29:447–462.

Barrow, N. J., J. W. Bowden, A. M. Posner, and J. P. Quirk. 1980. An objective method for fitting models of ion adsorption on variable charge surfaces. Aust. J. Soil Res. 18:37–47.

Barrow, N. J. 1985. Reaction of anions and cations with variable charge soils. Adv. Agron. 38:183–230.

Bowden, J. W., S. Nagarajah, N. J. Barrow, A. M. Posner, and J. P. Quirk. 1980a. Describing the adsorption of phosphate, citrate and selenite on a variable-charge mineral surface. Aust. J. Soil Res. 18:49–60.

Bowden, J. W., A. M. Posner, and J. P. Quirk. 1980b. Adsorption and charging phenomena in variable charge soils. *In* B. K. G. Theng (ed.) Soils with variable charge. N. Z. Soc. Soil Sci. Lower Hutt, New Zealand.

Bernasconi, C. F. 1976. Relaxation kinetics. Academic Press, New York.

Bohn, H. L., B. L. McNeal, and G. A. O'Connor. 1979. Soil chemistry. John Wiley, New York.

Bornemisza, E., and R. Llanos. 1967. Sulfate movement, adsorption and desorption in three Costa Rican soils. Soil Sci. Soc. Am. Proc. 31:356–360.

Bowden, J. W., S. Nagarajah, N. J. Barrow, and A. M. Posner. 1980. Describing the adsorption of phosphate, citrate and selenite on a variable-charge mineral surface. Aust. J. Soil Res. 18:49–60.

Breeuwsma, A., and J. Lyklema. 1973. Physical and chemical adsorption of ions in the electrical double layer on hemetite ($\alpha - Fe_2O_3$). J. Colloid. Interf. Sci. 43:437–448.

Bridger, K., R. C. Patel, and E. Matijevic. 1982. Thermodynamics and kinetics of iron (III) ion by picolinic and dipicolinic acids. Polyhedron, 1:269–275.

Bridger, K., R. C. Patel, and E. Matijevic. 1983. Thermodynamic and kinetic studies of hydroxo and chloro complexes of iron (III) in ethanol/water mixtures. J. Phys. Chem. 87:1192–1201.

Brown, M. J., and D. L. Cater. 1969. Leaching of added selenium from alkaline soils influenced by sulfate. Soil Sci. Soc. Am. Proc. 33:563–565.

Carski, T. H., and D. L. Sparks. 1985. A modified miscible displacement technique for investigating adsorption-desorption kinetics in soils. Soil Sci. Soc. Am. J.49:1114–1116.

Carter, D. L., M. M. Mortland, and W. D. Kemper. 1986. Specific surface. p.413–423. *In* A. Klute (ed). Methods of Soil Analysis, Part1. 2nd Ed. Am. Soc. Agron. and Soil Sci. Soc. Am., Madison, WI.

Cary, E. E., G. A. Wiecaonek and W. H. Allaway. 1967. Reaction of selenite-selenium added to soils that produce low selenium forages. Soil Sci. Soc. Am. Proc., 31:21-26.

Chang, M. L., and G. W. Thomas. 1963. A suggested mechanism for sulfate adsorption by soils. Soil Sci. Soc. Am. Proc. 27:281-283.

Chou, L., and R. Wollast. 1984. Study of the weathering of albite at room temperature and pressure with a fluidized bed reactor. Geochem. Cosmochim. Acta 48:2205-2217.

Davis, J. S., and H. Gutfreund. 1976. The scope of moderate pressure changes for kinetic and equilibrium studies of biochemical systems. FEBS Letters 72:199-207.

Davis, J. A. and L. O. Leckie. 1980. Surface ionization and complexation at oxide/water interface. III. Adsorption of anion. J. Colloid. Interf. Sci. 74:32-43.

Eigen, M., and L. De Maeyer. 1963. Relaxation Methods. *In* A. Weissbezger (ed.). Techniques in organic chemistry. Vol. VIII. Part 2. 2nd Ed. Wiley Interscience. New York

Elliott, H. A., and D. L. Sparks. 1981. Electrokinetic behavior of a Paleudult Profile in relation to mineralogical composition. Soil Sci. 132:402-409.

Evans, H. J., E. R. Purvis, and F. E. Bear. 1951. Effect of soil reaction on availability of molybdenum. Soil Sci. 71:117-124.

Fiskell, J. G. A., R. S. Mansell, H. M. Selim, and F. G. Martin. 1979. Kinetic behavior of phosphate sorption by acid, sandy soil. J. Environ. Qual. 8:579-584.

Fleming, G. A. 1980. Essential micronutrients. 2. Iodine and selenium. *In* B. E. Davies (ed.). Applied soil trace elements. John Wiley, New York.

Freney, J. R., W. J. Barrow, and K. Spencer. 1962. A review of certain aspects of sulfur as soil constituent and plant nutrient. Plant Soil 17:295-306.

Geering, H. R., E. E. Cary, L. P. Johnes and W. H. Llarvay. 1968. Solubility and redox criteria for the possible forms of selenium in soils. Soil Sci. Soc. Am. Proc. 32:35-40.

Gillman, G. P. 1974. The influence of net drainage on water disposable clay and sorbed sulfate. Aust. J. Soil Res. 12:173-176.

Giles, C. H., D. Smith, and A. Huitson. 1974. A general treatment and classification of the solute adsorption isotherm. I. Theoretical. J. Colloid Interface Sci. 47:755-765.

Goldberg, S. 1986. Chemical modeling of arsenate adsorption on aluminum and iron oxide minerals. Soil Sci. Soc. Am. J. 50:1154-1159.

Goldberg, S., and R. A. Glaubig. 1986. Boron adsorption on California soils. Soil Sci. Soc. Am. J. 50:1173–1176.

Goldberg, S., and R. A. Glaubig. 1988. Anion sorption on a calcareous montmorillonitic soil: Selenium. Soil Sci. Soc. Am. J. 52:954–958.

Goldberg, S., and G. Sposito. 1984a. A chemical model of phosphate adsorption by soils: I. Reference oxide minerals. Soil Sci. Soc. Am. J. 48:772–778.

Goldberg, S., and G. Sposito. 1984b. A chemical model of phosphate adsorption by soils: II. Noncalcareous soils. Soil Sci. Soc. Am. J. 48:779–783.

Goldberg, S., and G. Sposito. 1985. On the mechanism of specific phosphate adsorption by hydroxylated mineral surfaces: A review. Commun. Soil Sci. Plant Anal. 16(8):801–821.

Griffin, R. A., and R. G. Burau. 1974. Kinetic and equilibrium studies of boron desorption from soil. Soil Sci. Soc. Am. J.38:892–897.

Hachiya, K., M. Ashida, M. Sasaki, H. Kan, T. Inoue, and T. Yasunaga. 1979. Study of kinetics of adsorption-desorption of $Pb^{2+}$ on $\gamma - Al_2O_3$ surface by means of relaxation techniques. J. Phys. Chem. 83:1866–1871.

Hachiya, K., M. Ashida, M. Sasaki, M. Karasuda, and T. Yasunaga. 1980. Study of the adsorption-desorption of $IO_3^-$ on a $TiO_2$ surface by means of relaxation techniques. J. Phys. Chem. 84:2292–2296.

Hachiya, K., M. Sasaki, T. Ikeda, N. Mikami, and T. Yasunaga. 1984. Static and kinetic studies of adsorption-desorption of metal ions on a $\gamma - Al_2O_3$ surface. 2. Kinetic study by means of pressure-jump technique. J. Phys. Chem. 88:27–31.

Hansmann, D. D., and M. A. Anderson. 1985. Using electrophoresis in modeling sulfate, selenite, and phosphate adsorption onto goethite. Environ. Sci. Tech. 19:544–551.

Haque, I., and D. Walmsley. 1974. Movement of sulfate in two Caribbean soils. Plant Soil 40:145–152.

Harter, R. D. and R. G. Lehmann. 1983. Use of kinetics for the study of exchange reactions in soils. Soil Sci. Soc. Am. J.47:666–669.

Harward, M. E., and H. M. Reisenauer. 1966. Reactions and movement of inorganic sulfur. Soil Sci. 101:326–335.

Hayes, K. F. and J. O. Leckie. 1986. Mechanism of lead ion adsorption at the goethite–water interface. *In* J. A. Davis and K. F. Hayes (eds.). Geochemical processes at mineral surfaces. ACS SYM. 323. Am. Chem. Soc., Washington, DC

Hayes, K. F., and J. O. Leckie. 1987. Modeling ionic strength effects on cation adsorption at the hydrous oxide/solution interface. J. Colloid Interf. Sci. 115:564–572.

Hingston, F. J. 1981. A review of anion adsorption. *In* M. A. Anderson and A.J. Rubin (eds). Adsorption of inorganics at solid-liquid interfaces. Ann Arbor Science, Ann Arbor, MI.

Hingston, F. J., R. J. Atkinson, A. M. Posner, and J. P. Quirk. 1967. Specific adsorption of anions. Nature. 215:1459–1461.

Hingston, F. J., A. M. Posner and J. P. Quirk. 1968. Adsorption of selenite by goethite. Symposium on adsorption from aqueous solution. Adv. in Chem. Series. 70:82–90.

Hingston, F. J., A. M. Posner and J. P. Quirk. 1971. Competitive adsorption of negatively charged ligand on oxide surface. Discuss. Faraday Soc. 52:334-342.

Hingston, F. J., A. M. Posner and J. P. Quirk. 1972. Anion adsorption by goethite and gibbsite. I. The role of the proton in determining adsorption envelopes. J. Soil Sci. 23:177–192.

Hingston, F. J., A. M. Posner and J. P. Quirk. 1974. Anion adsorption by goethite and gibbsite. II. Desorption of anions from hydrous oxide surfaces. J. Soil Sci. 25:16–26.

Hodges, S. C., and G. C. Johnson. 1987. Kinetics of sulfate adsorption desorption by Cecil soil using miscible displacement. Soil Sci. Soc. Am. J. 50:323–331.

Hohl, H., and W. Stumm. 1976. Interaction of $Pb^{+}$ with hydrous $\gamma$-$Al_2O_3$. J. Colloid Interf. Sci. 55:281–288.

Huang, C. P. 1975. Adsorption of phosphate at the hydrous $\gamma - Al_2O_3$-electrolyte interface. J. Colloid Interf. Sci. 53:178–186.

Ikeda, T., M. Sasaki, R. D. Astumian, and T. Yasunaga. 1981. Kinetics of the hydrolysis of zeolite 4A surface by the pressure-jump relaxation method. Bull. Chemistry Society of Japan. 54:1885–1886.

Ikeda, T., M. Sasaki, K. Hachlya, R. D. Astumian, T. Yasunaga, and Z. A. Schelly. 1982a. Adsorption-desorption kinetics of acetic acid on silica-alumina particles in aqueous suspensions using the pressure-jump relaxation method. J. Phys. Chem. 86:3861–3866.

Ikeda, T., M. Sasaki, and T. Yasunaga. 1982b. Kinetic behavior of $\ell-$ Lysine on zeolite X surface using the pressure-jump method. J. Phys. Chem. 86:1680–1683.

Ikeda, T., M. Sasaki, and T. Yasunaga. 1982. Kinetics of hydrolysis of hydroxyl groups on zeolite using the pressure-jump method. J. Phys. Chem. 86:1678–1680.

Ikeda, T., J. Nakahara, M. Sasaki, and T. Yasunaga. 1983. Kinetic behavior of alkali metal ion on zeolite 4A surface using the stopped-flow method. J. Colloid Interf. Sci. 97:278-283.

Jarrell, W. M., and M. D. Donson. 1978. Sorption and availability of molybdenum in soils of Western Oregon. Soil Sci. Soc. Am. J. 42:412-415.

Jardine, P. M., and D. L. Sparks, 1984. Potassium-calcium exchange in a multireactive soil system. I. Kinetics. Soil Sci. Soc. Am. J.48:39-45.

Jones, L. H. P. 1957. The solubility of molybdenum in simplified systems and aqueous soil suspensions. J. Soil Sci. 8:311-327.

Johns, G. B., and G. B. Belling. 1967. The movement of copper, molybdenum and selenium in soils as indicated by radioactive isotopes. Aust. J. Agric. Res. 18:733-740.

Johnston, C. T., and G. Sposito. 1987. Disorder and early sorrow: Progress in the chemical speciation of soil surfaces. *In* L. L. Boersma et al. (eds.) Future developments in soil science research. Soil Sci. Soc. Am. Madison. WI

Kabatapendias, A. and H. Pendias. 1983. Trace elements in soils and plants. CRC Press Inc., Boca Raton. FL

Karimia, N., and F. R. Cox. 1978. Adsorption and extractability of molybdenum in relation to some chemical properties of soils. Soil Sci. Soc. Am. J. 42:757-761.

Knoche, W., and G. Wiese. 1974. An improved apparatus for pressure-jump relaxation measurements. Rev. Sci. Inst. 5:91-98.

Kuo, S., and E. G. Lotse. 1972. Kinetics of phosphate adsorption by calcium carbonate and Ca-kaolinite. Soil Sci. Soc. Am. Proc. 36:725-729.

Levesque, M. 1974. Some aspects of selenium relationships in eastern Canadian soils and plants. Canad. J. Soil Sci. 54:63-68.

Lopez-Quintela, M., W. Knoche, and J. Veith. 1984. Kinetics and thermodynamics of complex formation between aluminum(III) and citric acid in aqueous solution. J. Chem. Soc. Trans. 80:2313-2321.

Marsh, K. B., R. W. Tillman, and J. K. Syers. 1987. Charge relationships of sulfate sorption by soils. Soil Sci. Soc. Am. J. 51:318-323.

Martin, R. R., and R. S. C. Smart. 1987. X-ray photoelectron studies of anion adsorption on goethite. Soil Sci. Soc. Am. J. 51:54-56.

Mackenzie, R. M. 1983. The adsorption of molybdate on oxide surface. Aust. J. Soil Res., 21:505-513.

Mengel, K., and E. A. Kirkby. 1982. Principles of plant nutrition. 3rd Edition. Intl. Potash Inst. Bern, Switzerland.

Merrill, D. T., M. A. Manzione, J. J. Peterson, D. S. Parker, W. Chow, and A. O. Hobbs. 1986. Field evaluation of arsenic and selenium removed by iron coprecipitation. J. Water Pollut. Control Fed. 58:18–26.

Mikamii, N., M. Sasakl. K. Hachlya, R. D. Astumian, T. Ikeda, and T. Yasunaga. 1983. Kinetics of the adsorption-desorption of phosphate on the $\gamma - Al_2O_3$ surface using the pressure-jump technique. J. Phys. Chem. 87:1454–1458.

Mikami, N., M. Sasaki. K. Hachiya, and T. Yasunaga. 1983. Kinetic study of the adsorption–desorption of the uranyl ion on a $\gamma - Al_2O_3$ surface using the pressure–jump technique. J. Phys. Chem. 87:5478–5481.

Mikami, N., M. Sasaki, T. Kikuchi, and T. Yasunaga. 1983. Kinetics of adsorption–desorption of chromate on $\gamma - Al_2O_3$ surface using a pressure–jump technique. J. Phys. Chem., 87:5245–5248.

Miller, D. M., W. P. Miller, and M. E. Sumner. 1986. Kinetics of silicic acid sorption by goethite using a flow-through cell. Agron. Abstr. p. 169.

Mott, C. J. B. 1981. Anion and ligand exchange. *In* D.J. Greenland and M.H.B. Hayes (eds). The chemistry of soil processes. John Wiley, New York.

Motta, M. M., and C. F. Miranda. 1989. Molybdate adsorption on kaolinite, montmorillonite, and illite: Constant capacitance modddeling. Soil Sci. Sci. Am. J. 53:380–385.

Muljadi, M., A. M. Posner, and J. P. Quirk. 1966. The mechanism of phosphate adsorption by kaolinite, gibbsite, and pseudoboehmite. Part I. The isotherm and the effect of pH on adsorption. J. Soil Sci. 17:212–235.

Neal, R. H., G. Sposito, K. M. Holtzclaw and S. J. Traina. 1987a. Selenite adsorption on alluvial soils: I. Soil compositions and pH effects. Soil Sci. Soc. Am. J. 51:1161–1165.

Neal, R. H., G. Sposito, K. M. Holtzclaw and S. J. Traina. 1987b. Selenite adsorption on alluvial soils: II. Solution composition effects. Soil Sci. Soc. Am. J. 51:1165–1169.

Negishi, H., M. Sasaki, T. Yasunaga, and M. Inoue. 1984. Intercalation kinetics of $Na^+$ ion into $TiS_2$ using the pressure-jump technique. J. Phys. Chem. 88:1455–1457.

Novak, L. T., and D. C. Adriano. 1975. Phosphorus movement in soils: Soil–orthophosphate reaction kinetics. J. Environ. Qual., 4:261–266.

Ogwada, R. A., and D. L. Sparks, 1986a. A critical evaluation on the use of kinetics for determing thermodynamics of ion exchange in soils. Soil Sci. Soc. Am. J. 50:300–305.

Ogwada, R. A., and D. L. Sparks, 1986b. Kinetics of ion exchange on clay minerals and soils: I. Evaluation of methods. Soil Sci. Soc. Am. J. 50:1158–1162.

Ogwada, R. A., and D. L. Sparks, 1986c. Kinetics of ion exchange on clay minerals and soils: II. Elucidation of rate-limiting steps. Soil Sci. Soc. Am. J. 50:1162–1164.

Olson, O. E., E. I. Whitehead, and A. L. Moxon. 1942. Occurrence of soluble selenium in soils and its availability to plants. Soil Sci. 54:47–53.

Parks, G. A., and P. L. deBruyn. 1962. The zero point of charge of oxides. J. Phys. Chem. 66:967–973.

Parfitt, R. L. 1978. Anion adsorption by soils and soil materials. Adv. Agron. 30:1–50.

Parfitt, R. L., and J. D. Russell, 1977. Adsorption on hydrous oxides: IV. Mechanisms of adsorption of various ions on goethite. J. Soil Sci. 28:297–305.

Parfitt, R. L., J. D. Rusell, and V. C. Fraser, 1976. Confirmation of the surface of goethite ($\gamma$-FeOOH) and phosphated goethite by infrared spectroscopy. J. Chem. Soc. Farday Trans. I. 72:1082–1087.

Parfitt, R. L., and R. S. C. Smart. 1977. The mechanism of sulfate adsorption on iron oxide. Soil Sci. Soc. Am. J.42:48–50.

Patel, R. C., G. Atkinson, and R. J. Boe. 1974. Pressure jump apparatus for the study of fast reactions. Chem. Instrumentation 5:243–255.

Patel, R. C., F. Garland, and G. Atkinson. 1975. Dynamics of magnesium–bicarbonate interactions. J. Solution Chem. 4:161–174.

Patel, R. C., and R. S. Taylor. 1973. Kinetics of binding of pyrophosphate to magnesium ions. J. Phys. Chem. 77:2318–2323.

Phelan, P. J., and S. V. Mattigod. 1984. Adsorption of molybdate anion ($MoO_4^{2-}$) by sodium saturated kaolinite. Clays Clay Mineri. 32:45–48.

Rai, D., and I. P. Murarka. 1987. Evaluation of fundamental data needed to predict the geochemical behavior of elements. In L. L. Boersma et al., (eds.) Future developments in soil science research. Soil Sci. Soc. Am., Madison, WI.

Rajan, S. S. S. 1978. Sulfate adsorbed on hydrous alumina, ligands displaced, and changes in surface charge. Soil Sci. Soc. Am. J. 42:39–44.

Rajan. S. S. S. 1979. Adsorption of selenium. phosphate and sulfate on hydrous alumina. J. Soil Sci. 30:709–718.

Rajan. S. S. S.. K. W. Perott. and W. M. H. Saunders. 1974. Identification of phosphate-reactive sites of hydrous alumina from proton consumption during phosphate adsorption at constant pH values. J. Soil Sci. 25:438–447.

Rand. R. H. 1984. Computer algebra in applied mathematics: An introduction to MACSYMA. Pitman Advanced Publishing Program. London.

Reyes. E. D.. and J. J. Jurinak. 1967. A mechanism of molybdate adsorption on $\alpha Fe_2O_3$. Soil Sci. Soc. Am. Proc. 31:637–641.

Reisenauer. H. M.. A. A. Tabikh. and P. R. Stout. 1962. Molybdenum reactions with soils and the hydrous oxides of irom. aluminum. and titanium. Soil Sci. Soc. Am. Proc. 26:23–27.

Ryden. J. C.. J. K. Syers. and R. W. Tillman. 1987. Inorganic anion sorption and interaction with phosphate sorption by hydrous ferric oxide gel. J. Soil Sci. 38:211–217.

Russell, J. D., R. L. Parfitt. A. R. Fraser. and V. C. Farmer, 1974. Surface structure of gibbsite. goethite and phosphated goethite. Nature. 248:220–221.

Sasaki. M.. M. Morlya. and T. Yasunaga. 1983. A kinetic study of ion-pair formation of $\alpha$–FeOOH in aqueous suspension using the electric field pulse technique. J. Phys. Chem. 87:1449–1453.

Sasaki. M.. H. Negishi. M. Inoue. and T. Yasunaga. 1984. Intercalation kinetics of a proton into $TiS_2$ by the pressure-jump technique. J. Phys. Chem. 88:3082–3085.

Sawhney. B. L.. 1966. Kinetics of cesium sorption by clay minerals. Soil Sci. Soc. Am. Proc.. 30:364–369.

Schwarz. G. 1986. Theoretical basis of chemical relaxation. In C. F. Bernasconi (ed.) Investigation of rate and mechanism of reactions. Techniques of chemistry. Volume VI. John Wiley. New York.

Scott. N. M. 1976. Sulfate contents and sorption in Scottish soils. J. Sci. Food Agric. 27:367–372.

Sivasubramaniam. S.. and O. Talibudeen. 1972. Potassium-aluminum exchange in acid soils: I. Kinetics. J. Soil Sci. 23:163–176.

Sparks. D.L. 1989. Kinetics of soil chemical process. Academic Press. New York.

Sparks, D. L. 1987. Kinetics of soil chemical processes: Past progress and future needs. *In* L. L. Boersma et al. (eds.) Future development in soil science research. Soil Sci. Soc. Am. Madison, WI

Sparks, D. L., 1986. Kinetics of reaction in pure and mixed systems. *In* D. L. Sparks (ed.) Soil physical chemistry. CRC Press, Boca Raton, FL.

Sparks, D. L. 1985. Kinetics of ionic reactions in clay minerals and soils. Adv. Agron. 38:231–266.

Sparks, D. L., and P. M. Jardine, 1984. Comparison of kinetic equations to describe K-Ca exchange in pure and in mixed systems. Soil Sci. 138:115–122.

Sparks, D. L., L. W. Zelazny, and D. C. Martens. 1980. Kinetics of potassium desorption in soils using miscible displacement. Soil Sci. Soc. Am. J.,44:1205–1208.

Sposito, G. 1984. The surface chemistry of soils. Oxford University Press, New York.

Sposito, G. 1985. Chemical models of inorganic pollutants in soils. CRC Crit. Rev. in Environ. Control. 15:1–24.

Sposito, G. 1986. On distinguishing adsorption from surface precipitation. *In* J. A. Davis and K. F. Hayes (eds.) Geochemical processes at mineral surfaces. ACS SYM 323. Am. Chem. Soc. Washington D. C.

Sposito, G., J. C. M. De Wit, and R. H. Neal. 1988. Selenite adsorption on alluvial soils: III. Chemical modeling. Soil Sci. Soc. Am. J. 52:947–950.

Stout, P. R., W. R. Meagher, G. A. Pearson, and C. M. Johnson. 1951. Molybdenum nutrition of crop plants: I. The influence of phosphate and sulfate on the adsorption of molybdenum from soils and solution cultures. Plant Soil 3:51–87.

Strahm, U., R. C. Patel, and E. Matijevic. 1979. Thermodynamics and kinetics of aqueous iron (III) chloride complex formation. J. Phys. Chem. 83:1689–1695.

Stumm, W., R. Kummert, and L. Sigy. 1980. A ligand exchange model for the adsorption of inorganic and organic ligands at hydrous oxide interfaces. Croatica Chem. Acta. 53:291–312.

Swoboda, A. R., and G. W. Thomas. 1965. The movement of sulfate salts in soils. Soil Sci. Soc. Am. Proc. 29:540–544.

Takeda, K., and T. Yasunaga. 1973. Kinetic study of sodium decyl sulfate micelle dissociation by the relaxation method. J. Colloid Interf. Sci. 45:406–412.

Tripathi, P. S. M., R. Tripathi, and B. B. Prasad. 1975. Radiotracer studies of adsorption of sulfate ions on ignited alumina. Part A. Proc. Indiana Natl. Sci. Acad. 41:156–162.

Wedler, G. 1976. Chemisorption, an experimental approach. Translated by D. F. Klemperer. Butterworth & Co. Ltd. Boston, MA.

Westall, J. C. 1982. FITEQL, A program for determination of chemical equilibrium constants from experimental data (Version 2). Chemistry Department, Oregon State University, Corvallis, OR.

Wilhelmy, R. B., R. C. Patel, and E. Matijevic. 1985. Thermodynamics and kinetics of aqueous ferric phosphate complex formation. Inorg. Chem. 24:3290–3297.

White, R. E. 1981. Retention and release of phosphate by soil and soil constituents. *In* P. B. Tinker (ed.) Soils and Agriculture. Halsted Press, New York.

Yates, D. E., and T. W. Healy. 1975. Mechanism of anion adsorption at the ferric and chromic oxide/water interfaces. J. Colloid Interf. Sci. 52:222–228.

Zasoski, R. T., and R. G. Burau. 1978. A technique for studying the kinetics of adsorption in suspension. Soil Sci. Soc. Am. J.42:372–374.

Zhang, P. C., and D. L. Sparks. 1989. Kinetics and mechanisms of molybdate adsorption/desorption at the goethite/water interface using pressure-jump relaxation. Soil Sci. Soc. Am. J. 53:1028–1034.

Zhang, G. Y., X. N. Zhang, and T. R. Yu. 1987. Adsorption of sulfate and fluoride by variable charge soils. J. Soil Sci. 38:27–38.